SPECTRAL AND ELECTROCHEMICAL STUDY OF THE RESPONSE

MECHANISM OF IONOPHORE-BASED

POLYMERIC MEMBRANES

Except where reference is made to the work of others, the work described in this dissertation is my own or was done in collaboration with my advisory committee. This dissertation does not include proprietary or classified information.

_____

Robert F. Long II

Certificate of Approval:

_____	_____
Rik Blumenthal Assistant Professor Chemistry and Biochemistry	Eric Bakker, Chair Professor Chemistry and Biochemistry
_____	_____
Vince Cammarata Associate Professor Chemistry and Biochemistry	Curtis Shannon Professor Chemistry and Biochemistry

_____

Stephen L. McFarland
Acting Dean
Graduate School

SPECTRAL AND ELECTROCHEMICAL STUDY OF THE RESPONSE MECHANISM OF IONOPHORE-BASED POLYMERIC MEMBRANES

Robert F. Long III

A Dissertation

Submitted to

the Graduate Faculty of

Auburn University

in Partial Fulfillment of the

Requirement for the

Degree of

Doctor of Philosophy

Auburn, Alabama
August 7, 2006

SPECTRAL AND ELECTROCHEMICAL STUDY OF THE RESPONSE

MECHANISM OF IONOPHORE-BASED

POLYMERIC MEMBRANES

Robert F. Long III

_____
Signature of Author

_____
Date of Graduation

VITA

Robert Long, son of Phyllis Dykes Long and Robert Franklin Long Jr., was born in Savannah, Georgia on December 17, 1970. After graduating from high school in May 1989, he entered the Department of Chemistry at the University of Georgia the following fall. In 1996 he entered the Department of Chemistry at Armstrong Atlantic State University where he earned his degree of Bachelor of Science in Chemistry in the Spring of 1998. The following year was spent conducting environmental analysis for SAVANNAH LABORATORIES AND ENVIRONMENTAL SERVICES INC. He enrolled in the doctoral program in the Department of Chemistry, Auburn University, in the fall of 1999 and will obtain the degree of Doctor of Philosophy from Auburn University in August 2006. He is also brother to Jennifer Long Patterson, Mary Catherine Long, James Anthony Long and uncle to Morgan Ray Patterson and Phillip Anthony Patterson.

DISSERTATION ABSTRACT

SPECTRAL AND ELECTROCHEMICAL STUDY OF THE RESPONSE MECHANISM OF IONOPHORE-BASED POLYMERIC MEMBRANES

Robert F. Long III

Doctor of Philosophy, August 7, 2006
(B.S. , Armstrong Atlantic State University, 1998)

204 Typed Pages

Directed by Eric Bakker

Ion-Selective electrodes based on solvent polymeric membranes, typically plasticized poly-(vinyl chloride), are routinely used and fundamental studies on ion transfer mechanisms that dictate their practicality continue. This dissertation is aimed at elucidating some of the features of these ionophore-based sensors in hope of reaping the most benefit from their accurate response. The initial goal of this research was to develop a theory based on normal pulse voltammetry (NPV) applied to a conducting polymer membrane electrode doped with highly selective, lipophilic ion-complexing molecules. Upon discreet potential pulses (uptake of target ion) in a three-electrode setup, ions are selectively transferred from a conducting aqueous electrolyte phase into the polymeric membrane phase. After a short uptake pulse (1 s), the membrane is allowed to relax at a

potential 0.0 V (30 s). This allows the membrane to expel previously transferred ions back into the aqueous phase, renewing the original membrane composition prior to subsequent pulses.

This method was used to examine 18 neutral ionophores in an attempt to calculate ion-ionophore complexation constants. The NPV scans were conducted at 20 mV intervals. These scans were fit with a theory that depends on three separate regions of the NPV plot. The most striking feature in the NPV scans is the diffusion limited plateau in the current/potential plots. These plateau potentials vary in range for membranes containing different ionophores with different complex formation constants and different ion-ionophore stoichiometry.

The same principles mentioned above were also applied to polymeric films containing the proton-selective chromoionophore ETH 5294 without ionic sites. In addition, a calibration curve of potential versus pH was made and compared to similar potentiometric ion-selective membranes showing a Nernstian response and good lower and upper detection limits. The same NPV membranes (or ion amperometric membranes) used in the pH calibration were also fitted in a special transparent electrochemical cell coupled to a microscope and potentiostsat. The chromoionophore, ETH 5294, changes its absorbance maximum upon protonation. The cell was positioned under the microscope, a potential was then applied which transferred protons from an aqueous buffer into the polymer membrane protonating the chromoionophore and changing its

absorbance characteristics. The absorbance profiles were used to estimate the diffusion coefficient of the chromoionophore in the membrane.

In view of realizing accurate diffusion coefficients within solvent polymeric ion-selective membranes, an additional optical method was developed. ETH 5294 can be photobleached using ultra-violet light. This is not good for sensor performance, however, it was utilized to gain information on the effects of plasticizer and polymer content on the diffusion coefficient of ETH 5294. The method uses light from a high-pressure Hg arc lamp to photobleach a portion of a single polymer membrane containing ETH 5294. The microscope is then repositioned and absorbance measurements are taken over fixed time intervals, allowing for the estimation of the apparent diffusion coefficient of the chromoionophore in 20 different membranes. This method was also used to investigate other chromophores including an Indium(III) porphyrin and three grafted ionophores with an MMA-DMA copolymer backbone.

ACKNOWLEDGMENTS

I would like to thank Dr. Eric Bakker for his continuous support and guidance. I am indebted to him. I would also like to thank Dr. W. C. Neely for his encouragement. Many thanks to my committee members: Dr. Rik Blumenthal, Dr. Vincenzo Cammarata and Dr. Curtis Shannon for their patience. Good luck to other group members, Dr. Yu Qin, Dr. Martin Telting, Dr. Aleksander Radu, Dr. Smita Jadhav, Dr. Shane Peper, Dr. Ioannis Tsagkatakis, Dr. Sally Mathison, Dr. Alan Ceresa and Dr. Yanming Mi. I am also grateful for the financial support of The National Institutes of Health and The Petroleum Research Fund.

Without the help of my father and mother, I would not have been able to complete this work. So, I would love to thank Dr. Robert F. Long Jr. and his loving wife, Phyllis. I must also thank my brother, James Anthony Long, and my two sisters, Mary Catherine Long and Jennifer Elizabeth Patterson, simply for being who they are. Also, in fond memory of my Aunt Lynn Long Volk.

Style journal used Analytical Chemistry

Computer software used Microsoft Word, Adobe Illustrator, Mathematica, Microsoft Excel and Equation Editor.

TABLE OF CONTENTS

LIST OF TABLES

LIST OF FIGURES

Chapter 1

Introduction

Electrochemistry involves the chemical phenomena of charge separation and charge transfer. Over the last thirty years, advances in zero-current potentiometry and bulk optodes based on ionophores have established these methods and they are widely used in ion detection. An essential part of these ion-sensing methods is the ionophore contained within the sensing film, typically plasticized poly(vinyl chloride). Along with added lipophilic sites, the ionophore is responsible for the selective partitioning of target sample ions without counterions into the ion-selective (ISE) film or optode film. Many ionophores have been developed for both a variety of cations and anions, while other selective sensors were developed for neutral species, alcohols, organic amines and polyions.[1] With such a wide range of available ionophores, it makes perfect sense that

the complexation mechanism used in potentiometry and optodes would also find use in voltammetric and amperometric systems.[2-7]

1.1 Ion-Selective Electrodes (ISEs)

Ion selective sensing has been the corner stone of research in the field of electrochemistry known as potentiometry. A typical electrochemical cell most often used in potentiometry consists of two electrodes linked to a voltmeter through wires for electron transport and immersed in the same sample solution for ionic transport (See Figure 1-1). The first of the two electrodes is the reference electrode. There are several types including the saturated calomel electrode (SCE) and the silver/silver chloride electrode (Ag/AgCl) whose electrical contacts to the voltmeter are made through wires connected to the metal and ionic contacts through a saturated potassium chloride solution.[8] Commonly, the reference electrode is a double-junction electrode with a salt bridge (1 M lithium acetate) completing the ionic contact from the potassium chloride solution to the sample. It is important that the reference electrode maintains a constant and stable potential and is insensitive to changes in temperature and sample composition.[8]

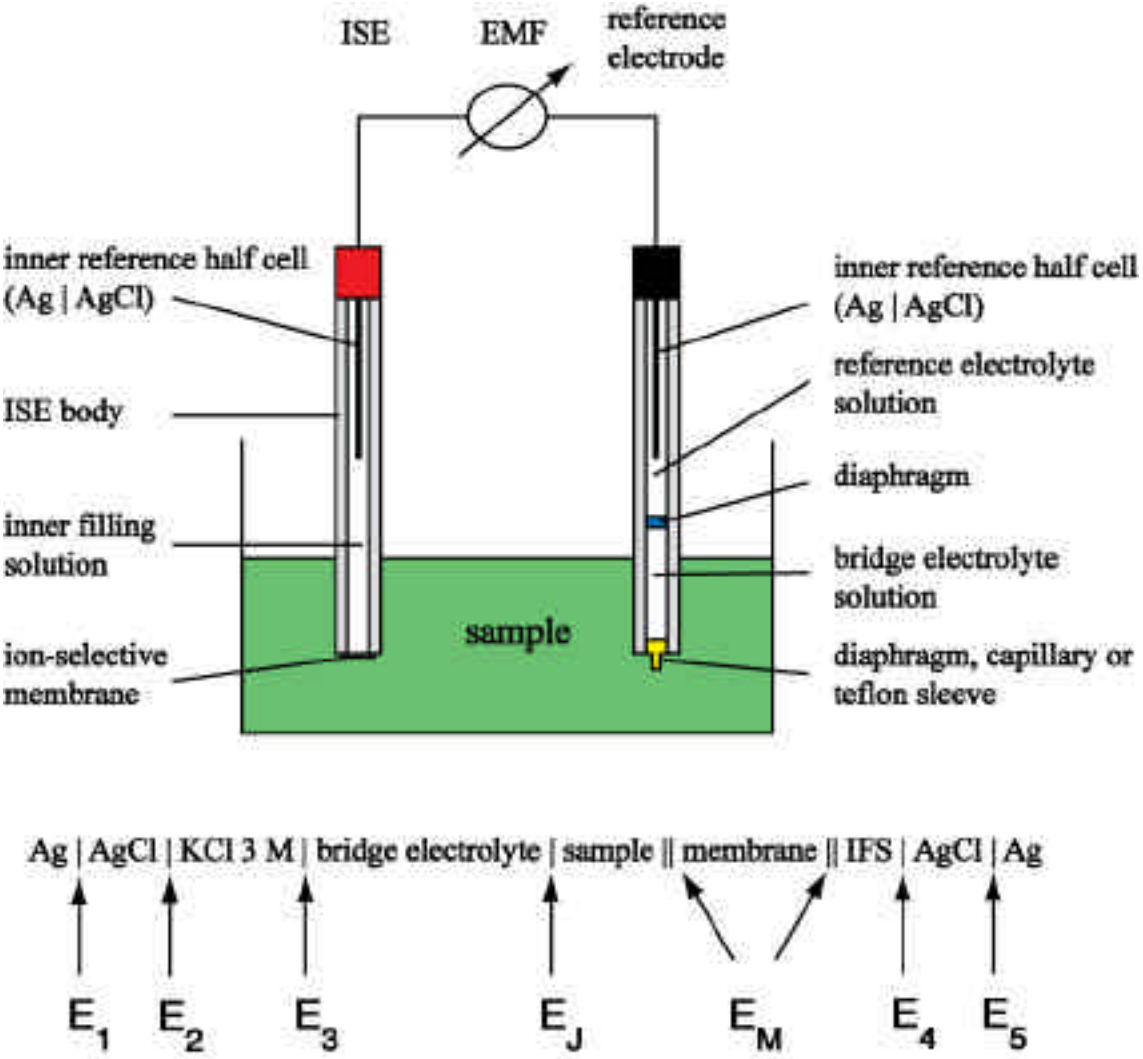

Fig. 1-1 Schematic of a potentiometric electrochemical cell showing the various contributors to the overall measured potential.

Next, the indicator electrode is an ion selective electrode (ISE) which is separated from the sample by a thin polymer membrane containing selective sensing components. On the other side of this ion-selective membrane and contained within the electrode body, there is another chloride salt solution called the inner filling solution (IFS) in contact with both the backside of the ISE membrane and an internal Ag/AgCl reference electrode wire. The wire is connected to the reference electrode through the high-impedance voltmeter. Once both electrodes are immersed in the sample the electrochemical cell is complete and the voltmeter may record the cell potential (EMF) in volts.

$$E_{cell} = E_1 + E_2 + E_3 + E_4 + E_5 + E_J + E_M \tag{1.1}$$

Potentials E_1 through E_5 include the sample independent contributions to the cell potential from both the reference electrode and the ISE. These potential contributions are constant and summed together as E°. Another potential develops between the salt bridge of the external reference electrode and the aqueous sample solution called the liquid junction potential, E_J, and another develops across the ISE membrane, E_M. This gives:

$$E_{cell} = E_0 + E_J + E_M \tag{1.2}$$

The salt bridge is typically more concentrated and contains ions with different sizes and mobilities than those in the contacting aqueous sample. This leads to a separation of charge due to differing rates of migration of the ions across the interface and thus a potential. The liquid junction potential is usually between 2-3 mV in this system and although it is not negligible it can be summed with the other sample independent

potentials.[9] This leaves the membrane potential, E_M, as the only sample dependent polarizable interface in the electrochemical cell. The phase boundary potential model describes the potentiometric response of an ISE membrane.[10] In this model, the membrane potential is divided into three separate potential contributions, the phase boundary potential between the sample and ISE membrane (E_{PB}), the phase boundary potential between the inner filling solution and the ISE membrane ($E_{PB'}$) and the internal diffusion potential of the membrane ($E_{diff.}$). Therefore, the membrane potential can be represented as:

$$E_M = E_{PB} + E_{PB'} + E_{diff.} \tag{1.3}$$

Recently, it has been shown that the diffusion potential is negligible and in most cases the membrane internal diffusion potential is zero due to the lack of concentration gradients within the membrane bulk.[11,12] The phase boundary potential at the interface between the sample and the polymer membrane is the only potential that is dependent on the sample composition. It is, therefore, assumed that the membrane potential (E_M) is the sum of the sample/ISE membrane phase boundary potential and a constant equaling the total contribution from the ISE membrane/inner filling solution phase boundary potential and the internal diffusion potential:

$$E_M = E_{PB} + E_{const} \tag{1.4}$$

The sample membrane phase boundary potential can be derived from thermodynamic considerations. Assuming that interfacial ion transfer kinetics are fast, equilibrium will be established at the sample/membrane interface and the electrochemical potentials of both the aqueous and the organic phase boundaries will be equal. Upon formulation of the electrochemical potentials for both phases in respect to the primary ion and rearrangement an expression for the phase boundary potential is established.[13]

$$E_{PB} = \Delta\Phi = -\frac{\mu^0(org) - \mu^0(aq)}{zF} + \frac{RT}{zF}\ln\frac{a_I(aq)}{a_I(org)} \qquad (1.5)$$

Here, φ is the electrical potential, μ° is the chemical potential under standard conditions, $a_I(org)$ is the activity of the primary ion I in the organic phase boundary, $a_I(aq)$ is the activity of the primary ion I in the aqueous phase boundary, z is the valency and R,T and F are the gas constant, temperature and Faraday constant, respectively. After inserting equation 1.4 into equation 1.5, and assuming that $a_I(org)$ is unaltered, the well-known Nernst equation is derived:[10]

$$E_M = E^0 + \frac{RT}{zF}\ln a_I(aq) \qquad (1.6)$$

In the above equation, all sample independent potential contributions are included in the constant E^o. The membrane potential and hence the cell potential will respond in a Nernstian manner giving a 59.2 mV increase in potential for every ten-fold increase in primary ion activity in the sample for monovalent cation selective electrodes (see Figure

1-2). Nernstian responses are dependent of course on maintaining a constant composition in the membrane bulk. Coextraction of ion pairs from the sample into the organic phase boundary will cause deviations from the expected Nernstian response by changing $a_I(org)$.[14,15]

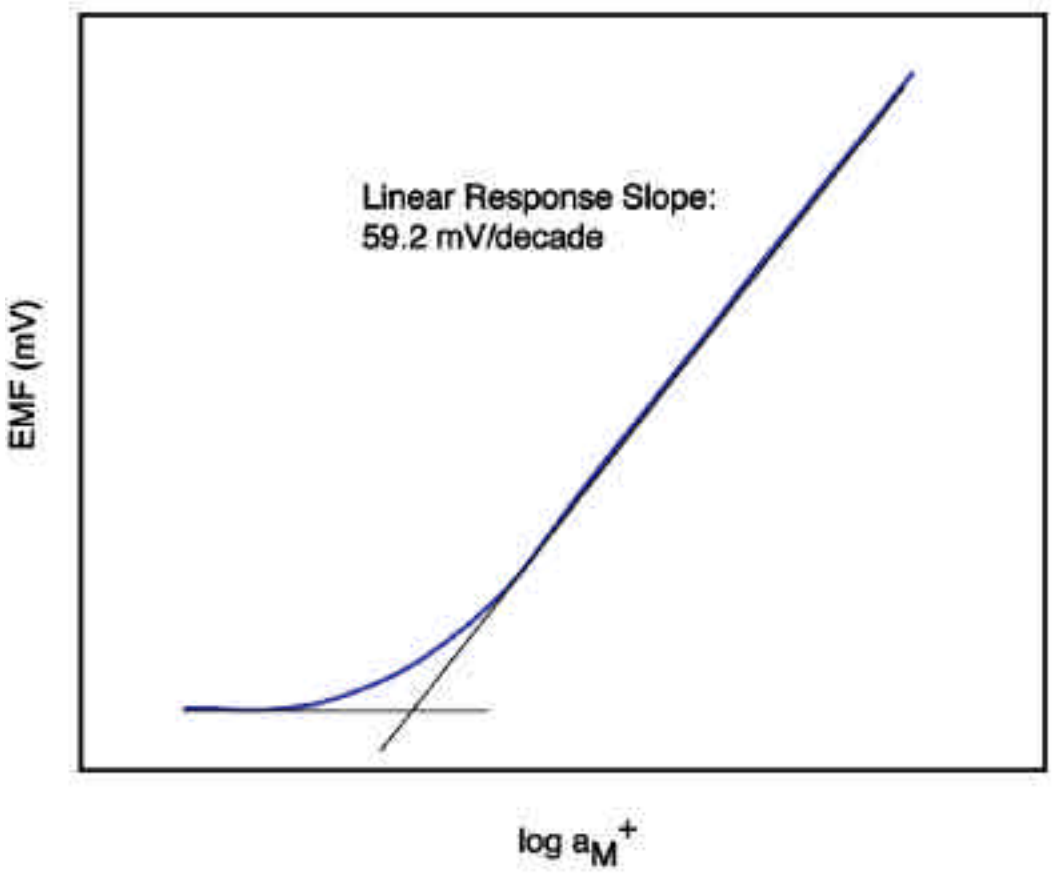

Fig. 1-2 A calibration curve for a cation selective electrode showing a Nernstian response to the changes in activity of the primary metal ion (M^+).

1.1.1 Membrane components:

Ionophores. In carrier-based ion-selective electrodes and optodes, the ionophore is responsible for the observed selectivity pattern, which corresponds to differences in the energy of hydration of the primary ion in the aqueous phase and the energy of complexation in the organic phase.[9] Naturally occurring ionophores like the potassium selective valinomycin and synthetic ones can transport ions in biological membranes as well as in synthetic polymer matrices like PVC.[16-18]

Ionophores are the target ion complexing ligands within carrier based ISE membranes. They can be either charged or uncharged depending on their uncomplexed form in the membrane phase. By selective complexation between the carrier (ionophore) and analyte, a target ion may be extracted into the membrane phase with specific stoichiometric ratios.[19-21] Ideally, the carrier should complex the target ion only, but not too tightly. This leads to the high selectivity of the electrode for a specific target ion over interfering ions.[22]

Some of the first ionophores used in ISEs were naturally occurring compounds like valinomycin and monactin.[16-18] Both showed good selectivity for the monovalent ion, potassium. Typically, cations are detected using neutral ionophores containing electron-donating atoms like nitrogen and oxygen (see Figure 1-3). After complexation with the analyte cation the ion-ionophore complex has a net positive charge that must be balanced in the membrane by a sufficient number of negatively charged lipophilic

counterions. Some of these cation-selective macromolecules include crown ethers[23-25] and calixarenes.[26,27]

For anionic analytes, the complexing carrier is usually an organometallic compound that allows for coordination with the negatively charged analyte that also must be balanced by a counterion within the membrane (see Figure 1-4). Some of the metalloporphyrins with various peripheral substituents have shown useful selectivities toward anions[28-33] through coordination with various central metal ions. Expanded porphyrins have also been used to detect anions by protonating the electron donor nitrogen atoms of the porphyrin ring.[34] To function as a viable ion-carrier in a solvent polymeric membrane electrode or optode, the ionophores must be sufficiently lipophilic both before and after complexing the target ion. One possibility to assure that the ionophore remains in the sensing matrix has been the covalent attachment of the carrier to the polymer backbone. [35]

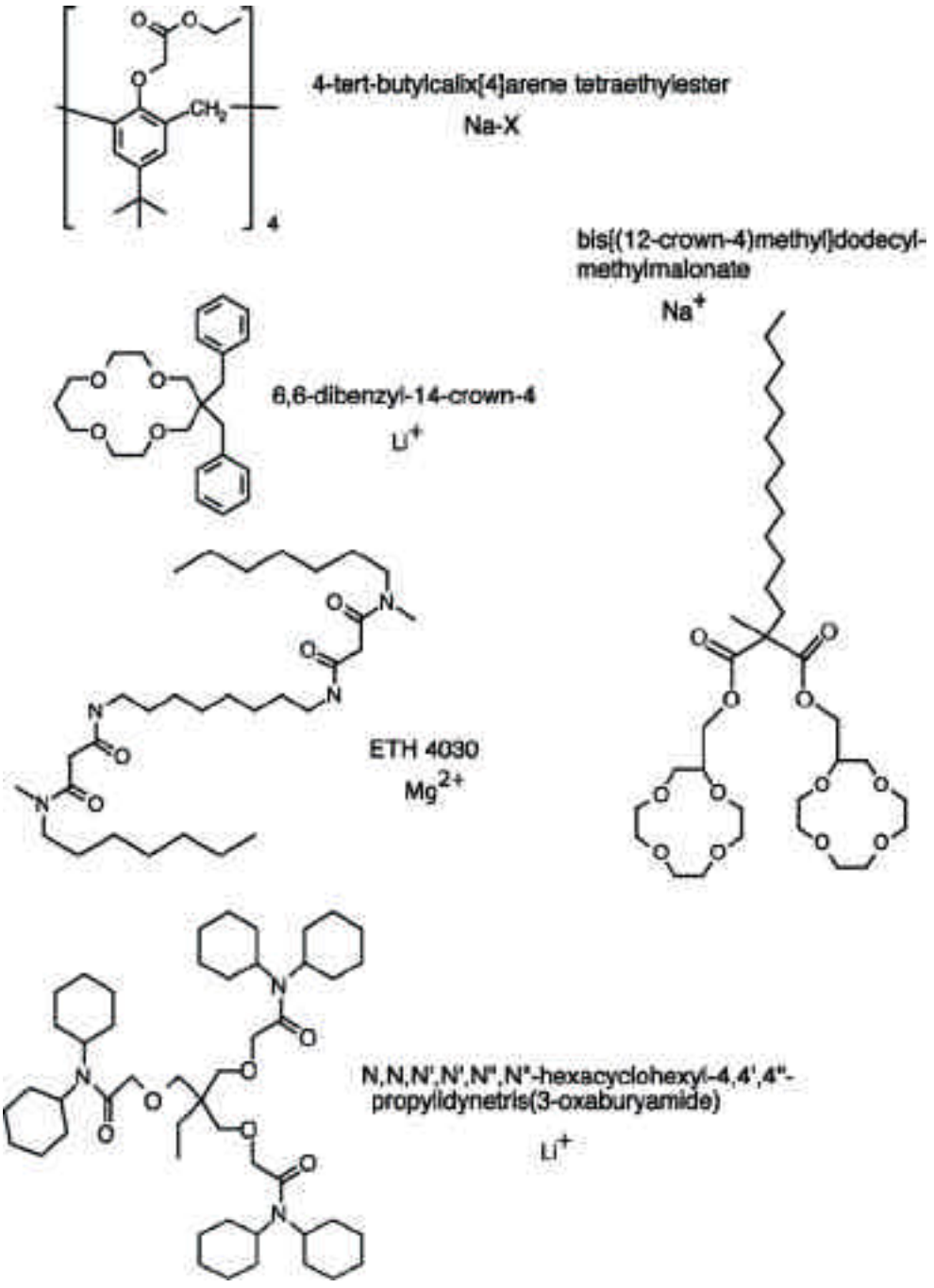

Fig. 1-3 Some ionophores used in cation sensing

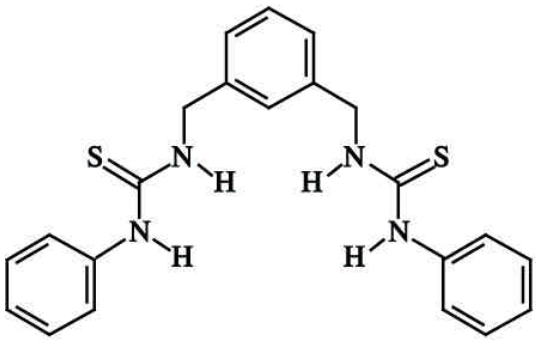

SO_4^{2-} -1

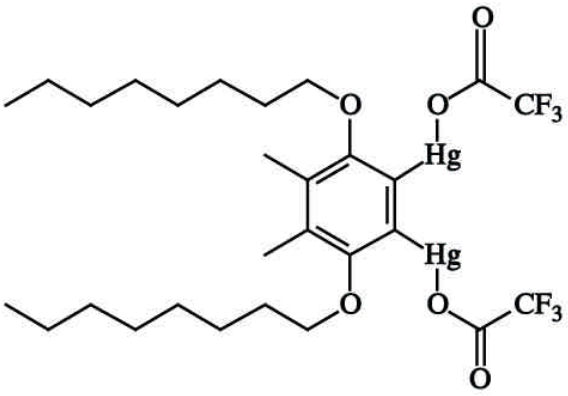

ETH 9009 (Cl^-)

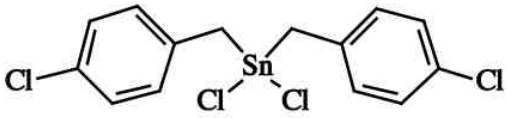

Phosphate-3

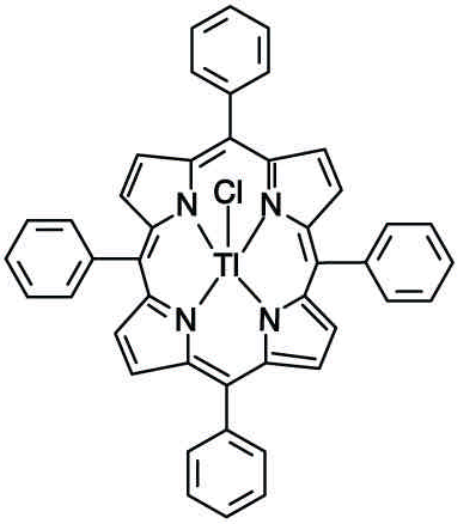

Tl (III) (TPP)Cl

Cl^-

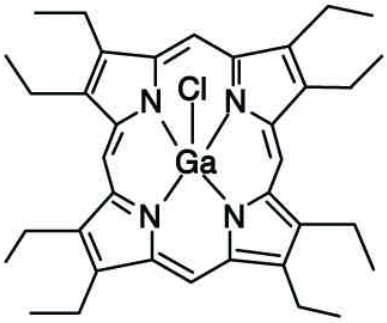

Ga (III) (OEP)Cl

F^-

Fig. 1-4 Some ionophore used in anion sensing.

Ionic sites. Ionic sites (ion exchangers) are salts containing lipophilic counterions to target sample ions and are dissolved within ISE membrane matrix. They are responsible for the permselectivity of the ISE, although it has been shown that impurities inherent in PVC manufacturing can also induce a potential response.[36,37] In neutral carrier-based ISEs, the ionic site selection in membrane preparation depends on the target ion being measured. Figure 1-5 shows two types of ion exchangers, an anionic site and a cationic site. Adding these compounds to the membrane composition also lowers the resistance of the membrane and may aid in the response of microelectrodes.[9]

For neutral carrier-based cation selective electrodes, a number of anionic sites should be added to the membrane matrix to ensure a Nernstian response and maintain selectivity.[38] The salt sodium tetra-phenyl borate (Na^+TPB^-) would be a good choice. The lipophilic anion TPB^- will remain mostly in the membrane phase while the more hydrophilic cation (Na^+) can exchange with sample target ions. The lipophilicity of the borate plays a role in the lifetime of the sensor, eventually leaching into the sample.[39] With added anionic sites in the membrane there will be less coextraction of sample anions preventing Donnan exclusion at high electrolyte concentrations and optimizes the Nernstian response range.[14,15]

For anion selective electrodes, a concentration of cationic sites in the membrane provides the same basic function. A salt containing a lipophilic cation like tri-dodecyl methyl ammonium ($TDMA^+$) and a more hydrophilic anion like chloride (Cl^-) which can exchange chloride ions with sample anions producing a Nernstian response. Again,

coextraction is limited due to the lipophilic cation that remains in the membrane. Anion selective membranes based on metalloporphyrins as ionophores exhibited non-Hoffmeister selectivity toward anions based on lipophilic cationic sites.[40] The Hoffmeister selectivity series measures the anions tendency to partition into a hydrophobic matrix based on differences in hydration and solvation energies.[41]

In the case of charged carrier-based ISEs, the ionophore aids in preventing Donnan exclusion in the same manner as the ionic sites in neutral carrier-based ISEs. Although ionic sites are not always needed to produce a Nernstian response, a small amount of lipophilic counterions is useful.[42] Ionic impurities in the membrane have been shown to act as ion-exchangers. In the case of monesin, an antibiotic, depending on the pH of the sample or the charge of the added ionic sites, the mechanism of complexation can be adjusted from a charged carrier-based ISE to a neutral carrier-based ISE.[43]

Ion exchangers are required in the ISE membrane to maintain permselectivity, which is the concept of selective complexation after ion transfer. These ion exchangers are usually lipophilic borate salts of alkaline metals or quaternary ammonium salts of chloride. With ion exchangers present, the membrane, in an attempt to maintain electroneutrality, can exchange hydrophilic membrane ions for sample ions in response to sample activity changes. This makes the coextraction of sample electrolyte into the membrane phase negligible if the ion exchanger (ionic site) concentration is sufficiently high and the target sample activity is not too large. Other compounds have been investigated as anionic additives. Dinonylnaphthalene-sulphonic acid (DNNS) and

Tetradodecyl-
ammonium
cation

$TDDA^+$

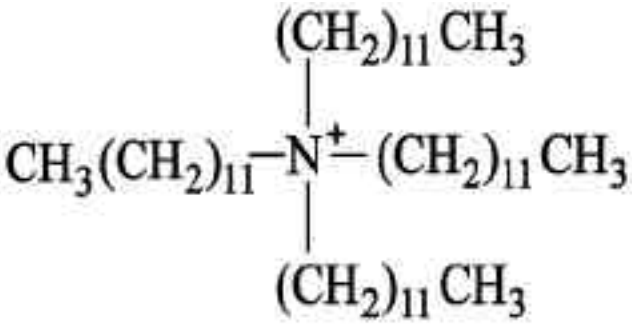

Tetrakis
(4-chlorophenyl) borate
anion

$TpClPB^-$

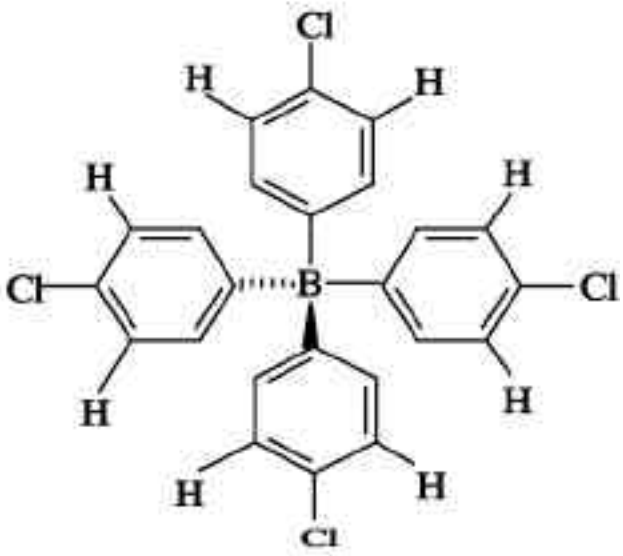

Fig. 1-5 Lipophilic ionic sites. The salt of these ions is known as ETH 500.

poly(2-acrylamido-2-methyl-1-propanesulphonic acid-co-styrene) were investigated and compared to traditional borate salts. The selectivity and detection limit were comparable, with one notable exception, an electrode based on the calcium selective ionophore ETH 1095 and DNNS as anionic site showed a preference for barium ions.[44]

Polymer matrix. The hydrophobicity of the polymer membrane is essential for permselectivity and sensor lifetime. The components of these ISE membranes may leach into the sample and into the inner filling solution. To prevent this from happening, covalent attachment of the sensing components has been proposed and implemented in certain cases.[35,45] Poly(vinyl chloride) is most widely used polymer support in potentiometric ISEs. The cost and mechanical properties make it most practical.[22]

In certain cases, PVC is not suitable as a support for the liquid-membrane ISE. This prompted researchers to find other supports for the sensing components of the ISEs. Other polymers including derivatized PVC, silicone rubbers, polyurethanes, polystyrene and methacrylates have all been used in ISEs.[9,22] All of the matrices must be compatible with the other sensor components for proper electrode response.

Plasticizer. To obtain proper function in ion transport, the membrane polymer support must have a glass transition temperature (T_g) that is less than room temperature.[46] For PVC-based membranes, this is accomplished by adding a plasticizer, typically, either nitrophenyl octyl ether (o-NPOE) or dioctyl sebacate (DOS) in a 1:2

weight ratio with the polymer support[47,48] (see Figure 1-6). At this ratio, the plasticized membrane is essentially a viscous liquid phase in which the plasticizer acts as the solvent for all membrane components.[22]

The difference in dielectric constants of the two plasticizers is believed to be the responsible for the difference in affinity for divalent ions in membranes whose composition is identical, with exception of the plasticizer. The membranes with the more polar plasticizer (NPOE) demonstrated a higher affinity for divalent ions.[9] Recently, methacrylic-acrylic copolymers have been used without added plasticizer in ISEs,[49] increasing sensor lifetime by decreasing the effects from leaching.

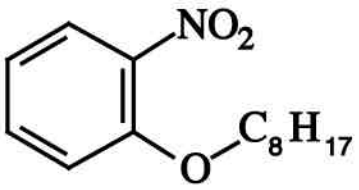

o-NPOE

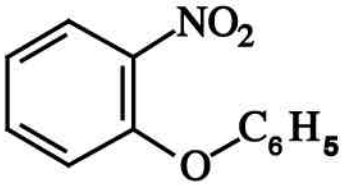

o-NPPE

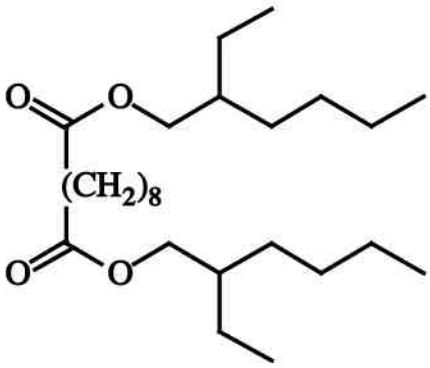

DOS

Fig. 1-6 Some common plasticizers.

1.1.2 Selectivity:

The ability to sense primary ion activities in samples containing interfering ions is a valuable measure of the ISE's utility as a sensor. From the Nernst equation for cation selective membranes (Eq. 1.6), the activity of the primary ion I in a solution without interfering ions, $a_I(I)$, is related to the measured potential. In a mixed sample containing more than one ion that will partition into the membrane and complex with the ion carrier (ionophore), the degree of preference for one ion over the other is defined by the selectivity coefficient. This characteristic can be quantified using the Nikolskii-Eisenman formalism:

$$E = E_I^0 + \frac{RT}{z_I F}\ln(a_I(IJ) + K_{IJ}^{pot} a_J(IJ)^{z_I/z_J}) \tag{1.7}$$

here, $a_I(IJ)$ is activity of primary ion I in the sample (IJ), $a_J(IJ)$ is the activity of interfering ion J in the sample and K_{IJ}^{pot} is the Nikolskii coefficient (selectivity coefficient). A more accurate expression was recently obtained that could account for different valencies of the primary and interfering ions.[50]

In the Nikolskii-Eisenman equation, the term for the primary ion potential contribution, $a_I(I)$, is replaced with a term relating the potentials created by the presence of more than one contributor. The selectivity coefficient, K_{IJ}^{pot}, can be related to the activity of ion I in a sample without interference, $a_I(I)$, and the activity of ion I in a mixed

sample, $a_I(IJ)$, if the measured potentials are identical for both solutions then the following equation should hold:

$$a_I(I) = a_I(IJ) + K_{IJ}^{pot} a_J(IJ)^{z_I/z_J} \quad (1.8)$$

Small values for K_{IJ}^{pot} indicate a greater amount of discrimination for ion I over ion J. Without compensation for interference from secondary ions on membrane potentials, the potential predicted by the Nernst equation for a specific primary ion activity in a sample will differ from the potential measured in a mixed sample. In the case where interference is small and/or the selectivity coefficient is extremely small (greater discrimination), a given activity of the primary ion I will produce identical membrane potentials in both a pure sample and in a mixed solution. However, as the interference of the secondary ion J is increased the required activity of I in the sample to produce the same potential as above is decreased due to the sum of both of the contributions to the potential.[12] Tabulated values of selectivity coefficients can be misleading if notice is not taken to the method used to obtain them.

In the separate solutions method (SSM) of selectivity coefficient determinations, the potential of individual aqueous solutions containing only the salt of the desired ion are determined.[51] If the potentials of the individual salt solutions are identical, substituting $a_I(IJ) = 0$ and $a_J(IJ) = a_J(J)$, the following relation is obtained to describe the selectivity coefficient in respect to ion activities:[12]

$$K_{IJ}^{pot} = \frac{a_I(I)}{a_J(J)^{z_I/z_J}} \tag{1.9}$$

Further substitution of the Nernst relations for the activities of both the primary and the interfering ions provides a means to calculate the selectivity coefficient based on the measured potentials of individual aqueous solutions. After substitution, we obtain:

$$K_{IJ}^{pot} = \exp\left[\left(E_J^0 - E_I^0\right)\frac{z_J F}{RT}\right] \tag{1.10}$$

where, $E°_J$ and $E°_I$ are the sums of the sample independent potentials for the measured electrode in each solution (see Figure 1-7). The selectivity coefficient determined by the SSM is expected to remain constant in a particular electrode if a Nernstian responses for the ions compared are observed in the activity range in which the measured potentials are recorded.[9] In a membrane conditioned in a solution of the primary ion prior to measurement, biased selectivity coefficients may be obtained. When the electrode is placed in a solution of interfering ions only, the preference for primary ions already present in the membrane prevents the interfering ions from fully displacing them from the membrane phase boundary. To avoid this, experimentally, the order in which the separate solutions are examined should follow from the least preferred ion to the most preferred ion and the membrane should be conditioned in solution of an interfering ion instead of the primary ion.[52]

The second method to determine accurate selectivity coefficients is the fixed interference method (FIM). In contrast to the SSM, the FIM more closely resembles the

target sample solution as the selectivity coefficients are extracted from mixed samples.[53] In the FIM, a calibration curve is generated from the measured membrane potential versus the activity of the primary ion, $a_I(IJ)$, in a background of a constant interfering ion activity, $a_J(IJ)$. Using the calibration curve, the low detection limit for the primary ion is calculated from extrapolation of the linear portions of curve, as seen in Figure 1-8. This provides a relation for selectivity coefficient, K_{IJ}^{pot}, where $a_I(DL)$ is the activity of ion I at the low detection limit, expressed as:

$$a_I(DL) = K_{IJ}^{pot} a_J^{z_I/z_J} \tag{1.11}$$

This is the basis for selectivity coefficient calculations using the FIM. As with the SSM, a Nernstian response is required for both the interfering and primary ions.[53]

The matched potential method (MPM) is also used to determine K_{IJ}^{pot}. It is an empirical method that begins by adding a specific amount of the primary ion to a reference solution and measuring the membrane potential. Next, an interfering ion is added to an identical reference solution until the potential is matched to the one recorded for the addition of primary ion.[54] The selectivity coefficient obtained with the matched potential method is denoted with a lower case to distinguish it from the Nikolskii coefficient, with the major difference being that it is not constant for a particular electrode (shown in Figure 1-9). It is defined as the ratio of the change in activities of the primary and interfering ions represented as:

$$k_{IJ}^{MPM} = \frac{\Delta a_I}{\Delta a_J} \tag{1.12}$$

The requirement of the other two methods, SSM and FIM, that the electrode responds in a Nernstian manner to both the primary and the interfering ions in the activity range used to obtain the selectivity coefficients does not exist in the matched potential method.[53] The experiments used to obtain these values are intuitive, however, the results can vary widely depending on experimental conditions.

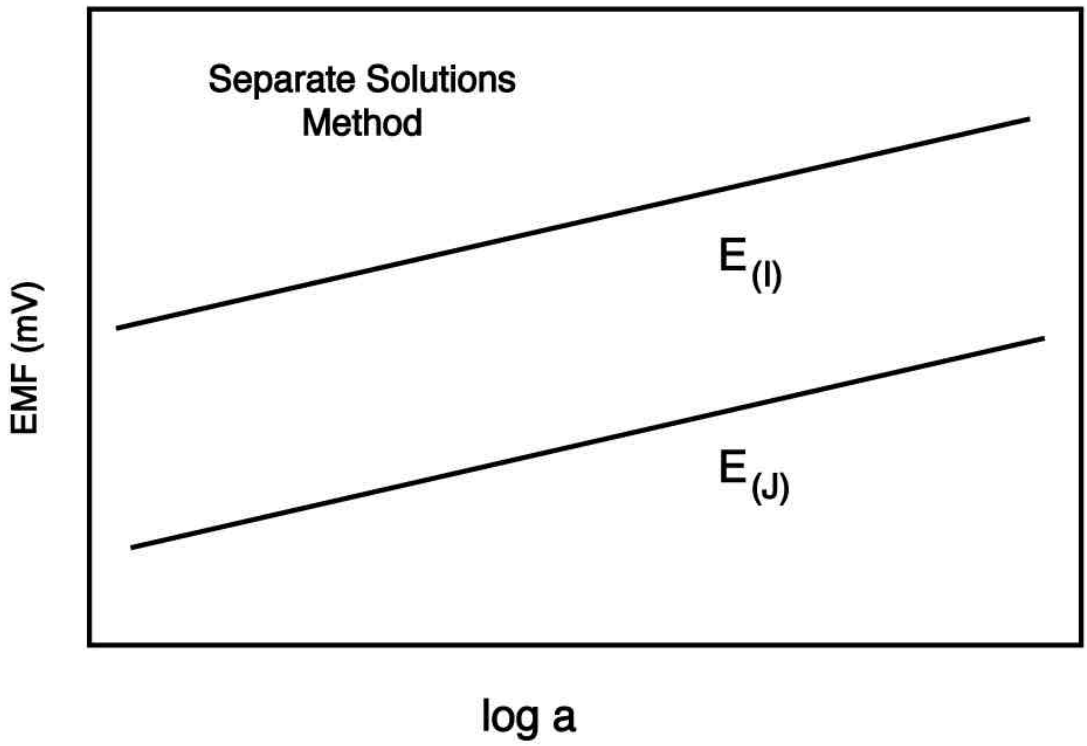

Fig. 1-7 The separate solutions method for selectivity coefficient calculations. Two separate calibration response curves of a cation selective solvent polymeric membrane are shown for both the primary ion (I) and the interfering ion (J). The electrode must respond in a Nernstian manner for both ions to obtain meaningful selectivity coefficients.

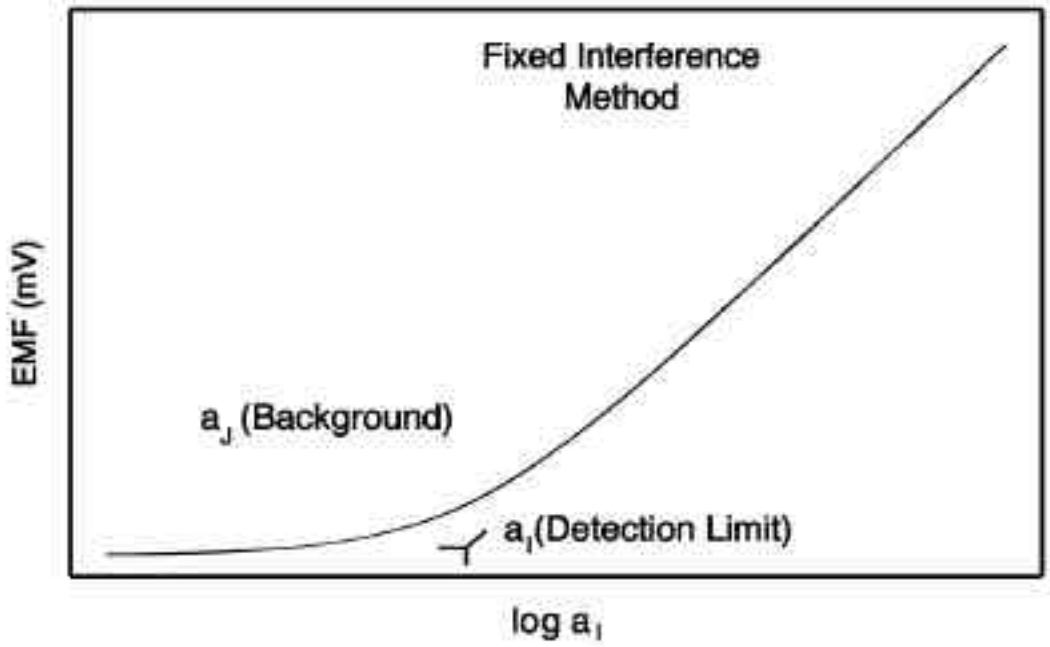

Fig. 1-8 This illustrates the fixed interference method of selectivity coefficient calculations. The lower detection limit from a calibration curve of the primary ion (I) in a mixed solution containing a constant concentration of interfering ion (J) is used for this determination.

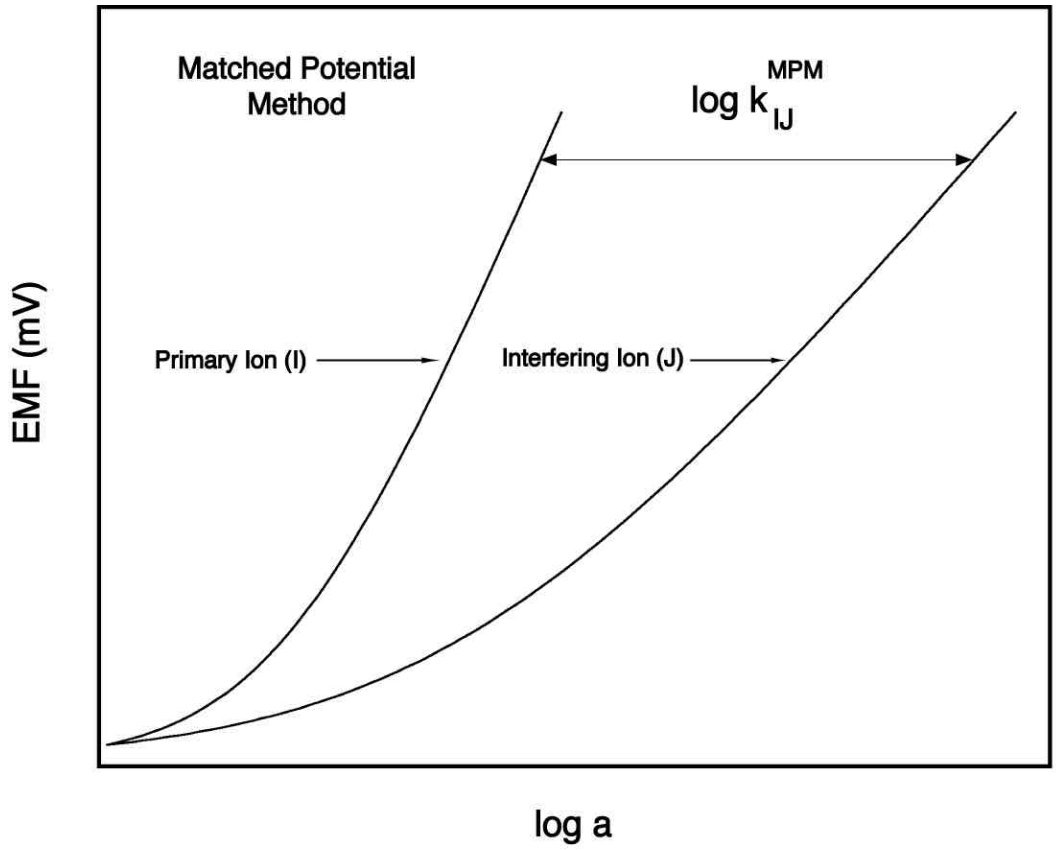

Fig. 1-9 This illustrates the matched potential method for selectivity coefficient calculations. In this method, the difference in the activities of separate solutions containing only the ion of interest that produce identical potentials is used to assess the selectivity coefficient.

Several methods have been introduced to ascertain accurate selectivity coefficients. Values obtained using these methods weigh heavily on the experimental conditions and sequence. Traditionally, a cation selective membrane was conditioned in an aqueous solution with a high concentration of the primary ion salt, which aids in providing stable and reproducible potentials. The membrane prefers the primary ion and discriminates in the interfacial exchange equilibrium against interfering ions. By conditioning in primary ion solutions, the preferred ion is embedded in the membrane phase boundary and it is not likely to be displaced fully by a discriminated ion when placed in a solution containing interfering ions only. It was proposed that the conditioning of the electrode be conducted in interfering ion solutions to prevent this. To obtain accurate measurements, the order in which the electrode membrane is exposed to ions in selectivity experiments is important. The least preferred ion should be interrogated first followed by the next preferred ion and so on, with the primary ion potential measured last.[52] Indeed, it was shown that Nernstian slopes could be obtained for interfering ions for several ISEs if the above conditions and sequence were used.

1.1.3 Detection limit:

Improving detection limits in ion selective electrodes is important in both theoretical and practical terms. The detection limit, according to IUPAC convention, is obtained from extrapolation of the linear portions of the Nernstian calibration curve. As

seen in Figure 1-10, the lower detection limit (LDL) is found at the point of intersection of the two linear segments.[55] At activities where the membrane phase boundary potential no longer responds in a Nernstian manner to activity changes, there exists an upper and a lower detection limit. The lower detection limit is dictated by the release of primary ions from the organic phase boundary into the aqueous phase boundary and competition from interfering ions. Leaching of primary ions from the membrane into the sample has been noted. It raises the local phase boundary activity of the primary ion above the activity found in the sample rendering the electrode non-responsive to sample activity changes.[56] Covalent attachment and copolymerization of a lead selective ionophore to a polyurethane supported liquid membrane reduced ion fluxes from the IFS giving a lower detection limit of 10^{-9} M Pb^{2+}.[57] It is now routine to reach micro-molar detection limits for most ISE systems and even lower limits have been reached in buffered systems,[55] where a primary ion-complexing ligand is placed in the sample (Ca^{2+} selective system). This has the effect of buffering the primary ion activity at the sample interface by complexing ions continuously released from the membrane through interfacial exchange. Buffering in the inner filling solution in an attempt to minimize transmembrane ion fluxes has also lowered the detection limit in the case of a Pb^{2+} selective electrode. The inner-filling solution was buffered with an ethylenediaminetetraacetic acid disodium salt (EDTA) and a millimolar amount of lead.[58] The resulting detection limit was lowered by nearly six orders of magnitude. Sample stirring effectively concentrates

sample ions in the aqueous phase boundary lowering the limit of Nernstian electrode response.

The upper detection limit (UDL) is also marked by a failure in the Nernstian response of the electrode. It is also determined by extrapolation of the linear segments of the calibration curve, as seen in Figure 1-10. At some point in the calibration curve, further addition of primary ions to the sample does not induce a potential change. Coextraction of sample cations with counterions into the membrane phase boundary is the cause for the deviation from Nernstian behavior.[9] At the upper detection limit, the available ionophore concentration in the phase boundary exists almost completely as an ion/ionophore complex. This complex acts as an ion-exchanger (ionic site) in the membrane changing the response of the electrode from a cation to an anion Nernstian response, reversing the sign of the slope of the potential change with increasing primary ion activity.[59]

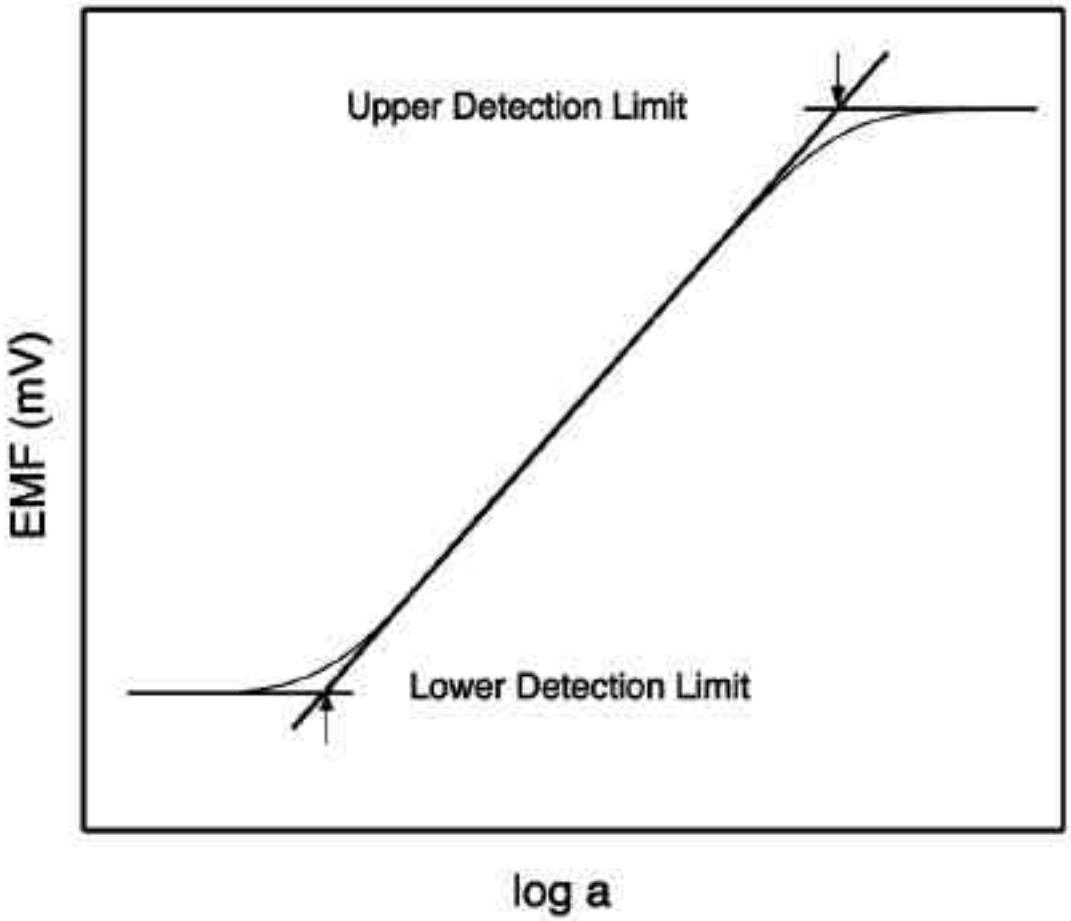

Fig. 1-10 Both the upper and lower detection limits for an ion selective electrode are obtained at the intersection of the extrapolated linear segments of the calibration response curve.

1.1.4 Segmented Sandwich membrane technique:

Investigation and characterization of membrane parameters that dictate the electrode response is essential for development of better sensors. One such parameter is the ionophore complex formation constant (stability constant). With accurate values for the complex formation constant of the ionophore and the other membrane components of ion selective electrodes, predictions can be made to enhance sensitivity, selectivity and lifetime of the sensor membrane.[9] Stability constants of ionophores have been determined in several solvents such as water, methanol and mixtures of polar solvents. Partitioning constants were also determined for electrolytes in similar solvents. Voltammetric analysis has also yielded values at the interface between two immiscible electrolyte solutions (ITIES)[60] and in solvent polymeric membranes.[61] Recently, a new method has been proposed and shown to give stability constants based on measured potentials. It has been dubbed the segmented sandwich membrane technique.[62]

In this method, two ISE membranes are prepared with identical compositions, differing only with the presence of an ionophore in one. Both membranes are conditioned to assure a constant primary ion distribution throughout both membrane bulks. The membranes are sandwiched together and placed in a potentiometric electrode setup with identical sample and inner filling solutions (shown in Figure 1-11). A single membrane electrode, with or without ionophore, placed in a similar electrochemical cell should induce a zero potential reading due to the symmetry of the cell and the homogeneity of

the membrane.[62] Non-zero potentials that develop in a symmetric cell across the sandwich membrane are a result of the presence of an ionophore in only one of the membrane segments. The presence of the ionophore creates an asymmetry in the continuum of primary ion distributions across both segments. The ionophore, in one segment, complexes the primary ion effectively lowering its free ion concentration in this segment and inducing a potential created by an ion gradient across the combined membranes.[9]

The previously mentioned phase boundary potential model is used to interrogate and explain the relevance of the sandwich membrane technique, dividing the membrane potential, E_M, into the two aqueous-membrane phase boundaries potentials and the internal diffusion potential. The internal diffusion potential is usually neglected[12] leaving the following expression for the membrane potential:

$$E_M = \frac{RT}{z_I F} \ln \frac{a_I(aq)}{a_I(org)} \frac{a_I(org)^{\cdot}}{a_I(aq)^{\cdot}} \qquad (1.13)$$

here, R, T and F have their usual meanings. The single dot (•) distinguishes the membrane -inner filling solution interface from the sample-membrane interface with the primary ion activities (a_I) represented in there respective phases. If the inner filling solution and the sample solution contain the same primary ion activity, then Equation 1-13 simplifies to:

$$E_M = \frac{RT}{z_I F} \ln \frac{a_I(org)^{\cdot}}{a_I(org)} \qquad (1.14)$$

To maintain electroneutrality, the concentration of free primary ion in the membrane segment, devoid of ionophore, must be equal to the concentration of added ionic sites, disregarding inherent ionic impurities.[62] This provides a relation between the activity of the primary ion in the membrane and the concentration of ionic sites also present in the membrane. This can be expressed as:

$$a_I = \frac{\gamma_I R_T}{z_I} \tag{1.15}$$

where R_T is the ionic site concentration and γ_I is the activity coefficient of ion I.

In the segment of the sandwich membrane with ionophore (L) and ionic sites (R), the primary ion activity is lower due to strong complexation with the ionophore. The degree of complexation between ion and ionophore is represented by the complex formation constant:

$$\beta_{IL_n} = \frac{a_{IL_n}}{a_I c_L^n} \tag{1.16}$$

where β_{IL_n} is the complex formation constant, a_{ILn} is the activity of the ion-ionophore complex, c_L^n is the concentration of uncomplexed ionophore in the membrane and n is the stoichiometry of the complex. The concentration of free ionophore in the membrane is related to the total amount of added ionophore (L_T) and upon substitution of the mass balance and charge balance equations from the membrane composition an expression for the primary ion activity is reached:[9]

$$a_I = \frac{\gamma_{IL_n} R_T}{z_I \beta_{IL_n} (L_T - nR_T / z_I)^n} \tag{1.17}$$

assuming the concentration of free ion in the membrane is much smaller than the concentration of the ion-ionophore complex.

An equation describing the relationship between the measured sandwich membrane potential, the complex formation constant of the ionophore, the total ionophore concentration and the concentration of ionic sites is formulated by inserting Equation 1.15 and Equation 1.17 into Equation 1.14:

$$E_M = \frac{RT}{z_I F} \ln \beta_{IL_n} \left(L_T - \frac{nR_T}{z_I} \right)^n \tag{1.18}$$

This equation was developed around several assumptions, the diffusion potential is negligible, the entire sandwich membrane is at equilibrium and negligible ion pairing exists between the ion-ionophore complex and the ionic sites.[62]

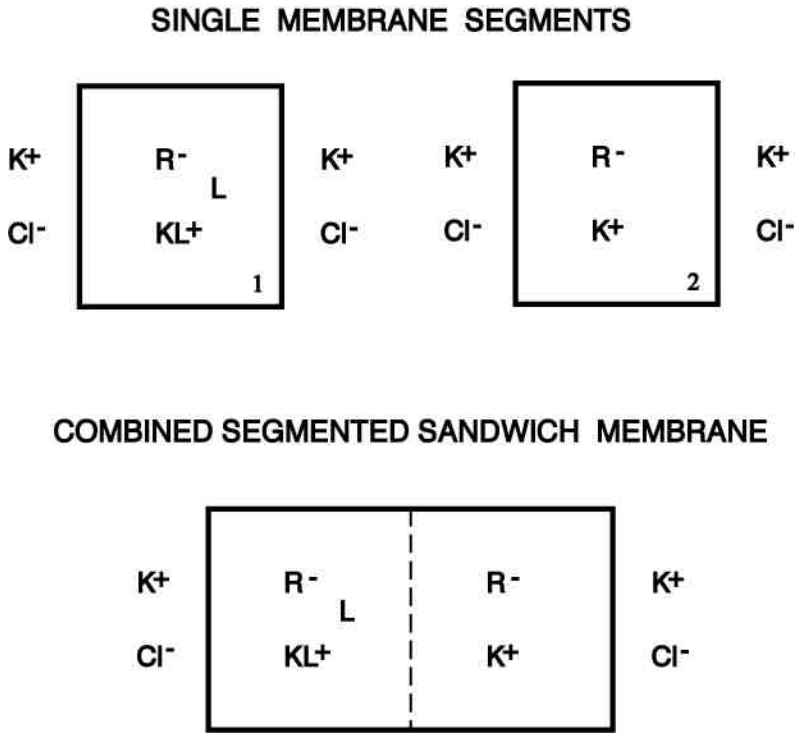

Fig. 1-11 Schematic of the preparation of a single, polarized membrane from two individual membranes. Membrane 1 contains anionic sites (R^-), ionophore (L) and has been conditioned in a chloride salt solution of the primary ion (K^+). Membrane 2 is identical, but does not include any ionophore (L).

If ion pairing is considered, two ion pair formation constants must be considered. The first, K_{IR}, relates the free ion activity in the membrane to the concentration of the ion pair complex between the anionic site and the primary ion. The second, K_{IL_nR}, relates the charged ion-ionophore complex to the concentration of the ion-ionophore-ionic site complex created by ion pairing.[62] Upon substitution, another relation is derived:

$$E_M = \frac{RT}{F} \ln \sqrt{\frac{K_{IL_nR}}{K_{IR}}} \beta_{IL_n} \left(L_T - nR_T\right)^n \tag{1.19}$$

which can be rearranged to solve for the complex formation constant as follows:

$$\beta_{IL_n} = \left(L_T - nR_T\right)^{-n} \sqrt{\frac{K_{IL_nR}}{K_{IR}}} \exp\left(\frac{E_M F}{RT}\right) \tag{1.20}$$

Again, the assumption that very little extracted primary ion exists in the membrane uncomplexed to an ionophore. Determining ionophore complex formation constants based on a measured potential and precisely known membrane quantities makes this method a useful tool to obtain ionophore complex formation constants and in the design of ISE membrane compositions. Recently, many ionophores have been examined using this technique to estimate the complex formation constant.[62,59]

1.2 Optical sensors:

Ion-selective optodes based on the same components found in potentiometric ion-selective electrodes and in hydrophilic matrices like hydrogels, have been described. Polymer optodes and films take advantage of a competitive exchange equilibrium between the two embedded ionophores, one selective for a metal ion (M^+) and the other selective for protons (H^+). In order to maintain electroneutrality, extraction of the metal ion into the membrane and complexation with the ionophore is coupled to the decomplexation of the proton and expulsion from the membrane. The sensing scheme uses the chromogenic properties of some H^+ ionophores (chromoionophores shown in Figure 1-12), namely a change in absorbance or fluorescence upon complexation.

These optodes have been termed bulk optodes due to the optical response's dependence on membrane bulk changes in the concentration of the protonated form of the chromoionophore. Several sensing schemes can be envisioned depending on the charges of the unprotonated chromoionophore and the uncomplexed metal selective ionophore. The equilibria for cation and anion selective bulk optodes are represented in Figure 1-13. For a bulk optode containing a neutral chromoionophore and a neutral ionophore selective for a primary cation (I^+), anionic sites are required to establish ion exchange in either a thin polymer film[63,64] or more recently in PVC-based microspheres.[65,66] The ion exchange

ETH 7075

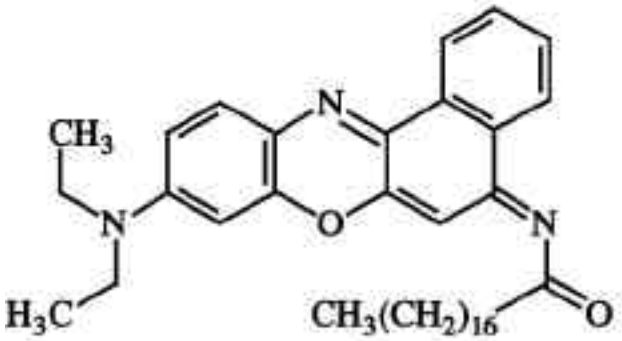

ETH 5294

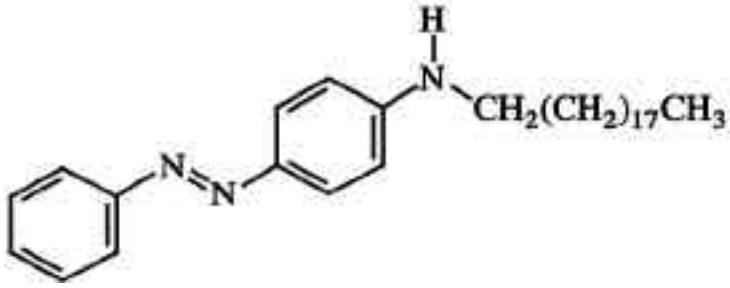

ETH 5315

Fig. 1-12 Chromoionophores used in proton (H^+) sensing.

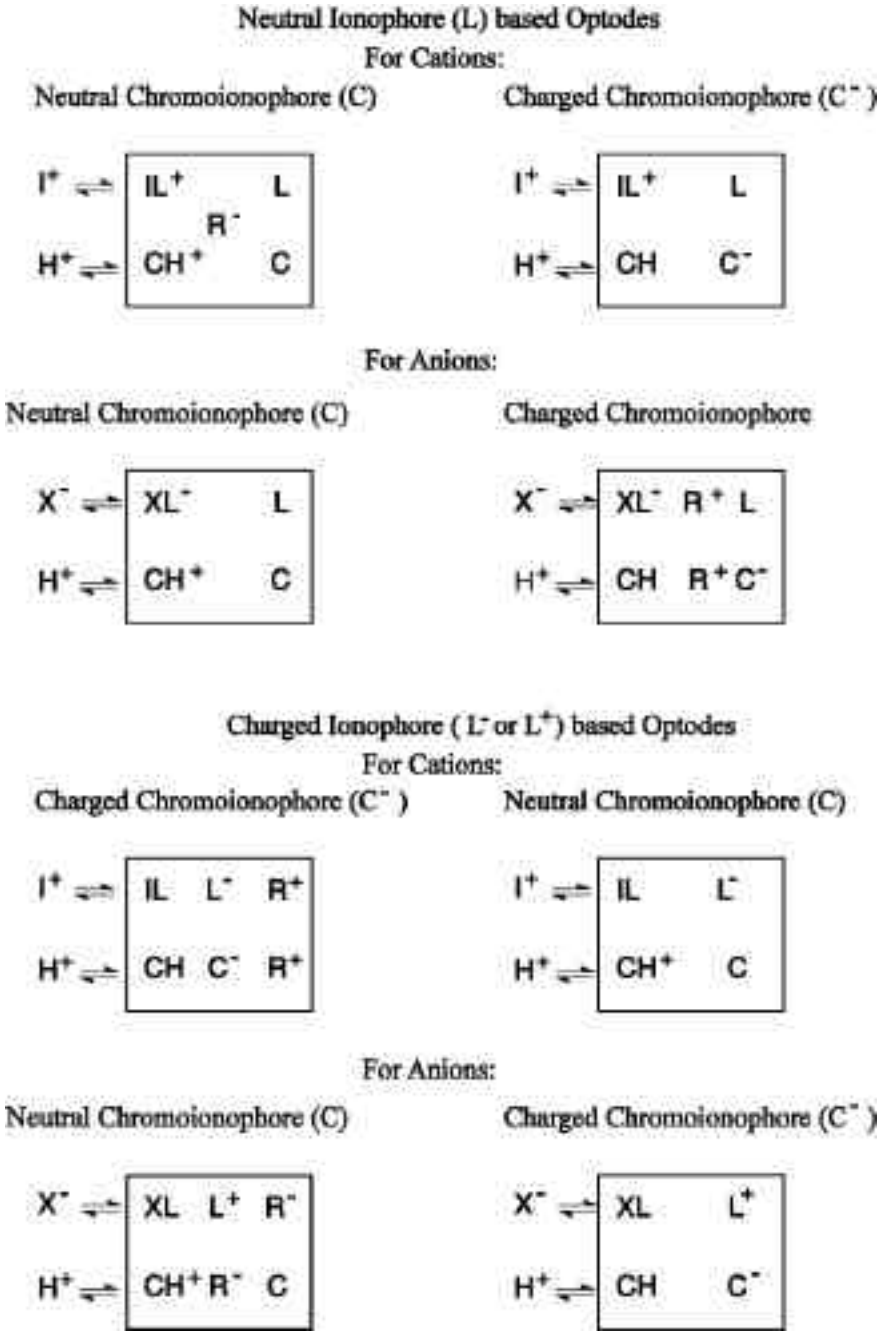

Fig. 1-13 Schematic of the various ion-exchange mechanisms for optodes.

equilibrium established in this system between the sample and bulk membrane is represented as:

$$I^{z+}(aq) + nL\,(org) + zCH^{+} \leftrightarrow IL_n^{z+}(org) + zC\,(org) + zH^{+}(aq) \qquad (1.21)$$

where *n* is the stoichiometry of the complex between the primary ion I and the ionophore L, *z* is the charge of the primary ion and C is the chromoionophore. In absorbance mode, the normalized absorbance (α) can be related to the absorbance of the fully protonated chromoionophore (A_P) and the absorbance of the fully deprotonated chromoionophore (A_D) with the observed absorbance (A) measured in a particular equilibrium, represented as:

$$\alpha = \frac{A_P - A}{A_P - A_D} \qquad (1.22)$$

α is the relative portion of the of the unprotonated chromoionophore.

From the ion-exchange equilibrium, a relation for the exchange constant $K_{exch}^{IL_n}$ is formulated:

$$K_{exch}^{IL_n} = \left(\frac{a_H[C]}{[CH^+]}\right)^z \frac{[IL_n^{z+}]}{a_I[L]^n} = \left(\frac{K_a}{k_H}\right)^z k_I \beta_{IL_n} \qquad (1.23)$$

It is a function of the stability constant for the ion-ionophore complex (β_{IL_n}), the dissociation constant for the chromoionophore (K_a) and the relative lipophilicities of the proton and the primary ion (k_H and k_I, respectively). Substituting the charge balance for

the anionic sites and the mass balance equations for the ionophore and chromoionophore, an optode response function is derived assuming the optode is in equilibrium with the sample and that the concentrations within the bulk are proportional to the activities, shown as:

$$a_I = \left(zK_{exch}^{IL_n}\right)^{-1}\left(\frac{\alpha}{1-\alpha}a_H\right)^{z}\left(\frac{R_T^- - (1-\alpha)C_T}{L_T - \left(R_T^- - (1-\alpha)C_T\right)\left(\frac{z}{n}\right)}\right)^{n} \qquad (1.24)$$

where C_T is the total chromoionophore concentration in the film or microsphere. The response curve is sigmoidal and seen in Figure 1-14 as a plot of 1-α versus the log of the primary ion activity. This curve can be shifted to access different measuring ranges of the primary ion by changing the film components to those with different acidity constants for the chromoionophore and different stability constants for the ionophore. Buffering the sample pH is essential in obtaining reliable responses. A constant proton activity in the sample ensures a proper ratiometric response in the film. Figure 1-15 shows the effect of pK_A changes of the chromoionophore on the position of the curve and the measuring range. A similar methodology was applied to bulk optodes used in fluorescence mode.

Optodes based on ion-selective sensing schemes suffer from interference in mixed samples, which must be taken into account when describing their response. In analogy to ion-selective electrodes, the selectivity of the film in discriminating between primary and interfering ions is essential for the realization of a mixed sample response. Introducing a second equilibrium exchange constant ($K_{exch}^{JL_{nJ}}$) for the interfering ion J and a complex

formation constant (β_{JL_n}) for the interfering ion-ionophore complex, an equation for the optical selectivity coefficient is derived as

$$K_{IJ}^{opt} = \frac{\left\{ z_J K_{exch}^{JL_{nJ}} \left(L_T - \frac{n_J}{z_J}\{R_T - (1-\alpha)C_T\} \right)^{n_J} \right\}^{\frac{z_I}{z_J}}}{z_I K_{exch}^{JL_{nI}} \left(L_T - \frac{n_I}{z_I}\{R_T - (1-\alpha)C_T\} \right)^{n_I}} \{R_T - (1-\alpha)C_T\}^{1-\frac{z_I}{z_J}} \quad (1.25)$$

The selectivity coefficient is determined for optodes using the SSM in which separate calibration curves are made containing the salt of only one cation. The horizontal distance between curves obtained in solutions with identical pH is required to calculate meaningful selectivity coefficient values. The effect on the sigmoidal shape of the calibration curve when interfering ions contribute to the optical signal is shown in Figures 1-14 and 1-15.

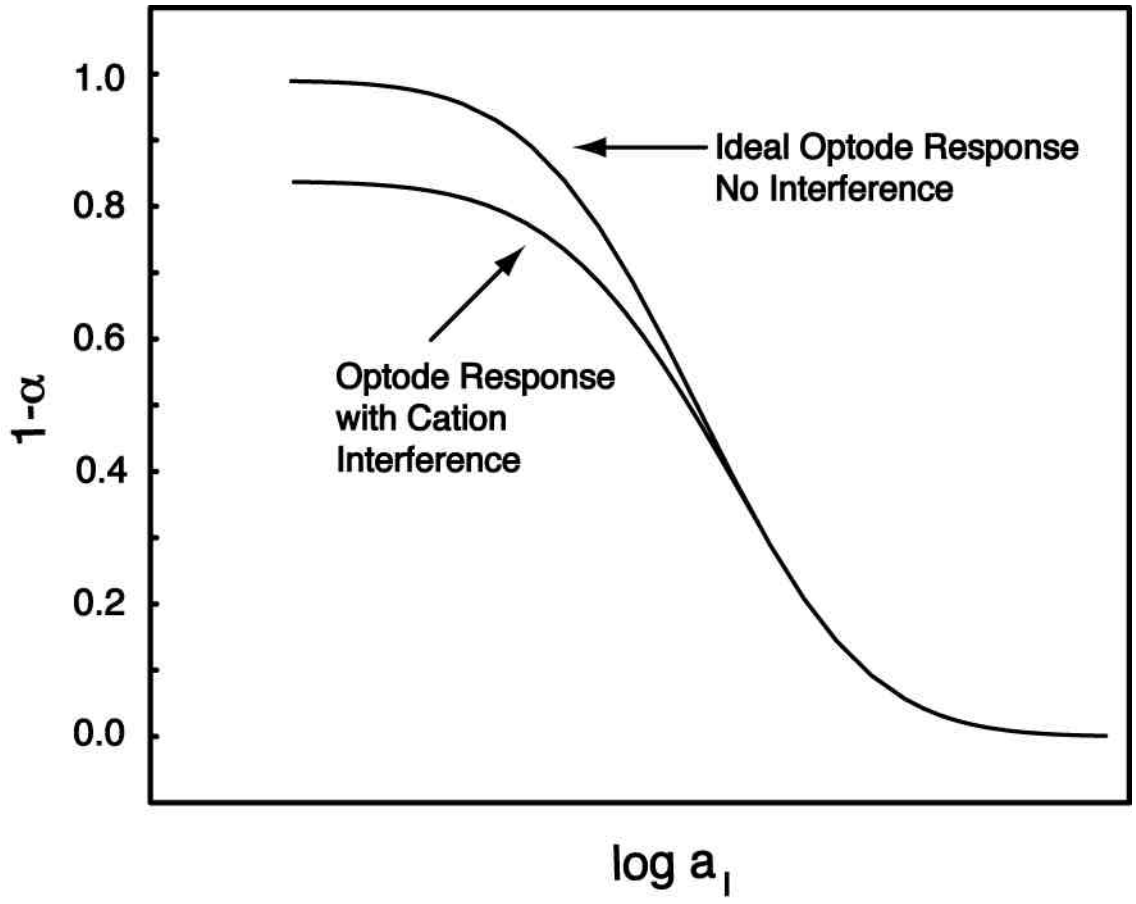

Fig. 1-14 Normalized optode response to changes in the primary ion activity in a pure sample and in a mixed sample containing interfering ions.

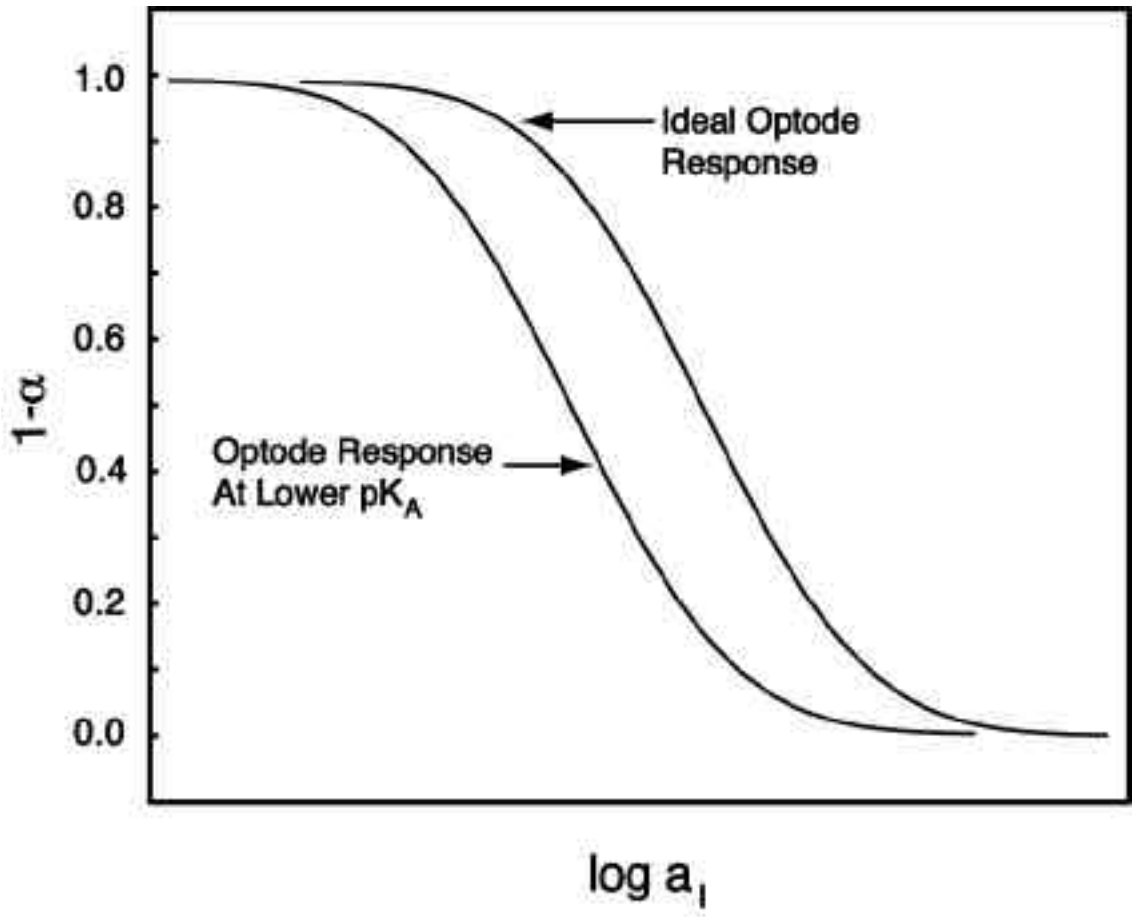

Fig. 1-15 Normalized optode response to changes in the primary ion activity in an ideally pH buffered sample and in an identical sample but with a chromoionophore with a lower pK_A.

1.3 Voltammetry

Metal-Liquid Interface. In contrast to zero current potentiometry and the competitive exchange equilibrium of optodes, voltammetry has the added dimension of an applied potential that leads to a current measured across the electrochemical cell. For typical solvent polymeric ion-selective electrodes, normal pulsed voltammetry (NPV) was chosen to interrogate the current-potential responses dictated by the applied potential and membrane components. This method requires a different electrochemical cell configuration than potentiometry with the addition of a third electrode (the counter electrode) immersed in the sample with the working and reference electrodes as seen in Figure 1-16.

Electrolysis at a metal working electrode is perhaps the best starting point for extension of voltammetric techniques to ISEs. For this purpose, the sample solution is made sufficiently conducting to provide a low enough solution resistance for current to easily flow through the cell in response to changes in the applied potential. The three-electrode setup ideally measures the current that flows between the counter and working electrodes and is dependent on the applied potential difference that develops between the reference electrode and the working electrode. A computer, that is connected to a potentiostat and records the resulting current, also controls the applied potential. The current considered in this microelectrode example occurs as a result of electron transfer

from the electrode surface to a sample species. The following half-reaction for this reversible process is represented as

$$A + ne^- \leftrightarrow P \tag{1.26}$$

Diffusion is defined, here, by the rate of transport of species *A* to the electrode surface. This species is subsequently reduced to form species *P* and is transported away from the electrode surface.[8] This process gives rise to concentration gradients in a small area immediately adjacent to the electrode surface known as the Nernst diffusion layer. Beyond this region, the bulk concentrations of *A* and *P* remain constant over the time scale of the experiment.

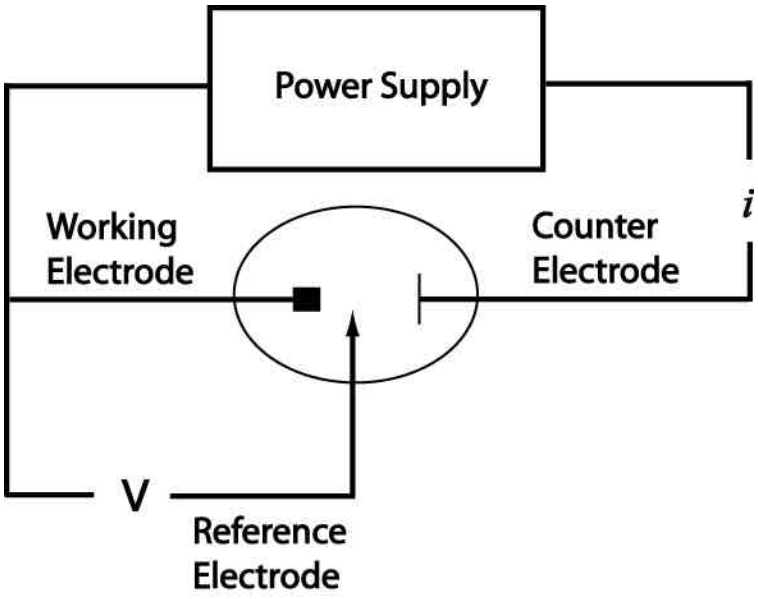

Fig. 1-16 Schematic of a three-electrode setup with notation for the different electrodes.

If we assume that the electrode reaction is rapid and reversible, then the concentrations of *A* and *P* can be described at any instant by the Nernst equation:

$$E_{appl} = E_A^0 - \frac{0.0592}{n} \log \frac{c_P^0}{c_A^0} - E_{ref} \quad (1.27)$$

where $c_P°$ and $c_A°$ are the molar concentrations of *P* and *A* at the surface of the electrode and E_{appl} is the applied potential between the working electrode and reference electrode. In NPV, the potential is stepped from zero to a non-zero value and the concentrations of *A* and *P* are adjusted to satisfy the Nernst relation. The potential step and current response are illustrated in Figure 1-17A and 1-17B. In Figure 1-17B, the initial current response to the potential step gives rise to the greatest current as essentially all of the available concentration of *A* at the electrode surface is converted into *P*. Figure 1-18 shows the concentration profiles of *A* as a function of time (*t*) and distance from the electrode (*x*). After this initial surge, the current quickly decreases with increasing time due to depletion of *A* at the electrode surface. In a system in which solution convection (stirring) is not involved, the mass transport of species *A* to the electrode surface is limited by its diffusion and after the initial potential step, in which the all of the available *A* at the surface is converted to *P*, the distance that species *A* must travel to reach the electrode is increased. Consequently, there is a drop in current.

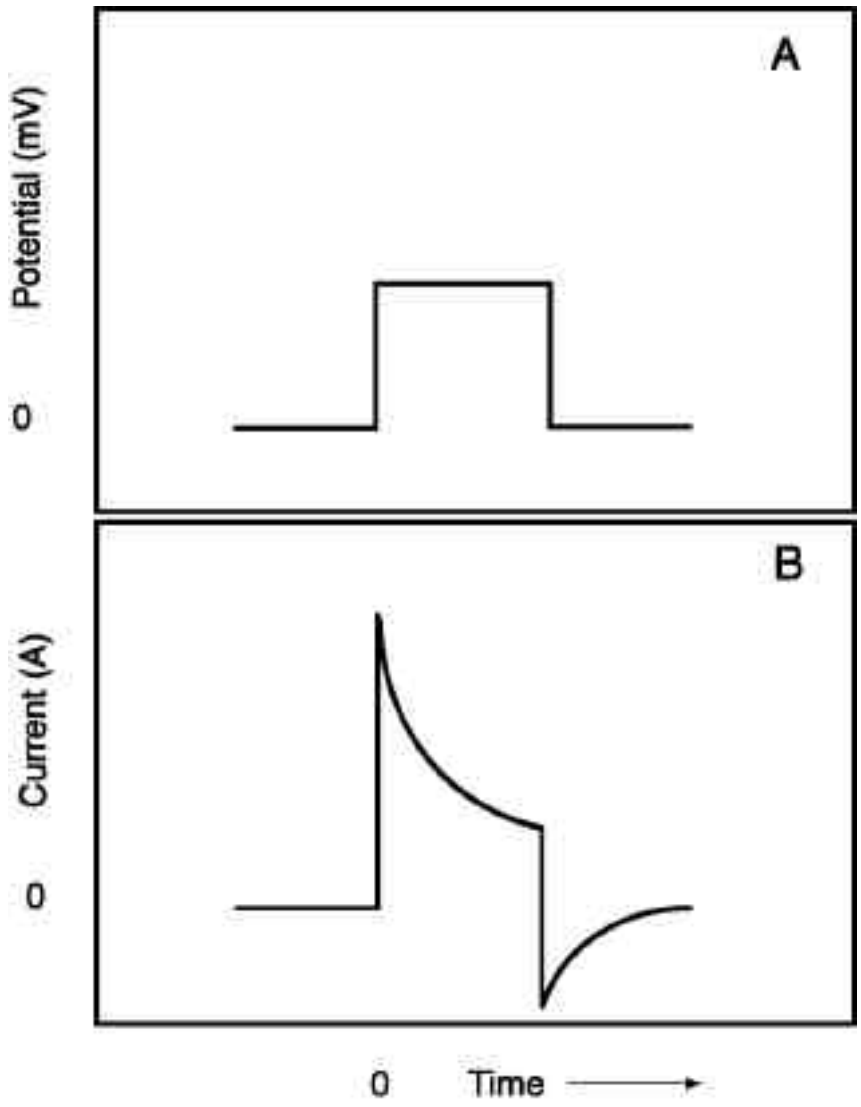

Fig. 1-17 Schematic of a normal pulse voltammetric experiment showing A: the potential step from 0 V to a non-zero value and back, B: the current generated from the potential step.

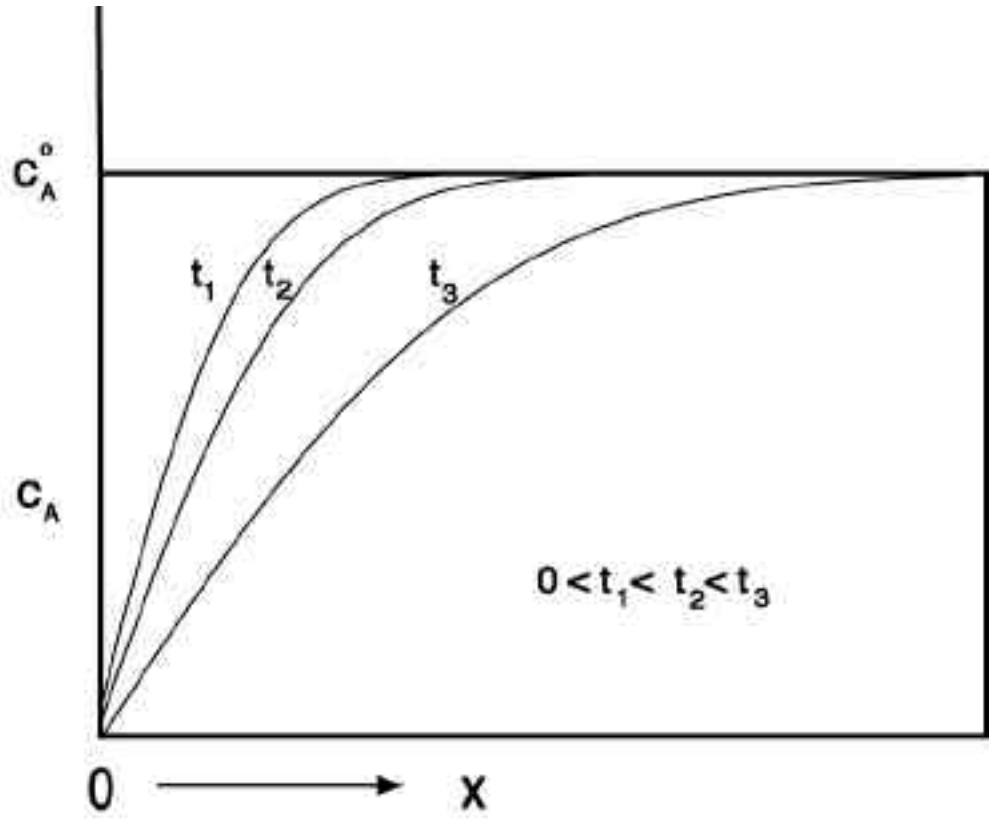

Fig. 1-18 Concentration gradient showing the depletion of species A in an area immediately adjacent to the electrode surface as a function of time (t) and distance (x).

The rate of diffusion is limited by the concentration gradients represented by Fick's first law of diffusion:

$$J = -D\frac{dc_A}{dx} \tag{1.28}$$

where the flux (J) is a function of the linear concentration gradient $\left(\frac{dc_A}{dx}\right)$ and the proportionality constant known as the diffusion coefficient (D). Next, by considering the change in the concentration gradient as a function of time (t) one reaches an expression for diffusion in a one-dimensional system known as Fick's second law:[8]

$$\frac{dc_A}{dt} = D\frac{d^2c_A}{dx^2} \tag{1.29}$$

In a practical case of a planar metal electrode immersed in a sample solution of *A*, whose random motion processes are known as semi-infinite linear diffusion, the current (i) is expressed by:

$$i = nFAD\frac{dc_A}{dx} \tag{1.30}$$

where $i=nFADJ$, x is the distance from the electrode and c_A is the concentration of A in the solution. Solving Fick's second law with the following boundary conditions:

$$t = 0, \quad c_A^{\circ} = c_{A,\infty} \qquad \text{(no electrode reaction)} \tag{1.31}$$

$$t \geq 0, \quad \lim_{x \to \infty} c_A = c_{A,\infty} \qquad \text{(bulk solution)} \tag{1.32}$$

$\left.\begin{matrix} t>0 \\ x=0 \end{matrix}\right\}$, $c_A^{\circ} = 0$ (diffusion-limited current, i_d) (1.33)

this reduces to another expression for the diffusion limited current known as the Cottrell equation, represented below:

$$i(t) = i_d(t) = \frac{nFAD^{1/2}}{(\pi t)^{1/2}} \tag{1.34}$$

Here, the current decreases with $t^{1/2}$, limiting the length of time in which this relation is valid due to changes in the concentration gradients from natural convection.[8]

This concept of the relation between the flux (J) and current permeates all voltammetric and amperometric analyses. It is obvious in this case that increasing the diffusion coefficient or the area of the electrode will effectively increase the current. The geometry and considerations pertaining to a liquid-liquid interface presented in the next section are quite different. In particular, the interface is not as distinct and the diffusing ions of interest are not oxidized or reduced. They are transported from one phase to another in a non-Faradaic charge transfer reaction.

Liquid-liquid interface. From an unmodified solid contact scenario where the chemical species involved in producing current through the electrochemical cell are contained in the same solution phase, ion transfer studies were extended to liquid-liquid systems. In this configuration, two conducting solutions form an interface due to their immiscible characteristics, such as the water/1,2-dichloroethane[67-69] interface or the

water/nitrobenzene interface.[70-73] Over twenty years ago, a novel approach to ion sensing emerged based on selective partitioning of ions from an aqueous phase to an organic phase. The method was termed ITIES (interface between two immiscible electrolyte solutions), which is an electrochemical technique based on the transfer kinetics and transfer energies of ions across a liquid-liquid interface. In contrast to zero current potentiometry, ITIES allows for tuning of an applied potential for selective ion extraction from one liquid to another. Koryta first reported an example of ITIES used in the transfer of potassium ions from water into nitrobenzene.[70] The extraction of potassium was aided by the presence of a natural antibiotic, valinomycin, in the organic phase. This antibiotic selectively binds potassium ions lowering the Gibbs transfer energy from the aqueous to the organic phase.

Studying charge transfer reactions using ITIES has provided information on ion-receptor complexation and extraction. This method allows one to probe the kinetics and thermodynamics associated with these electrochemical processes by measuring the rate at which ions are transported across the interface. The energy required for this transport of ions is related to the dehydration and resolvation energies of the ions and to the applied potential across the interface. "The difference between the standard Gibbs energies of hydration and solvation is effectively the work that is required in transferring an ionic species, j, from the bulk aqueous phase (w) to the bulk organic phase (o) ".[74] In order to transfer an ion from one phase to another, the interface must be polarized so that the

difference in the Galvani (or inner) potential (Φ) of each phase compensates the Gibbs energy of transfer. The Galvani potential difference is represented as:

$$\Delta_o^w \Phi = \Delta\Phi^w - \Delta\Phi^o \tag{1.35}$$

At equilibrium, the equal electrochemical potentials of ion J in each phase provides the Nernst equation for ion transfer from the aqueous (w) phase to the organic (o) phase:

$$\Delta_o^w \Phi = \Delta_o^w \Phi_J^\circ + \frac{RT}{z_J F} \ln\left(\frac{a_J^o}{a_J^w}\right) \tag{1.36}$$

where a_J and z_J are the activity and charge of ion J, repectively. R, T and F have their usual meanings. The standard Gibbs energy of transfer is related to the standard potential of transfer according to the following equation:

$$\Delta_o^w \Phi_J^\circ = \frac{\Delta G_{tr,J}^{\circ,w\to o}}{z_J F} = \frac{\mu_J^{\circ,o} - \mu_J^{\circ,w}}{z_J F} \tag{1.37}$$

where z_J is the charge of the transferring ion and F is the Faraday constant, $\Delta G_{tr,J}^{\circ,w\to o}$ is standard Gibbs energy of transfer of ion J, $\Delta_o^w \Phi_J^\circ$ is the standard potential of transfer of ion J, $\mu_J^{\circ,w}$ is the standard Gibbs energy of hydration of J and $\mu_J^{\circ,o}$ is the standard Gibbs energy of solvation.

In order to use this method to selectively transfer ions, the competing ions in both phases must have different Gibbs transfer energies. Since the transfer energies are related to the applied potential, according to the above equation, a system using differential pulse

voltammetry (DPV) can be used to measure the rate of ion transfer for a variety of ions, both cationic and anionic.[75] Standard Gibbs energies of transfer are most commonly scaled versus the "TATB" assumption, which states that the "cation and anion of tetraphenylarsonium tetraphenylborate (TPAsTPB) have equal standard Gibbs energies of transfer for any pair of solvents, assuming that the solvation energies of both the cation and the anion are equal".[74] The cation ($TPAs^+$) and anion (TPB^-) are both highly lipophilic and will remain mostly in the organic phase. From this basis, one can calculate the transfer potential for a set of counterions in the aqueous phase.

Experimentally, both the aqueous and organic phases must be made conducting by adding salts to both. Ideally, the base electrolyte for the aqueous phase should contain a salt whose cation and anion are highly hydrophilic, while the base electrolyte for the organic phase should contain a salt with highly hydrophobic cations and anions. Figure 1-19 shows a voltammogram consisting of two separate sweeps starting at $i = 0$ and proceeding in opposite directions with a sweep rate of 5 mVs^{-1}.[76] Luggin capillaries were placed in close proximity to the ITIES interface containing 10^{-2} M LiCl in the aqueous phase and 10^{-3} M TPAsTPB in the organic phase (NPOE). The cell was completed with Ag/AgCl reference electrodes immersed in 10^{-2} M LiCl for the aqueous phase and 10^{-2} M TPAsCl (aqueous) in contact with the NPOE phase containing the same tetraphenylarsonium cation. The two sweeps determine the zero potential scale according to the TATP assumption for NPOE. The non-zero potential value where the current/potential curves meet is subtracted from values obtained for other ions. The

voltammograms, of the four ions investigated, showed that the transfer processes were reversible. Table 1-1 reports the half-wave potentials, the conditional potential difference of ion transfer and the calculated Gibbs energies of transfer for the tetramethylammonium (TMA^+) and tetraethylammonium (TEA^+) cations and for picrate (Pi^-) and perchlorate (ClO_4^-) anions.[76] The Gibbs energies of transfer for each ion from the aqueous to the organic phase show that the perchlorate anion prefers the NPOE phase most and the tetramethylammonium cation prefers it least.

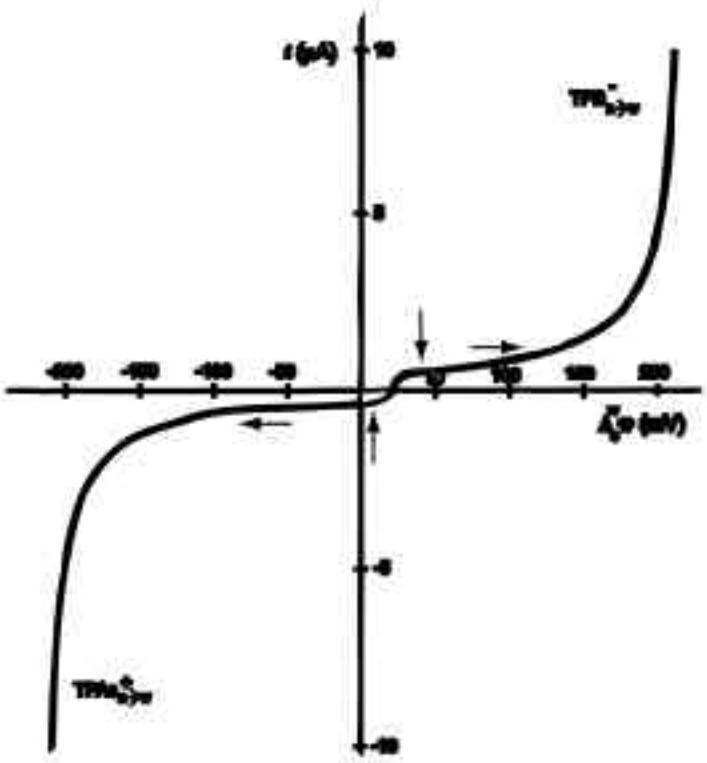

Fig. 1-19 TATB assumption is used to determine the zero of the potential scale in NPOE. Two single voltammetric sweeps (5 mVs^{-1}) proceeded in opposite directions and started at i=0. The aqeous phase contained 10^{-2} M LiCl and the NPOE phase contained 10^{-3} M TPAsTPB. The residual currents marked by the arrows were subtracted from each voltammogram in order to determine the currents associated with the transfer of $TPAs^{+}$ and TPB^{-}.[76]

Ion	$\Delta_o^w\Phi_{1/2}$ (mV)	$\Delta_o^w\Phi_J^\circ$ (mV)	$\Delta G_{tr,J}^{\circ,w\rightarrow o}$ (kJ mol^{-1})
TMA^+	+166± 3	+196± 3	-18.8± 0.3
TEA^+	-3± 3	+27± 3	-2.6± 0.3
Pi^-	+8± 3	+38± 3	+3.7± 0.3
ClO_4^-	-187± 5	-157± 3	+15.1± 0.3

Table 1-1 This table reports the half wave potentials, the conditional ion transfer potential differences and the Gibbs energies of ion transfer for the specified ions. [76]

Ion transfer at a single polarized interface of the conducting base electrolyte at an ITIES produces a potential window for examining ion transfer rates of other target ions. Figure 1-19 can be used as an example in which the transfer of the $TPAs^+$ and TPB^- ions take place at more extreme negative and positive potentials. Here, there exists a "window" between -125 mV and 125 mV in which neither the base electrolyte (LiCl) nor

the target ions ($TPAs^+$ and TPB^-) contribute to the observed current. If an additional salt of more desired ions is added to these sample solutions, it must have standard transfer potentials within this potential window. Otherwise, the voltammograms will continue to monitor the ion transfer of the TPAsB salt. This makes the investigation of each desired ion highly dependent on the electrochemical cell setup, especially the choice of base electrolyte. Figures 1-20 and 1-21 show an example of a modern four-electrode setup for an ITIES with the accompanying phase compositions.[77]

Addition of an ion-complexing molecule (ionophore) into the organic phase of the ITIES has the effect of lowering the Gibbs ion transfer energy and shifting the ion transfer potential. In conjunction with an appropriate base electrolyte, an ionophore can shift the potential resulting in current from the target ion into the range of the potential window where the base electrolytes are not transferred from one phase to another. LiCl is a typical hydrophilic base electrolyte for the aqueous phase while typical lipophilic salts like n-tetrapentylammonium tetrakis(4-chlorophenyl)borate[78] and bis(triphenyl-phosphoranylidene) ammonium tetrakis(4-chlorophenyl)borate[68] have been used to widen the potential window range. Within this window, ion transfer processes have been studied using cyclic voltammetry (CV),[67-72,79] normal pulse voltammetry (NPV)[73,80] and differential pulse voltammetry (DPV).[75,81]

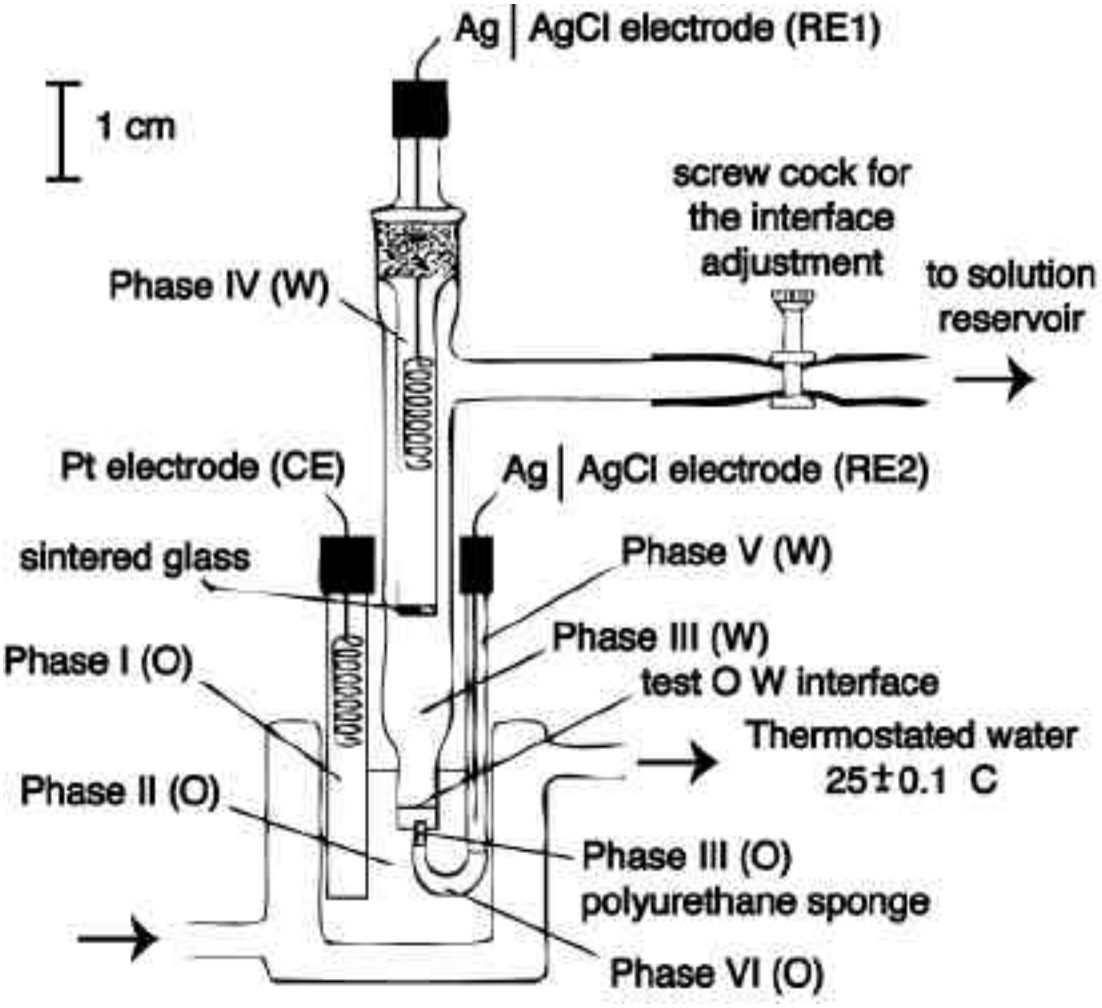

Fig 1-20 Schematic of the ITIES electrochemical setup of a four electrode system used in the ion transfer analysis across the water/1,6-DCH interface of various ions including choline and acetylcholine.[77]

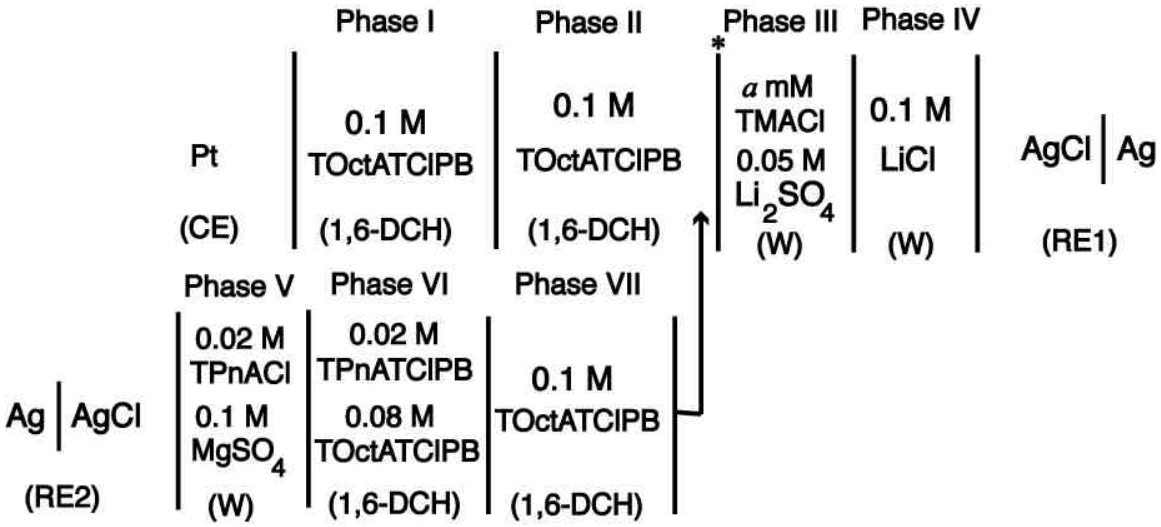

Fig.1-21 Schematic showing the individual phase concentrations used in Fig. 1-20. [77]

Recently, a trend toward miniaturization of the ITIES interface in an attempt to decrease the *iR* drop has produced micropipette devices in which the interface between phases is contained within the pipette or at the tip of the pipette.[68,82-84] Other efforts

include the supported liquid membrane electrodes[74,81,85,86] and phospholipid layers that have been adsorbed onto the ITIES interface in an attempt to mimic biological membranes.[69,87-89]

In a case of a supported liquid membrane, the organic phase was separated from two aqueous phases by an array of 35 μm holes that were drilled into polyethylene terephthalate (PET) by UV laser photoablation.[85] This creates two polarizable interfaces and doubles the potential window for ion transfer as compared to a single polarizable interface.[89] This produced a potential window with a range of about 1600 mV in which other target ions could be studied through ion transfer processes.

Special care must be taken in the theoretical treatment of currents associated at the ITIES, due to the geometrical surface area of the various electrodes. Several mathematical representation of the current/potential curves generated from an ITIES have been proposed.[78,91,92] Some are quite complicated taking into account successive complex formation constants and their specific ion pairing in both phases. It was shown that no single mathematical representation will apply universally to all ion transfer processes at an ITIES for they are dependent on the mechanism of complexation.[92] A common factor in these theoretical explanations is that mass transfer of the ions is diffusion limited. The peak current and peak potential obtained from the cyclic voltammograms is used to evaluate the reversible half-wave potential of ion transfer and the diffusion coefficients. The reversible half-wave potential can be related to either the Gibbs energy of ion transfer or the standard ion transfer potential, shown as:

$$\Delta_O^W \Phi_{1/2,J}^{rev} = \Delta_O^W \Phi_J^\circ + \frac{RT}{z_J F} \ln\left(\frac{D_J^O}{D_J^W}\right)^{1/2} + \text{constant} \tag{1.38}$$

Here, $\Delta_O^W \Phi_{1/2,J}^{rev}$ is the reversible half-wave potential of transfer of ion J, $\Delta_O^W \Phi_J^\circ$ is the standard ion transfer potential of J across the O/W interface, R, T and F have their usual meanings, z is the charge of ion J including the sign, D_J^W and D_J^O are the diffusion coefficients of J in each phase. If ion transfer is assisted by an ionophore (L) that forms 1:1 complexes with the specified ion and its concentration is held in excess, the reversible half-wave potential will shift negatively by a value that is related to the complex formation constant by:

$$\Delta_O^W \Phi_{1/2,J}^{rev} = -\frac{RT}{z_J F} \ln \beta_{JL}(o) c_L^\circ(o) \tag{1.39}$$

From this relation values for the formation constants are obtained and suitable ionophores with appropriate base electrolytes are chosen for ion transfer experiments.

Liquid-solvent polymeric membrane interface. From the progress made in the field of ITIES at both the liquid-liquid interface and the supported liquid membrane interface, a novel approach to ion amperometry was proposed only a few years ago. The method involves using traditional potentiometric type solvent polymeric membrane electrodes in voltammetry to assess a variety of aspects in ion transfer across the water plasticized PVC interface. Samec *et al.* has recently shown using cyclic voltammetry that the standard ion transfer potentials of PVC-based membranes show a small effect

from the added polymer compared to the water-NPOE interface without polymer.[93] Since a typical solvent polymeric membrane electrode separates the sample from the inner-filling solution (IFS), an analogy to the ITIES with two polarizable interfaces can be drawn. Horvath and Horvai have recently demonstrated the ability to modify the type of ion transfer interface from ideally polarized to diffusion limited by changing the bathing ions of the base electrolyte.[79] A series of articles were published explaining the methodology, theoretical response and practical applications[3,94-97] of these amperometric ISEs.

Having two ideally polarized interfaces was seen as a practical benefit for this type of analysis in contrast to many of the traditional studies done at an ITIES.[70,71,80] Using a three electrode setup (Figure 1-16) in which the working electrode membrane is in contact on one side with the sample and on the other side with the IFS, dictates that upon applying a negative potential cations are forced into the membrane from the sample and anions are forced into the membrane from the IFS to maintain electroneutrality (see Figure 1-22). Further investigation concluded that the voltammetric wave form used in normal pulse voltammetry (NPV) was best suited for this electrochemical configuration. This offers a method of renewing the ion concentrations at the membrane phase boundary by sequential potential pulses in which a stripping pulse at 0.0 V is imposed between each uptake pulse forcing the previously extracted ions back into their respective phases. The length of time imposed on the stripping pulse to remove 95% of the ions transferred during the uptake pulse was 100 times longer, although a ten fold increase in the length of

time of the stripping pulse should remove 85% of the previously transferred ions.[95] From the initial studies,[93-95] the theory of the response mechanism for this amperometric ISE was extended to include the selectivity of multi-analyte detection.[3] It is here that the basis for the amperometric sensor is explained. In analogy to traditional potentiometric sensors whose response mechanism is based on selective extraction of target sample ions into the membrane phase contingent on the ion-exchange mechanism provided by added lipophilic salts, the amperometric counter part uses an applied external potential to achieve the same result. It is therefore imperative to remove the ion-exchangers as they have been shown to produce an ohmic response in these amperometric ISEs.[94] It was accomplished by adding a high concentration of the lipophilic salt ETH 500 (shown in Figure 1-5), which had the added benefits of lowering the membrane resistance and decreasing ion migration. A second condition requires the use of neutral ionophores only, because the current associated with the applied potential should be limited to the transferred ions.

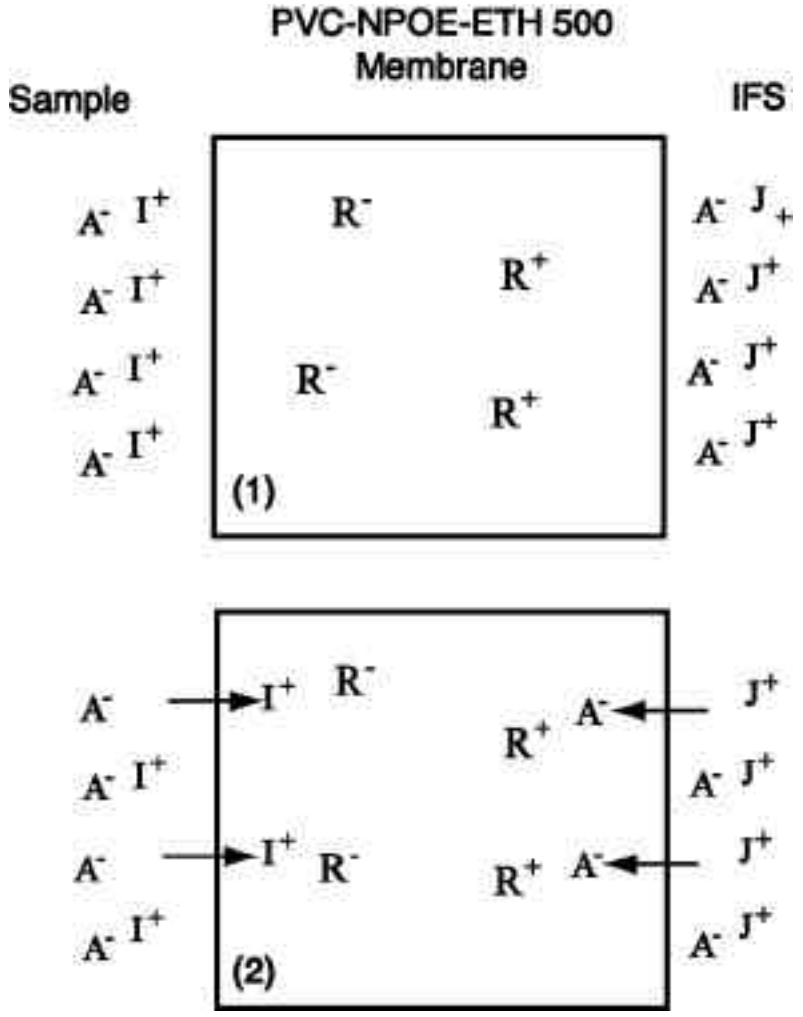

Fig. 1-22 Schematic of the two ideally polarized interfaces created by the polymer membrane electrode. (1) shows the membrane composition before the uptake potential pulse and contains only the cation and anion of the salt ETH 500. (2) shows the influx of cations at the sample side and simultaneous influx of anions from the IFS side as a result of an applied negative potential pulse in a NPV scan.

It is known that the membrane potential can be divided into the sample-membrane phase boundary potential (E_{PB}), the IFS-membrane phase boundary potential ($E_{PB'}$) and the internal membrane potential or iR_{drop}, represented as:

$$E_M = E_{PB} + E_{PB'} + iR_{bulk} \tag{1.40}$$

where I and R_{bulk} are the observed current and bulk membrane resistance, respectively, and $(\cdot)$ denoted the inner phase boundary. Since the diffusion coefficients in plasticized PVC membranes are about 1000 times slower than those found in aqueous solutions,[9] the current is assumed to be limited by the diffusion of the extracted sample ions in the membrane phase. According to Equation 1.40, the current is also dependent on the concentrations of extracted ions and can be expressed in analogy to Equation 1.30 for a microelectrode as:

$$i = AFD\frac{[I^+]_{PB} + [IL^+]_{PB} + [J^+]_{PB} + [JL^+]_{PB}}{\delta} \tag{1.41}$$

where A is the electrode area, F is the Faraday constant, D is the diffusion coefficient, δ is the Nernst diffusion layer thickness in the membrane phase, $[I^+]_{PB}$, $[IL^+]_{PB}$, $[J^+]_{PB}$ and $[JL^+]_{PB}$ are the concentrations of free and complexed primary and interfering ions at the membrane phase boundary. It is assumed that the Nernst diffusion layer thickness is the same prior to each uptake potential pulse of the NPV scan.

To maintain electroneutrality, for every cation transferred into the membrane from the sample side, an anion must be transferred into the membrane from the IFS side. Represented here as:

$$[A^-]_{PB'} = [I^+]_{PB} + [IL^+]_{PB} + [J^+]_{PB} + [JL^+]_{PB} \quad (1.42)$$

where $[A^-]_{PB'}$ denotes the anion concentration at the IFS-membrane phase boundary and allows for an equivalent expression for the current in terms of the extracted anions:

$$i = AFD\frac{[A^-]_{PB'}}{\delta} \quad (1.43)$$

The phase boundary potential at the sample-membrane interface is a function of any ion found in both boundary regions, expressed, here, for the monovalent cation $[I^+]$ as:

$$E_{PB} = \frac{RT}{F}\ln\frac{k_I a_I(aq)}{[I^+]_{PB}} = s\log\frac{k_I a_I(aq)}{[I^+]_{PB}} \quad (1.44)$$

where R,T and F have their usual meanings, k_I is a function of the standard chemical potential difference of I^+ in both phases, a_I is the activity of the uncomplexed cation in the aqueous phase boundary and $[I^+]$ is its concentration in the organic phase boundary. The ion exchange constant can be defined as:

$$\frac{k_J}{k_I} = \frac{a_I(aq)[JL^+]}{a_J(aq)[IL^+]} \quad (1.45)$$

Inserting this relation into the phase boundary potential formulated for the anions gives:

$$E_{PB} = \frac{RT}{F}\ln\frac{k_A a_A(aq)}{[A^-]_{PB}} = s\log\frac{k_A a_A(aq)}{[I^+]_{PB}+[IL^+]_{PB}+[J^+]_{PB}+[JL^+]_{PB}} \quad (1.46)$$

If the membrane contains a lipophilic neutral ionophore (L), the complex formation constants for the primary ion (I^+) and interfering ion (J^+) are expressed as:

$$\beta_{IL} = \frac{[IL^+]}{[I^+][L]} \quad (1.47)$$

and

$$\beta_{IJ} = \frac{[JL^+]}{[J^+][L]} \quad (1.48)$$

Assuming only 1:1 complexes between ion and ionophore, the total ionophore concentration is represented by:

$$L_T = [L]_{PB} + [IL^+]_{PB} + [JL^+]_{PB} \quad (1.49)$$

A later chapter extends this theory to accommodate multivalent ions and higher complex stoichiometries. By combining the appropriate equations and under the condition that the measured currents are from the potential range where uncomplexed ions in the membrane phase are extremely small, a relation for the membrane phase boundary potential is obtained:

$$E_M = iR_{bulk} + s\log\frac{k_A a_A}{\beta_{IL}} + s\log\frac{L_T - i\delta/AFD}{(i\delta/AFD)^2} + s\log\left(a_I + \frac{\beta_{JL}k_J}{\beta_{IL}k_I}a_J\right) \quad (1.50)$$

Here, the ion transfer potential, resulting in the current from both ions, is related to the complex formation constants with the ionophore. Analogous to potentiometric analysis, the selectivity also depends on the ratio of the complex formation constants in this voltammetric interpretation of the membrane phase boundary potential.[3]

Using this theory, interesting results on the ion transfer mechanisms of solvent polymeric membrane electrodes have been studied. In an attempt to gain further control over these types of amperometric sensors, a new methodology has recently been introduced in which the transfer of sample target ions is dictated by a controlled current during the uptake and a controlled potential during the stripping of previously transferred ions from the membrane.[5] This pulsed chronopotentiometric method has distinct advantages over the previously described NPV technique. By applying a specific current density to the membrane electrode, a specific amount of sample ions will be transferred into the membrane and the resulting potential can be measured. By developing the theoretical response of these sensors with traditional potentiometric ion-selective electrode formalisms, a direct comparison is possible to the potentiometric electrode counter-parts. The basic starting point in this approach utilizes the same membrane components found in the NPV membranes. A 1:2 ratio of PVC:NPOE is dissolved in THF along with 10% by weight of the lipophilic salt ETH 500 and 10 kg^{-1} of the ionophore.

In an identical case to the conditions presented for the NPV theory, the applied currents are held below the limiting current dictated by the total ionophore concentration

in the membrane. In this case the chronopotentiometric theoretical derivation gives the phase boundary potential as a function of the applied current for monovalent ions:

$$E_{PB} = \frac{RT}{F}\ln\frac{-k_I FA\beta_{IL.n}\sqrt{\frac{D_{org}}{t}}}{2i}\left(L_T + \frac{2i}{FA}\sqrt{\frac{t}{D_{org}}}\right)^n + \frac{RT}{F}\ln\left\{a_I(aq,pb) + \frac{\beta_{JL,n}}{\beta_{IL.n}}K_{ex}a_J(aq,pb)\right\} \quad (1.51)$$

here, the terms have their same meanings with the activities denoting ions in the aqueous phase boundary and a relation for the Nernst diffusion layer thickness is substituted from:

$$\delta = 2\sqrt{Dt} \quad (1.52)$$

The last term in equation 1.51 is identical in meaning to the last term in equation 1.50 giving the selectivity coefficient for competing ions as a function of the exchange constant (K_{ex}) times the ratio of the complex formation constants.[9]

The most striking difference between these two methods is the ability of the chronopotentiometric technique to apply a known current of fixed duration to achieve a constant activity of I in the organic phase boundary. A constant current uptake of -5 μA for 1 second was applied followed by a stripping potential pulse for 10 seconds in a membrane containing the ionphore (*tert*-butyl calix[4]arene tetramethyl ester) selective for sodium.[5] Nernstian responses were obtained for Na^+ and K^+ upon application of a cathodic current. The sign of the applied current was then reversed giving a Nernstian

response to Cl^-, showing another distinct advantage of this method. This technique and theory have also, recently, been used to distinguish between the response of free calcium activities from that of the total calcium concentration based on the magnitude of the applied current.[99] A novel fully reversible sensor for the polyion, protamine, was also realized based on the above method.[100] These so-called pulsetrodes have provided an avenue of research that has the potential to combine the sensor fields of ion detection.

References

1 Bühlmann, P.; Pretsch, E.; Bakker, E. *Chem. Rev*. **1998**, *98*, 1593.

2 F. Reymond, F.; Carrupt, P.; Girrault, H. H. *J. Electroanal. Chem.* **1998**, *449*, 49.

3 Jadhav, S.; Bakker, E. *Anal. Chem.* **2001**, *73*, 80.

4 Iglehart, M.L.; Buck, R.P.; Pungor, E. *Anal. Chem.* **1988**, *60(4)*, 290.

5 Shvarev, A.; Bakker, E. *Anal. Chem.* **2003**, *75*, 4541.

6 Katano, H.; Kuboyama, H.; Senda, M. *J. Electroanal. Chem.* **2000**, *483*, 117.

7 Samec, Z.; Samcova, E.; Girault, H.H. *Talanta* **2004**, 63, 21.

8 Brett, C.M.A.; Brett, A.M.O. *Electrochemistry Principles, Methods and Applications*; Oxford University Press, New York, **2000**.

9 Bakker, E.; Bühlmann, P.; Pretsch, E. *Chem. Rev*. **1997**, *97*, 3083.

10 Bakker, E.; Bühlmann, P.; Pretsch, E. *Talanta* **2004**, *63*, 3.

11 Pungor, E. *Pure Appl. Chem.* **1992**, 64, 503.

12 Bakker, E.; Nagele, M.; Schaller, U.; Pretsch, E. *Electroanalysis*, 7 (1995) 817.

13 Gugenheim, E.A. *J. Phys. Chem.* **1930**, *34*, 1540.

14 Yajima, S.; Tohda, K.; Bühlmann, P.; Umezawa, Y. *Anal. Chem.***1997**, *69(10)*, 1919.

15 Buck, R.P.; Cosofret, V.V.; Lindner, E. *Anal. Chim. Acta* **1993**, *282*, 273.

16 Stefanac, Z.; Simon, W. *Chimia* **1966**, *20*, 436.

17 Stefanac, Z.; Simon, W. *Microchem. J.* **1967**, *12*, 125.

18 Pioda, L.A.R.; Stanova, V.; Simon, W. *Anal. Lett*. **1969**, *2*, 665.

19 Umezawa, Y.; Sugawara, M.; Kataoka, M.; Odashima, K.; Pungor, E. *Ion-sel Electrodes* , 5, Proc. Symp. (5th), **1989**, 211.

20 Sugawara, M.; Yoshida, H.; Henmi, A.; Umezawa, Y. *Anal. Sci*. **1991**, *7*, 141.

21 Cox, J.A.; Poopisut, N. *Anal. Chem.* **1992**, *64*, 423.

22 Johnson, R.D.; Bachas, L.G. *Anal. Bioanal. Chem* **2003**, *376*, 328.

23 Shono, T.; Okahara, M.; Ikeda, I.; Kimura, K.; Tamura, H. *J. Electroanal. Chem.* **1999**, *132*, 99.

24 Xie, R.Y.; Christian, G.D. *Anal. Chem.* **1986**, *58*, 1806.

25 Kitazawa, S.; Kimura, K.; Yano, H.; Shono, T. *J. Am. Chem. Soc.* **1984**, *106*, 6978.

26 Diamond, D.; Svehla G.; Seward, E.M.; McKervey, M.A. *Anal. Chim. Acta* **1988**, *204*, 223.

27 Yamamoto, H.; Shinkai, S. *Chem. Lett.* **1994**, *6*, 1115.

28 Zhang, W.; Rozniecka E.; Malinowska, E.; Parzuchowski, P.; Meyerhoff, M.E. *Anal. Chem*. **2002**, *74*, 4548.

29 Steinle, E.D.; Schaller, U.; Meyerhoff, M.E. *Anal. Sci.* **1998**, *14*, 79.

30 Chaniotakis, N.A.; Chasser, A.M.; Meyerhoff, M.E. *Anal. Chem.* **1988**, *60*, 188.

31 Badr, I.H.A.; Meyerhoff, M.E. *Anal. Chem.* **2005**, *77*, 6719.

32 Messik, M.S.; Krishnan, S.K.; Hulvey, M.K.; Steinle, E.D. *Anal. Chim. Acta* **2005**, *539*, 223.

33 Malinowska, E.; Gorski, L.; Meyerhoff, M.E. *Anal. Chim. Acta* **2002**, *468*, 133.

34 Umezawa, K.; Tohda, K.; Lin, X.M.; Sessler, J.L.; Umezawa, Y. *Anal. Chim. Acta* **2001**, *426*, 19.

35 Qin, Y.; Bakker, E. *Anal. Chem.* **2004**, *76*, 4379.

36 Lindner, E.; Graf, E.; Nigreisz, Z.; Toth, K.; Pungor, E.; Buck, R.P. *Anal. Chem*. **1988**, *60*, 295.

37 van den Berg, A.; van der Wal, P.D.; Skowronska-Ptasinska, M.; Sudholter, E.J.R.; Reinhoudt, D.N.; Bergveld, P. *Anal. Chem.* **1987**, *59*, 2827.

38 Ammann, D.; Pretsch, E.; Simon, W.; Lindner, E.; Bezegh, A.; Pungor, E. *Anal. Chim. Acta* **1985**, *171*, 119.

39 Bakker, E.; Pretsch, E. *Anal. Chim. Acta* **1995**, *309*, 7.

40 Bakker, E.; Malinowska, E.; Schiller, R.D.; Meyerhoff, M.E. *Talanta* **1994**, *41*, 881.

41 Hofmeister, F. *Arch. Exp. Pharmakol.* **1888**, *24*, 247.

42 Mi, Y.; Bakker, E. *J. Electrochem. Soc*. **1998**, *114(2)*, L27.

43 Schaller, U.; Bakker, E.; Pretsch, E. *Anal. Chem.* **1995**, *67*, 3123.

44 Rozatzin, T.; Bakker, E.; Suzuki, K.; Simon, W. *Anal. Chim. Acta* **1997**, *280*, 197.

45 Malinowska, E.; Gawart, L.; Parzuchowski, P.; Rokicki, G.; Brzozka, Z. *Anal. Chim. Acta* **2000**, *421*, 93.

46 Fiedler, U.; Ruzicka, J. *Anal. Chim. Acta* **1973**, *67(1)*, 179.

47 Craggs, A.; Moody, G. J.; Thomas, J. D. R. *J. Chem. Educ.* **1974**, *51*, 541.

48 Moody, G. J.; Oke, R. B.; Thomas, J. D. R. *Analyst* **1970**, *95*, 910.

49 Heng, L. Y.; Hall, E. A. H. *Anal. Chem.* **2000**, *72*, 42.

50 Bakker, E.; Meruva, R. K.; Pretsch, E.; Meyerhoff, M. E. *Anal. Chem*. **1994**, *66*, 3021.

51 Guilbault, G.G.; Durst, R.A.; Frant, M.S.; Freiser, H.; Hansen, E.H.; Light, T.S.; Pungor, E.; Rechnitz, G.; Rice, N.M.; Rohm, T.J.; Simon, W.; Thomas, J.D.R. *Pure Appl. Chem.* **1976**, *48*, 127.

52 Bakker, E. *J. Electrochem. Soc*. **1996**, *143(4)*, L83.

53 Bakker, E.; Pretsch, E.; Bühlmann, P. *Anal. Chem.* **2000**, *72(6)*, 1127.

54 Gadzekpo, V.P.Y.; Christian, G.D. *Anal. Chim. Acta* **1984**, *164*, 279.

55 Bakker, E.; Bühlmann, P.; Pretsch, E. *Electroanalysis* **1999**, *11(13)*, 915.

56 Mathison, S.; Bakker, E. *Anal. Chem.* **1998**, *70(2)*, 303.

57 Puntener, M.; Vigassy, T.; Baier, E.; Ceresa, A.; Pretsch, E. *Anal. Chim. Acta* **2004**, *503(2)*, 187.

58 Sokalski, T.; Ceresa, A.; Zwickl, T.; Pretsch, E. *J. Am. Chem. Soc.* **1997**, *119(45)*, 11347.

59 Qin, Y.; Bakker, E. *Anal. Chem.* **2002**, *74(13)*, 3134.

60 Sabela, A.; Koryta, J.; Valent, O. *J. Electroanal. Chem. Interfac. Electrochem.* **1986**, *204(1-2)*, 267.

61 Lee, H.J.; Beriet, C.; Girault, H.H. *J. Electroanal. Chem*.**1998**, *453(1-2)*, 211.

62 Mi, Y.; Bakker, E. *Anal. Chem.* **1999**, *71*, 5279.

63 Lerchi, M.; Bakker, E.; Rusterholz, B.; Simon, W. *Anal. Chem.* **1992**, *64(14)*, 1534.

64 Rosatzin, T.; Holy, P.; Seiler, K.; Rusterholz, B.; Simon, W. *Anal. Chem*. **1992**, *64(18)*, 2029.

65 Tsagkatakis, I.; Peper, S.; Bakker, E. *Anal. Chem.* **2001**, *73*, 315.

66 Tsagkatakis, I.; Peper, S.; Retter, R.; Bell, M.; Bakker, E. *Anal. Chem*. **2001**, *73(24)*, 6083.

67 Dassie, S.A.; Yudi, L.M.; Baruzzi, A.M. *J. Electroanal. Chem*.**1999**, *464*, 54.

68 Cacote, M.H.M.; Pereira, C.M.; Tamaszewski, L.; Girault, H.H.; Silva, F. *Electrochim. Acta* **2004**, *49*, 263.

69 Manzanares, J.A.; Allen, R.M.; Konturri, K. *J. Electroanal. Chem*.**2000**, *483*, 188.

70 Koryta, J. *Electrochim. Acta* **1979**, *24(3)*, 293.

71 Samec, Z.; Marecek, V.; Koryta, J.; Khalil, M.W. *J. Electroanal. Chem*. **1977**, *83*, 393.

72 Koryta, J.; Du, G.; Ruth, W.; Vanysek, P. *Faraday Discuss. Chem. Soc.* **1984**, *77*, 209.

73 Katano, H.; Senda, M. *Bull. Chem. Soc. Jpn*. **1999**, *72*, 2085.

74 Qian, Q.; Wilson, G.S.; Bowman-James, K.; Girault, H.H. *Anal. Chem*. **2001**, *73(3)*, 497.

75 Koryta, J. *Electrochim. Acta* **1984**, *29(4)*, 445.

76 Valent, O.; Koryta, J.; Panoch, M. *J. Electroanal. Chem*. **1987**, *226*, 21.

77 Katano, H.; Tatsumi, H.; Senda, M. *Talanta* **2004**, *63*, 185.

78 Katano, H.; Senda, M. *Bull. Chem. Soc. Jpn*. **1997**, *70* 2493.

79 Horvath, V.; Horvai, H. *Anal. Chim. Acta* **1993**, *273*, 145.

80 Senda, M.; Katano, H.; Yamada, M. *J. Electroanal.Chem*. **1999**, *475*, 90.

81 Qian, Q.; Wilson, G.S.; Bowman-James, K. *Electroanalysis* **2004**, *16(6)*, 1343.

82 Shoup, D.; Szabo, A. *J. Electroanal. Chem*. **1984**, *160*, 27.

83 Beattie, P.D.; Delay, A.; Girault, H.H. *J. Electroanal. Chem*. **1995**, *380*, 167.

84 Fang, Y.; Leddy, J. *Anal. Chem.***1995**, *67*, 1259.

85 Beriet, C.; Girault, H.H. *J. Electroanal. Chem*. **1998**, *444*, 219.

86 Ulmeanu, S.M.; Jensen, H.; Samec, Z.; Bouchard, G.; Carrupt, P-A.; Girault, H.H. *J. Electroanal*. Chem. **2002**, *530*, 10.

87 Konturri, A.K.; Konturri, K.; Murtomaki, L.; Quinn, B.; Cunnane, V.J. *J. Electroanal. Chem*. **1997**, *424*, 69.

88 Cunnane, V.J.; Schriffrin, D.J.; Fleischmann, M.; Gebelwicz, G.; Williams, D. *J. Electroanal. Chem*. **1988**, *243*, 455.

89 Allen, R.M.; Williams, D.E. *Faraday Discuss.* **1996**, *104*, 281.

90 Shirai, O.; Kihara, S.; Suzuki, M.; Ogura, K.; Matsui, M. *Anal. Sci*. **1991**, *7*, 607.

91 Du, G.; Koryta, J.; Ruth, W.; Vanysek, P. *J. Electroanal. Chem. Interfacial Electrochem*. **1983**, *159*, 413.

92 Reymond, F.; Lagger, G.; Carrupt, P-A.; Girault, H.H. *J. Electroanal. Chem*. **1998**, *451*, 59.

93 Langmaier, J.; Stejskalova, K.; Samec, Z. *J. Electroanal. Chem*. **2001**, *496*, 143.

94 Bakker, E.; Jadhav, S. *Proceed, Electrochem. Soc*. **1999**, *99-13*, 390.

95 Jadhav, S.; Bakker, E. *Anal. Chem.* **1999**, *71*, 3657.

96 Jadhav, S.; Meir, A.J.; Bakker, E. *Electroanalysis* **2000**, *12*, 1251.

97 Jadhav, S.; Bakker, E. submitted.

98 Makarychev-Mikhailov, S.; Shvarev, A.; Bakker, E. *Anal. Chem.* **2006**, *78(8)*, 2744.

99 Shvarev, A.; Bakker, E. *Talanta* **2004**, *63*, 195.

100 Shvarev, A.; Bakker, E. *Anal. Chem.* **2005**, *77*, 5221.

Chapter 2

Spectral Imaging and Electrochemical Study on the Response Mechanism of Ionophore-Based Polymeric Membrane Amperometric pH Sensors

2.1 Introduction

Amperometric sensors based on ion transfer voltammetry, inspired by the important work of Koryta,[1] have been studied by growing number of researchers, for example by Girault for the miniaturization and detection in fluidic systems,[2-4] by Cammann for miniaturization,[5] by Horvath and Horvai to study the voltammeric behavior of plasticized membranes and the relationship to ion-selective electrodes,[6,7] by Marecek for the determination of ionophores,[8], by Senda for introducing pulsed amperometry and gelified membranes with more stable interfaces,[9,10] by Sawada and Osakai for lithium detection in artificial serum[11] and Samec for fundamental

characteristics of ion-selective membrane materials.[12] They are known to function in many ways in analogy to metal electrodes.[3,13] Nonetheless, the underlying chemistry is very different, since the applied potential forces the ion of interest to distribute unevenly across a liquid–liquid interface, often with the assistance of an ionophore dissolved in the organic phase. Unfortunately, potentiometric and amperometric sensors based on the same membrane materials and ionophores have rarely been compared to each other directly by the same research groups. Indeed, ion-selective electrodes have long ago successfully transitioned from liquid membrane electrodes used in academic settings to miniaturized, polymer-based, engineered devices that are used in clinical laboratories all over the world.[14] In contrast, the corresponding amperometric sensors have only recently been evaluated in fluidic platforms[15] or with modified materials.[5,16,17] This discrepancy in the speed and direction of development is perhaps partly due to the different academic environments pursuing research in those areas, with analytical chemists focusing more on potentiometric sensors, and fundamental physical chemists on their amperometric counterparts. On the other hand, the sensing material of amperometric sensors was required to be a simple organic liquid phase in order to guarantee a low resistance and high diffusion coefficients in the organic phase. Such membranes are known to respond to ionic species with very similar response mechanisms as their metal electrode counterparts. Consequently, recent efforts have focused on following the advances made with metal electrodes, by introducing microinterfaces for enhanced mass transport and consequently achieving lower detection limits.[15] This approach requires one to deal with

simple organic solvents, which are difficult to handle and are prone to leach into the sample, and that limit the lifetime of the sensors. Success was obtained in gelifying the organic liquids with a small amount of poly(vinyl chloride) for easier handling and to obtain a sharper liquid–liquid interface.[10,18]

Recently, we have started to study amperometric ion sensors based on the very same membrane materials as their potentiometric counterparts in an effort to critically compare both transduction principles to each other. Owing to the high polymer content in the plasticized PVC membranes, the diffusion coefficients of extracted ions and other active membrane components are, with about 10^{-8} cm^2 s^{-1}, and known to be much smaller than in pure organic liquids.[19] As a consequence, it was suggested that the current observed in the amperometric experiments is typically given by limited mass transport in the organic, not aqueous phase.[20] Koryta has previously also described systems (containing the ionophore monensin) where the same processes were assumed to be rate limiting, by utilizing a low ionophore concentration in the organic phase and a high electrolyte concentration in the aqueous phase.[21] Because of this alternate response mechanism, it was postulated that these amperometric sensors resemble the corresponding ion-selective electrodes much more closely than many previously studied systems.[22,23] The membranes contained no added ion-exchanger, but a high concentration of inert lipophilic salt. Normal pulse voltammetry, rather than cyclic voltammetry, was suggested as a preferred interrogation method for these sensing membranes since repeatable current readings require the re-establishment of a membrane

void of extracted ions between discrete potential pulses.[23] The sensing selectivity was found to be dependent on the magnitude of the observed current, which was used for multianalyte detection purposes.[22] A theoretical model was developed that satisfactorily explained the experimental results. In particular, the observed current in a normal pulse voltammetric experiment was compared to the function of the concentration of ion-exchanger in a potentiometric membrane.[22]

This chapter introduces a more direct approach to understanding amperometric ion sensors based on ionophores dissolved in hydrophobic polymeric membranes. Real time spectroscopic imaging experiments were performed on pH responsive ion-selective membranes containing a H^+-selective chromoionophore. The results are explained in light of the current response theory for these amperometric sensors, and correlated to the corresponding normal pulse voltammetric responses. The excellent selectivity,[24] imaging capability[19] and well-studied behavior in ion-selective membranes[25] make these H^+-chromoionophores ideal candidates for a critical comparative study of amperometric and potentiometric transduction principles.

2.2 Experimental

Reagents. The salts used for aqueous solutions were puriss quality or better and were dissolved in Nanopure distilled water. High molecular weight poly(vinyl chloride) (PVC), *o*-nitrophenyl octyl ether (NPOE), tetradodecylammonium tetrakis(4-chlorophenyl) borate (ETH 500), Selectophore grade tetrahydrofuran (THF), 9-(diethylamino)-5-octadecanoylimino-5H-benzo[a]phenoxazine (ETH 5294), potassium tetrakis[3,5-bis(trifluoromethyl)phenyl] borate (KTFPB), citric acid, boric acid and all salts were obtained from Fluka Chemical Corp. (Milwaukee, WI). Sodium hydroxide, sodium phosphate monobasic and sodium phosphate dibasic were obtained from Fisher Scientific (Fair Lawn, NJ).

Membrane Preparation. All membranes were prepared by dissolving PVC and NPOE (1:2 by weight) into Selectophore grade THF along with various amounts of two other components. For potentiometric membranes, 10 mmol/kg of the chromoionophore ETH 5294 and 5 mmol/kg KTFPB was added. The amperometric ISE membranes contained 10 wt% ETH 500 and 10 mmol/kg ETH 5294, whereas the ring membranes were prepared in complete analogy, but with 0.5 mmol/kg ETH 5294 to reduce the optical density. This cocktail was shaken mechanically for a few minutes and then poured into a glass ring with an inner diameter of 22 mm mounted on a microscope slide. The solvent

THF was allowed to evaporate overnight leaving membranes that were approximately 200 μm thick.

Instrumentation. A model AFRDE5 potentiostat (Pine Instruments, Grove City, PA) was used with a three electrode system to measure current versus applied potential. The Normal Pulse Amperometric data were recorded using LabView 5.0 software (National Instruments, Austin, TX) on a Macintosh computer equipped with a 16-bit data acquisition board (National Instruments, Austin, TX).[23] The imaging data were collected using a Nikon Eclipse E400 microscope equipped with a Pariss imaging spectrometer (LightForm, Inc., Belle Meade, NJ) and a model 4920 Peltier cooled CCD camera (Cohu, Inc., San Diego, CA).[26]

Electrodes. A saturated KCl, Ag/AgCl reference electrode containing a 1.0 M lithium acetate bridge electrolyte was used for all measurements. The potentiometric and amperometric working electrodes were prepared by mounting a piece of the ion-selective membrane onto a Philips electrode body (IS-561, Glasbläserei Möller, Zürich, Switzerland) with an i.d. of 4.0 mm and conditioning the electrode overnight in the inner filling solution (0.1 M NaCl). This inner solution composition is not optimal for the potentiometric sensor, but was chosen for maximum consistency in the experimental comparison. The potentiometric measurements were made with a two electrode setup, whereas the amperometric system required a three-electrode setup with a Pt cage counter

electrode immersed in the sample with the ion-selective working electrode. The sample was 0.1 M NaCl in 6.6 mM citric acid, 11 mM boric acid and 10 mM phosphoric acid, buffered with varying amounts of HCl to encompass the desired pH range.

The imaging experiments were done in a cell with a small Ag/AgCl working electrode separated from the reference electrode and much larger Ag/AgCl counter electrode by the ring shaped ISE membrane. Otherwise, this setup is similar to that reported in the literature for spectropotentiometric studies.[19] The membrane was cut into a donut-shaped ring with an o.d. of 8 mm and an i.d. of 6 mm and mounted onto a polished plexiglass cell bottom, in the center, forming two concentric rings separating the IFS and identical sample. The outer circle (34 mm i.d.) was a circular rubber gasket. The cell was covered with a 2" x 1/8" piece of quartz, fitted with a plastic cover slip and mounting screws. The rubber gasket and ISE membrane form two chambers between the plexiglass and quartz which are filled through channels with an identical 0.1 M NaCl solution buffered to pH 6.8 with 10 mM Na_3HPO_4 + 10 mM NaH_2PO_4. Ag/AgCl wire working and counterelectrodes were inserted through the fluidic channels and placed in close vicinity of the ring membrane and connected to the potentiostat. The cell was then mounted under a microscope and a section of the ISE membrane, approximately 430 µm deep, was studied in transmission mode as a function of time at a specified applied potential. The spectral camera recorded transmission spectra between 390 and 860 nm. Absorbance data were calculated by comparing the initial transmittance of the cell without mounted membrane ring to the transmittance of the final setup at a given time. For the

imaging experiment polarized at -1000 mV, the absorbance change was calculated relative to the transmittance with mounted membrane before application of the voltage pulse (in which case the chromoionophore was in its deprotonated form). This approach gave similar results, but with a lower noise in the relative absorbance profiles.

2.3 Results and Discussion

The response mechanism of polymeric membrane amperometric ion sensors was studied here with the H^+-selective chromoionophore ETH 5294 as a model system. This chromoionophore has been thoroughly studied earlier for use in optical and potentiometric polymeric sensors and likely represents an adequate system to study the mechanism of such amperometric sensors. Potentiometric sensors based on ETH 5294 are known to yield excellent pH electrodes owing to the high selectivity of this chromoionophore to hydrogen ions.[25,27] On the other hand, the absorbance and fluorescence properties of this compound have repeatedly been used to fabricate optical sensing films on the basis of competitive ion-exchange or coextraction equilibria.[24,26,28] In these cases, the extent of protonation of the chromoionophore is followed spectroscopically and related to the ion concentration of interest. This same chromoionophore has recently also been utilized in order to image the concentration profiles within ion-selective membranes under zero current conditions.[19,29] A drastic pH change on one membrane side, for example, promotes either the exchange with interfering

ions[19] or the coextraction of hydrogen ions and anions,[29] which gradually alters the concentration profiles within the entire sensing film. These processes were imaged in real time and yielded diffusion coefficients of the chromoionophore as well as an improved fundamental understanding of potentiometric sensors.

In the matrix of interest, PVC plasticized with o-NPOE in a ratio of 1:2, the chromoionophore ETH 5294 has recently been shown to exhibit negligible binding affinity to alkali metals.[30] Its pK_a value in this hydrophobic environment has been determined as 14.8 by utilizing the so-called sandwich membrane method.[30] Its lipophilicity is normally adequate in basic and neutral pH values, but has been reported to be insufficient under acidic sample conditions.[24] The absorbance maxima for the protonated and unprotonated forms are around 660 nm and 560 nm, respectively.[24] With the exception of its somewhat less than optimal lipophilicity, this chromoionophore is expected to be an adequate system for fundamental studies of amperometric sensors based on assisted ion transfer into a polymeric membrane.

In accordance with earlier work involving alkali metal selective ionophores,[20,22] membranes containing ETH 5294 were measured with normal pulse voltammetry. The purpose of alternating each incrementally applied potential with a baseline potential (here at 0 V) is to re-establish the membrane surface region devoid of extracted ions before each potential pulse. Figure 2-1 shows a typical normal pulse voltammogram for a PVC–NPOE membrane containing the chromoionophore ETH 5294 in contact with a pH 6.0 solution. As with earlier studies on the basis of other ionophores, a fairly wide

limiting current region is observed between -600 and -800 mV. It has been suggested that the current in these systems is predominantly dictated by the limited mass transport of ions from the sample–membrane interface into the polymer bulk (and not from the sample bulk to the membrane surface). Consequently, the limiting current region shown in Fig. 2-1 is believed to reflect the limited availability of ionophore in the membrane. As its concentration is exhausted, the interfacial concentration of extracted hydrogen ions can no longer increase, even at more extreme applied potentials. Eventually, the applied potential is sufficiently large so that an ionophore-mediated process is no longer necessary to extract sample cations in the membrane. This is thought to mark the end of the limiting current region shown in Fig. 2-1, and the selectivity of the membrane is now no longer reflected by the ionophore binding affinity but by the relative lipophilicity of the cations. Indeed, it results in a drastic selectivity change (lipophilic ions are preferred over hydrophilic ones) relative to the voltammetric response at lower currents (where ionophore-mediated selectivity is observed). The effect was exploited to use such membranes for multianalyte detection purposes.[22]

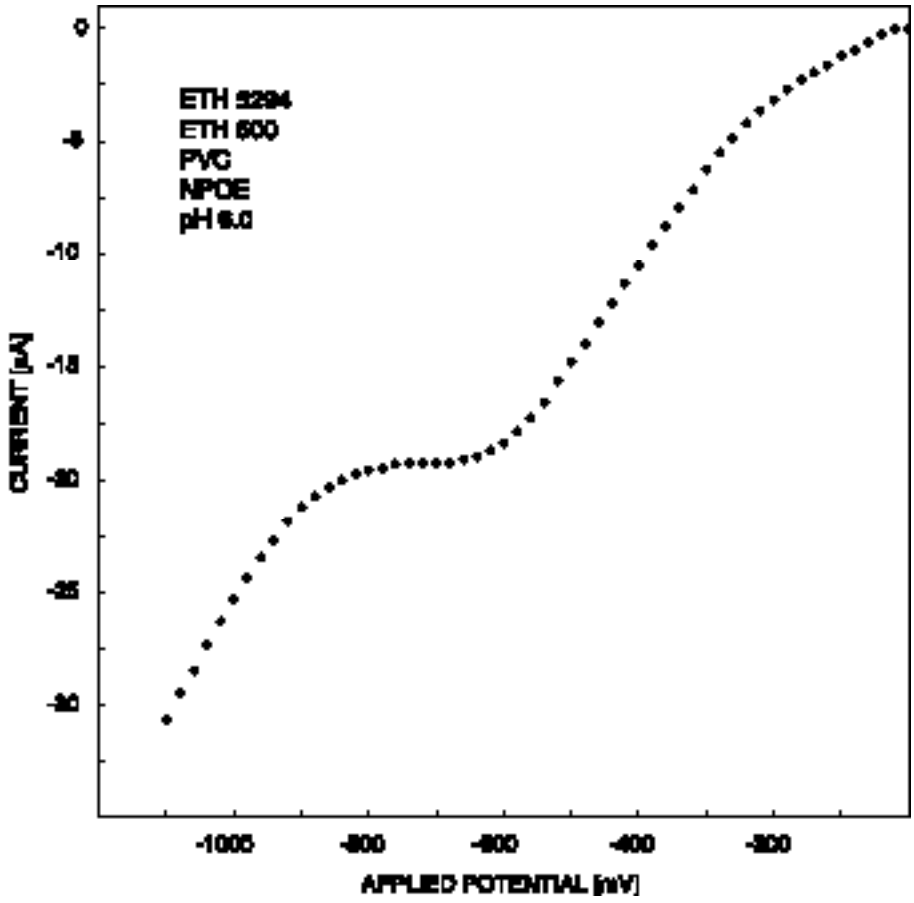

Fig. 2-1 Normal pulse voltammogram for a PVC-NPOE membrane containing ETH 5294 and the inert lipophilic salt ETH 500 in contact with a 0.1 M NaCl sample buffered at pH 6.0. Inner solution: 0.1 M NaCl. Uptake times: 1 s; Stripping times: 30 s at 0.0 V.

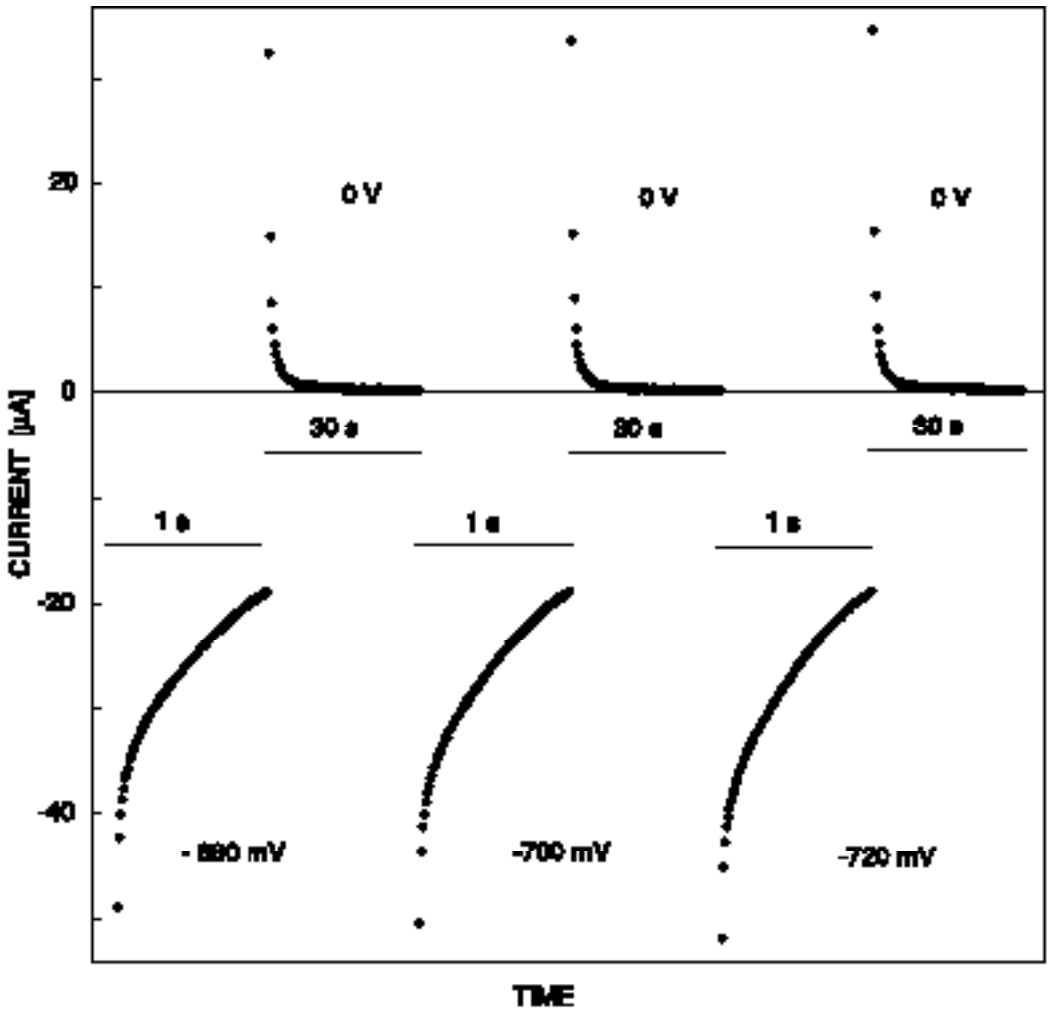

Fig. 2-2 Current responses for experiment shown in Figure 2-1 in the indicated potential range (limiting current).

Figure 2-2 shows the current response upon three applied potentials of increasing magnitude, separated by a longer baseline potential, in the range of the limiting current (-500 mV). Obviously, the current decays continuously within one pulse and does not appear to reach a limiting value. With classical amperometric metal electrodes, the limiting current is given by mass transport from the sample bulk to the electrode surface, and the processes can be described in an analogous fashion. In that case, however, a steady-state concentration profile across the stagnant diffusion layer, and hence a steady-state current, is eventually achieved. Here, it is believed that the rate limiting step is diffusion into the membrane interior. Diffusion coefficients are known to be rather small (on the order of 10^{-8} cm^2 s^{-1}),[19] and the membrane thickness is on the order of 200 μm. It would take many hours to reach a steady-state current. In principle, the current response for this situation (at the limiting current) may be described in complete analogy to a potential step experiment with a classical metal electrode: the interfacial concentration is suddenly forced from zero to a constant value due to the applied potential, and the current is given by diffusion of the reaction product away from the interface into the sample bulk. The Cottrell equation is known to describe this process (it is normally formulated to describe a potential step experiment at a metal electrode):

$$i(\mathrm{t}) = \frac{nFAD^{1/2}C^*}{\pi^{1/2}t^{1/2}} \qquad (2.1)$$

where i(t) is the observed current as a function of time, n is the number of electrons (in this case, the charge of +1 of the hydrogen ion), F is the Faraday constant, A is the surface

area of the electrode, D is the diffusion coefficient, C^* is the constant phase boundary concentration of the diffusing species (in this case that of the protonated chromoionophore), and t is the time after applying the potential step. With the experiment shown in Fig. 2-2, the interfacial concentration C^* in Equation 2.1 is approximated by the chromoionophore concentration (assuming that the diffusion coefficients of protonated and unprotonated chromoionophore are similar). The corresponding Cottrell fit (current versus the inverse of the square root of time) for the uptake current at -700 mV is shown in Fig. 2-3. A linear relationship is found at times larger than 200 ms, and a least squares analysis for the last 500 ms of the pulse yields a diffusion coefficient of 1.0×10^{-8} cm^2 s^{-1}. This value is in excellent correspondence with literature values found under zero-current conditions.[19] This suggests that electrical migration is a minor contribution to the mass transport of the protonated chromoionophore in the membrane, likely because of the very high concentrations of inert lipophilic salt used in the membrane. In this experiment, the influence of the iR drop across the membrane bulk was not compensated for, and this could introduce an error. However, in the limiting current region, this error is expected to have only a small influence on the Cottrell experiment since a small change in the applied phase boundary potential would have little consequence on the phase boundary concentration of the diffusing species. This would not be the case with potential values outside the limiting current window. The Cottrell experiment was only analyzed at times larger than 0.5 s, where the current decay was comparatively small. With a membrane resistance of 10 kΩ,

the observed current change of 8 μA (see Figures 2-2 through 2-4) would give a potential change of ca. 80 mV. This is much smaller than the width of the limiting current plateau (see Fig. 2-1) and perhaps sufficiently small to ensure that the phase boundary concentrations did not change appreciably in the course of the experiment.

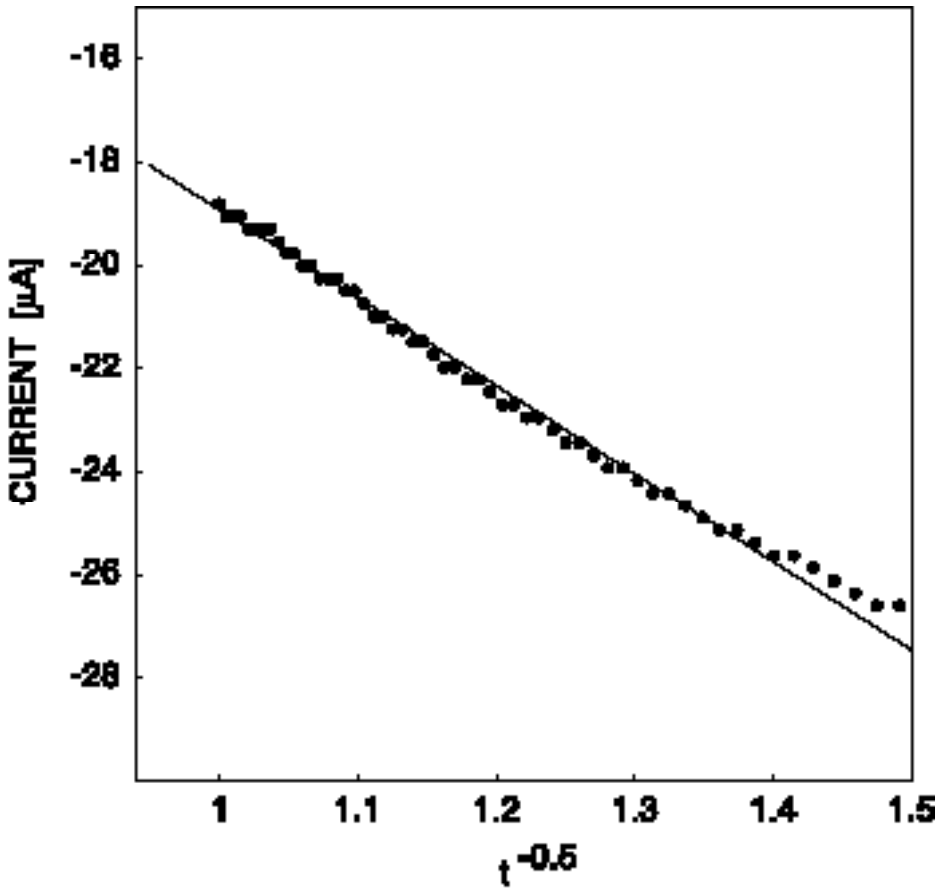

Fig. 2-3 Cottrell fit for current response shown in Figure 2-2 upon application of a -700 mV potential pulse (see Equation 2-1). Other conditions as in Figure 2-1.

The hydrogen ion extraction and diffusion processes into polymeric membranes doped with ETH 5294 upon the application of an external voltage were further studied by direct spectroscopic imaging. In analogy to earlier zero-current experiments,[19] the setup involved a ring-shaped ion-selective membrane that could be imaged under the microscope. The ring membrane separated two buffered solutions that were each in contact with a working and a pair of reference and counter electrodes, in similar to earlier reports.[22] Time-dependent absorbance spectra were recorded with an optical microscope fitted with a UV/Vis spectrometer and CCD detector.

Figure 2-4 shows spatially resolved absorbance spectra as a function of time upon the application of a constant potential of -500 mV. The profiles were described with the known diffusion equation:[31]

$$A(x,t) = A_l \frac{x}{l} + \frac{2}{\pi} \sum_{n=1}^{\infty} \frac{A_l \cos(n\pi)}{n} \sin\left(\frac{n\pi x}{l}\right) \exp\left(-\frac{Dn^2\pi^2 t}{l^2}\right) \qquad (2.2)$$

where A(x,t) is the absorbance as a function of distance x from the interface and time t and A_l is the absorbance of the disturbance at distance, *l*, and D is the diffusion coefficient.

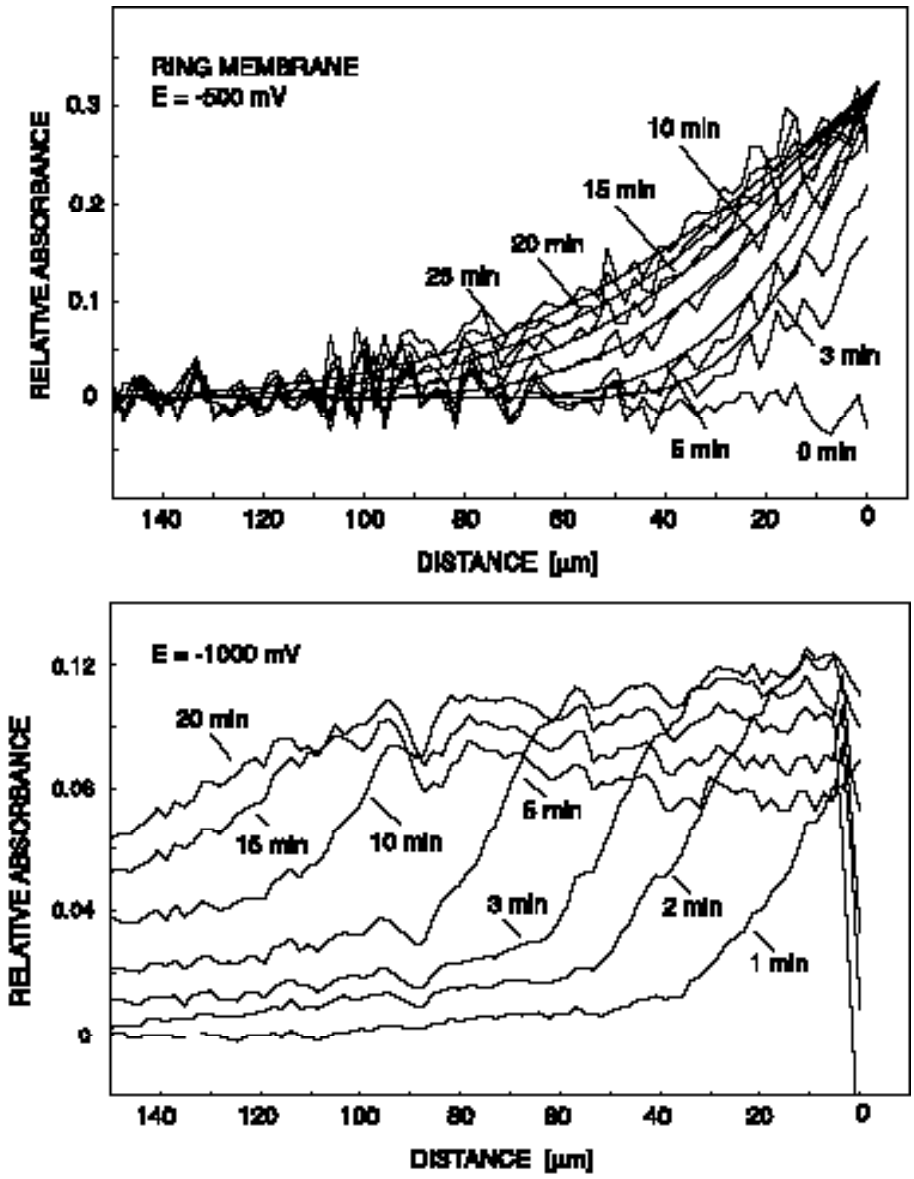

Fig. 2-4 Time dependent absorbance of a PVC-NPOE memnbrane containing ETH 5294 (protonated form, at 650 nm) in contact with a pH 6.8 solution upon external application of a single (top) -500 mV or (bottom) -1000 mV potential pulse. Solid lines in top figure according to Equation 2.2.

All theoretical curves shown in Fig. 2-4 were obtained with Eq 2.2, with the parameters D_{org} = 1.05 x 10^{-8} cm^2 s^{-1} and l = 0.10 cm. Obviously, all theoretical curves originate at the same calculated point at the interface, suggesting that this experiment was performed in the limiting current region where all chromoionophore molecules at the interface become protonated. Note that it is impossible in this experiment to accurately image the surface region spectroscopically because of optical scattering effects.[19] The diffusion coefficient obtained from this experiment is in good agreement with literature values obtained under zero-current condition,[19] and is also in excellent agreement with the Cottrell fit discussed above. Consequently, the earlier notion that such polymeric membrane electrodes function according to mass transport processes within the polymer phase, not the sample phase, appears to be consistent with the experimental data obtained here.

Figure 2-4 (bottom) shows the same experiment as for the top figure, but at a more extreme potential of -1000 mV. Here, obviously, the concentration profile appears to be different from the ideal case shown in Fig. 2-4 (top). The protonated chromoionophore starts to assume its maximum value for an increasingly larger distance away from the interface as time progresses. This can be explained by the substantial extraction of uncomplexed hydrogen ions into the membrane owing to the more extreme applied potential. In this case, the proton gradient would no longer be dictated by the gradient of protonated chromoionophore alone. Diffusion appears to be much more rapid than for the case shown in Fig. 2-4 (bottom). Similar effects have been observed earlier in

zero-current transport experiments of simple acids in membranes containing this chromoionophore. This behavior is also fully in line with the earlier interpretation of the extraction of undissociated electrolyte at potentials beyond the limiting current region. Note that the phase boundary concentration of protonated chromoionophore continuously decreases with time. This effect is believed to reflect a gradual concentration polarization of total chromoionophore in the membrane, which originates from membrane transport effects.[32] While this principle does not appear to be problematic in the normal function of amperometric ion sensors, which are pulsed at short times, it has been used by Lindner[33] to estimate the concentration of membrane components remaining in the membrane. Also note that the potentials applied in the ring membrane experiments are not directly comparable to the ones applied in the Philips electrode body because of the differences in the experimental setup (different membrane resistance and non-uniform membrane thickness owing to the ring shape, and a smaller concentration of chromoionophore). Unfortunately, the non-uniform membrane thickness and lower ionophore concentration made it difficult to record useful normal pulse voltammograms directly with the ring-shaped membranes, which would have enabled a direct correlation between spectroscopic imaging information and amperometric response. Nonetheless, the correlation to separate amperometric experiments appears to be convincing.

The basic mechanism of the amperometric sensors studied here can be summarized as follows. Upon the application of a given interfacial potential, ions are forced to partition from the sample into the organic phase boundary region in order to satisfy the

phase boundary potential condition. Since the sample solution is well buffered, ion depletion on the sample side is unimportant. Instead, ions extracted into the polymeric membrane phase will spontaneously diffuse in direction of the membrane bulk, which is devoid of those ions. This ion flux leads to a replenishment at the phase boundary, which dictates the observed current. Initially, at mild potentials, the extraction and diffusion of ions in the polymeric membrane is assisted by the neutral ionophore. As the applied potential increases, the ionophore will eventually saturate, that is, there will be a limiting concentration of ionophore at the phase boundary beyond which no hydrogen ions can be extracted into the polymeric membrane. This defines the limiting current. In this potential range, the observed current decay for a given pulse can be adequately described with the Cottrell equation because the phase boundary concentration of ionophore is constant as a function of time. Further increase of the applied potential leads eventually to the extraction of uncomplexed ions that no longer require the assistance of the ionophore to be extracted into the polymer. In order to obtain repeatable current readings in a practical experiment, normal pulse voltammetry is a recommended method.[23] The baseline potential applied intermittently will allow the ions extracted during a previous applied potential pulse to be adequately displaced again from the membrane.

If these notions are accurate, it should be possible to use such membranes containing a H^+-ionophore to measure pH voltammetrically. Indeed, the phase boundary concentration of extracted ions is thought to depend directly on the applied interfacial potential and the pH. If the membrane is effectively renewed before a given applied

potential so that the membrane diffusion layer thickness is always identical, the resultant current should be a direct function of pH. This is in agreement with recent theory describing standard hydrogen ion transfer potentials in biphasic systems containing a lipophilic base.[34] Figure 2-5 shows different normal pulse voltammetric response curves as a function of the sample pH. Obviously, the half-wave potentials appear to be directly dependent on pH. At those equal half-wave potential currents, the phase boundary concentration of extracted hydrogen ions is thought to be identical from voltammogram to voltammogram. Consequently, they should ideally represent a direct Nernstian relationship between half-wave potential and the sample pH, in accordance to the phase boundary potential equation. The half-wave potentials (at the constant current of -10 μA) are separately plotted as a function of the sample pH in Figure 2-6, lower trace. The relationship is indeed Nernstian in a wide pH range, with an experimental slope of -58.5 mV pH^{-1}. Interestingly, the same membranes were found to show very poor slopes of ca. -15 mV pH^{-1} when measured potentiometrically. Indeed, these membranes contain no deliberately added ion-exchanger, but a very high concentration of inert lipophilic salt, and are therefore not optimized for potentiometric experiments. The complete lack of pH response can probably be best explained by some leaching of the tetraphenylborate from the membrane, thus creating a membrane with gradual anion-exchange, rather than cation-exchange properties, or by the presence of some impurities. In contrast, the voltammetric response is analyzed at relatively high currents where a small residual ion-exchange property of the membrane is without consequence. Indeed, a visual inspection of the

applied potentials in Fig. 2-4 required to reach much smaller currents, below 1 µA, suggests that pH response is much less sensitive in this range, which is consistent with the potentiometric results. Since the half-wave potentials represent the point where the ionophore is thought to be half-protonated at the phase boundary (giving half the limiting current), the voltammetric response was compared to potentiometric measurements on membranes that contained 50 mol-% cation-exchanger with otherwise the same composition. The potentiometric response is shown in the upper trace Fig. 2-6 and is now nearly identical to the voltammetric pH responses shown in the same figure.

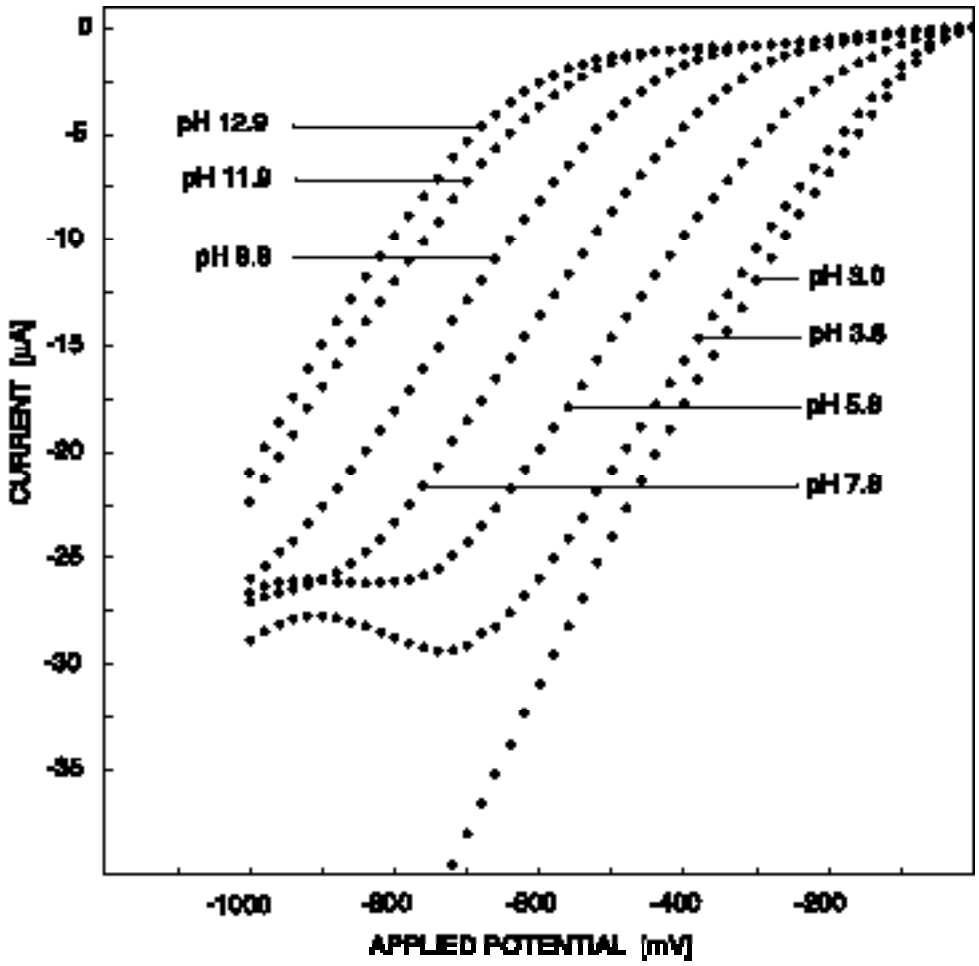

Fig. 2-5 Normal pulse voltammograms for a PVC-NPOE membrane containing ETH 5294 and the inert lipophilic salt ETH 500 in contact with sample solutions of various pH. Other conditions as in Figure 2-1.

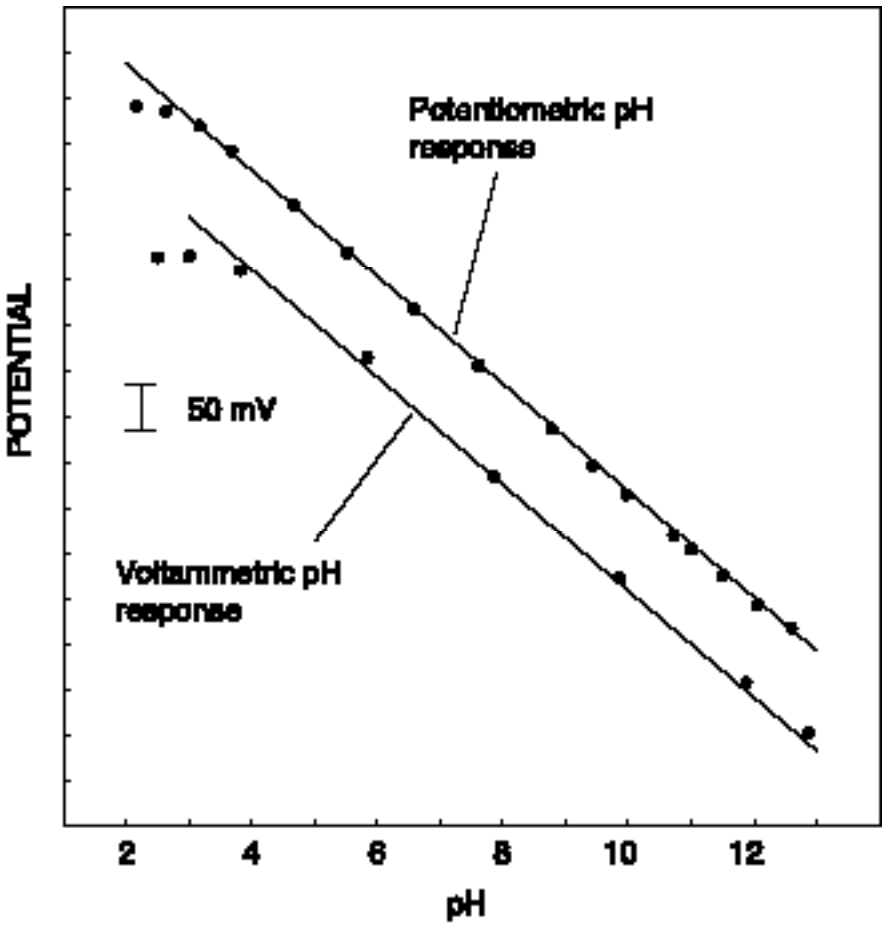

Fig. 2-6 Bottom data: galvanostatic potential values (at i = -10 µA) of data shown in Figure 2-5 as a function of the sample pH. Solid line with slope of -58.5 mV/pH. Top data: Potentiometric zero-current response of corresponding ion-selective membrane containing the cation-exchanger NaTFPB in addition to ETH 5294.

The normal pulse voltammograms as shown in Figure 2-5 start to exhibit unusual behavior at low pH. The limiting current gradually starts to increase at pH 4 until, at pH 3, a complete loss of any limiting current is observed. Although this seems to be very surprising at first, it can be explained by comparing it to the known behavior of the potentiometric and optical counterparts at low pH. If no external potentials are applied, PVC–NPOE membranes containing the ionophore ETH 5294 are known to exhibit anion-interference starting around pH 3.5 (see Fig. 2-6, upper trace). This originates from a spontaneous coextraction of protons and chloride ions into the polymeric membrane.[35] With ion-selective electrodes, this results in a breakdown of the Nernstian pH response slope and defines the upper detection limit (see Fig. 2-6). With the voltammetric sensors discussed here, spontaneous coextraction of electrolyte into the membrane effectively renders the interface non-polarizable: a substantial phase boundary concentration of hydrogen ions is spontaneously present at all times at both sides of the interface. This leads to a featureless voltammetric response curve and to breakdown of the Nernstian pH response range as well (see Figs 2-4 and 2-5). Voltammetric sensors appear to be more susceptible to this effect than their potentiometric counterparts, since the latter show a Nernstian response that are extended by about a one pH unit (see Fig. 2-6).

2.4 Conclusions

Spectral imaging experiments on amperometric hydrogen ion sensing membranes revealed that the limiting current region of the voltammogram is given by saturation of the ionophore at the phase boundary. The time-dependent diffusion profiles could be conveniently correlated to common diffusion theory, and yielded diffusion coefficients that agreed with experiments on ion-selective membranes under zero-current conditions. The imaging results also suggested that the observed current decay curves under the same conditions may be described by the Cottrell equation, and the correspondence was indeed good, with very similar diffusion coefficients as for the imaging experiments. This good correlation suggested that the underlying response principles of the amperometric ion sensors are well understood. As expected, and in contrast to regular amperometric sensors, the voltammetric responses were analyzed galvanostatically and found to relate to the sample pH in a Nernstian fashion. Their response range was compared to that of the corresponding ion-selective electrodes, and the origin of the upper detection limit at low pH was discussed. The response characteristics and diffusion profile measurements obtained here are in agreement with the expected response mechanism formulated earlier.

References

1 Samec, Z.; Marecek, V.; Koryta, J.; Khalil, M.W. *J. Electroanal. Chem.* **1977**, *83*, 393.

2 Lee, H.J.; Beriet, C.; Girault, H.H. *J. Electroanal. Chem.* **1998**, *453*, 211.

3 Lee, H.J.; Girault, H.H. *Anal. Chem.* **1998**, *70*, 4280.

4 Beriet, C.; Girault, H.H. *J. Electroanal. Chem.* **1998**, *444*, 219.

5 Henn, D.; Cammann, K. *Electroanalysis* **2000**, *12*, 1263.

6 Horvath, V.; Horvai, G.; Pungor, E. *Mikrochim. Acta* **1990**, *I*, 217.

7 Horvath, V.; Horvai, G. *Anal. Chim. Acta* **1993**, *273*, 145.

8 Marecek, V.;Janchenova, H.; Brezina, M. *Anal. Chim. Acta* **1991**, *244*, 15.

9 Osakai, T.; Nuno, T.; Yamamoto, Y.; Saito, A.; Senda, M. *Bunseki Kagaku* **1986**, *38*, 479.

10 Osakai, T.; Kakutani, T.; Senda, M. *Bunseki Kagaku* **1984**, *33*, E371.

11 Sawada, S.; Torii, H.; Osakai, T.; Kimoto, T. *Anal. Chem.* **1998**, *70*, 4286.

12 Langmaier, J.; Stejskalova, K.; Samec, Z. *J. Electroanal. Chem.* **2001**, *496*, 143.

13 Koryta, J.; Vanysek, P.; Brezina, M.; *J. Electroanal. Chem.* **1977**, *75*, 211.

14 Cosofret, V.V.; Ernosy, M.; Johnson, T.A.; Buck, R.P.; Ash, R.B.; Neuman, M.R. *Anal. Chem.* **1995**, *67*, 1647.

15 Lee, H.J.; Pereira, C.M.; Silva, A.F.; Girault, H.H. *Anal. Chem.* **2000**, *72*, 5562.

16 Roberts, M.A.; Rossier, J.S.; Bercier, P.; Girault, H.H. *Anal. Chem.* **1997**, *69*, 2035.

17 Rossier, J.S.; Roberts, M.A.; Ferrigno, R.; Girault, H.H. *Anal. Chem.* **1999**, *71*, 4294.

18 Marecek, V.; Colombini, M.P. *J. Electroanal. Chem.* **1988**, *241*, 133.

19 Schneider, B.; Zwickl, T.; Federer, B.; Pretsch, E.; Lindner, E. *Anal. Chem.* **1996**, *68*, 4342.

20 Jadhav, S.; Bakker, E. *Anal. Chem.* **1999**, *71*, 3657.

21 Koryta, J.; Du, G.; Ruth, W.; Vanysek, P. *Faraday Discuss. Chem. Soc.* **1984**, *77*, 209.

22 Jadhav, S.; Bakker, E. *Anal. Chem.* **2001**, *73*, 80.

23 Jadhav, S.; Meir, A.J.; Bakker, E. *Electroanalysis* **2000**, *12*, 1251.

24 Bakker, E.; Lerchi, M.; Rosatzin, T.; Rusterholz, B.; Simon, W. *Anal. Chim. Acta* **1993**, *278*, 211.

25 Cosofret, V.V.; Nahir, T.M.; Lindner, E.; Buck, R.P. *J. Electroanal. Chem* **1992**, *327*, 137.

26 Tsagkatakis, I.; Pepper, S.; Bakker, E. *Anal. Chem.* **2001**, *73*, 315.

27 Bakker, E.; Pretsch, E. *Anal. Chem.* **1998**, *70*, 295.

28 Seiler, K.; Simon, W. *Anal. Chim. Acta* **1992**, *266*, 73.

29 Lindner, E.; Zwickl, T.; Bakker, E.; Lan, B.T.T.; Tóth, K.; Pretsch, E. *Anal. Chem.* **1998**, *70*, 1176.

30 Qin, Y.; Bakker, E. *Talanta* **2002**, *58*, 909.

31 Crank, J. *The Mathematics of Diffusion* New York **1993**.

32 Iglehart, M.L.; Buck, R.P.; Horvai, G.; Pungor, E. *Anal. Chem.* **1988**, *60*, 1018.

33 Pendley, B.D.; Lindner, E. *Anal. Chem.* **1999**, *71*, 3673.

34 Gobry, V.; Ulmeanu, S.; Reymond, F.; Bouchard, G.; Carrupt, P-A.; Testa, B.; Girault, H.H. *J. Am. Chem. Soc.* **2001**, *123*, 10684.

35 Bakker, E.; Nägele, M.; Schaller, U.; Pretsch, E. *Electroanalysis* **1995**, *7*, 817.

Chapter 3

Voltammetric Screening of Ionophores in Ion-Selective Polymeric Membranes

3.1 Introduction

In recent years, a variety of methods have become available to assess the complex formation constants of highly selective hydrophobic receptor molecules (ionophores) in solvent polymeric sensing membranes.[1] Such ionophores are responsible for the selective recognition process in a variety of chemical sensors, and the resulting selectivity is directly related to the extraction of ions into and complexation with an ionophore within a polymeric membrane phase. Since the sensing selectivity reflects the competitive extraction between sample ions, selectivity determinations alone are not sufficient to assess the binding constants of ionophores.

Earlier methods focused on determinations of complex formation constants in model solvents only, and were of limited value to the chemical sensing field since a quantitative correlation to sensing selectivity was not generally possible. More recent research has introduced new methods that allow one to perform such measurements in actual ion-selective membrane phases. One method involves optical or potentiometric experiments on membranes containing an ideally selective reference ionophore (typically a H^+-ionophore) in addition to the ionophore to be measured.[2,3] The interference from H^+ is quantified and related to the complex formation constant of the ionophore with a reference experiment on a membrane without the ionophore of interest. A second method utilizes unbiased selectivity determinations on regular membranes, without any reference ionophore, relative to a reference ion in the sample (such as tetramethylammonium) assumed not to interact with the ionophore. This method was utilized, for example, for the characterization of Pb^{2+} ionophores where the assumption most likely holds.[4] The third method is the so-called sandwich membrane method, where the experimental zero current potential of a concentration polarized membrane is related to the activity ratio in both membrane segments.[5,6] Since the total concentration in each segment is known (only one side contains the ionophore), the membrane potential may be related to the effective complex formation constant in the membrane. All three methods have been shown to give comparable results. While the last one is experimentally more complicated than the other two, it is the most general method and, if properly performed, gives reproducibilities on the order of just a few millivolts.

Voltammetric measurements at the interface of two immiscible electrolyte solutions (ITIES) has also been used in the past to assess binding constants of ionophores in organic phases. This approach was mainly utilized by Koryta[7] and later also by others.[8,9] The applied interfacial potential forces the transfer of sample ions into the organic phase, which occurs at smaller values if this process is assisted by an ionophore in the organic phase. This decrease in the effective free energy of transfer is a measure of the complex formation constant. Senda has recently summarized how different experimental protocols can be used to assess ionophore binding constants in the organic phase.[10] The final equation that relates the binding constant to the shift in the half-wave potential depends primarily on the mechanism that limits the observed current in the voltammetric experiment. The simplest and most direct relationship may be observed if the current is limited by mass-transport processes in the organic, not the aqueous phase.

Since the days of Koryta, the fields of ion-selective electrodes and the ITIES community have undegone separate developments with rather limited scientific contact. Consequently, a direct comparison of voltammetric and potentiometric techniques to assess ionophore binding constants has not been performed. Recently, our group has reported on how voltammetric ion-selective electrodes based on essentially unmodified plasticized poly(vinyl chloride) membranes can be fabricated and characterized. This chapter offers an evaluation of a rapid voltammetric screening technique for ionophores and quantitatively compares the results to established potentiometric protocols.

3.2 Theory

The basic response theory of pulsed voltammetric ion-selective electrodes has been described before and is here extended to multivalent ions in view of determining ionophore complex formation constants. Upon discrete negative potential pulses, cations from the sample and anions from the inner filling solution are transferred into the membrane and the resulting current is measured. Between each uptake potential pulse, a baseline potential is applied for a sufficiently long time to effectively remove all of the previously extracted ions back into the sample and inner filling solutions. This provides for a reproducible phase boundary prior to the next pulse. In order to present a theoretical treatment of the responses of these sensors, it is assumed that the Nernst diffusion layer thickness is constant prior to each uptake pulse. Using the segmented potential model, the membrane potential E_M is subdivided into the sample-membrane phase boundary, E_{PB}, the membrane-inner filling solution phase boundary, $E_{PB'}$, and the membrane internal potential:

$$E_M = E_{PB} + E_{PB'} + iR_{bulk} \tag{3.1}$$

where i and R_{bulk} are the observed current and membrane resistance, respectively. Due to the relatively high concentration of the primary ion in the aqueous phase and the relatively small diffusion coefficients of the ions in the plasticized polymer membranes, the current i is assumed to be limited by the diffusion of the extracted ions from the phase

boundary into the bulk of the membrane. Here, we assume that the diffusion of complexed and uncomplexed primary ions have equal diffusion coefficients (*D*) within the membrane. This approximation is a possible source of error compared to the potentiometric methods discussed above. By knowing the exposed area of the electrode membrane and assuming that the bulk concentrations of complexed and uncomplexed ions in the bulk membrane are much smaller than the phase boundary concentrations, the current can be described as:

$$i = -\frac{AFDz}{\delta}\sum_{n=0}^{n_{max}} c_{IL_n}(pb) \tag{3.2}$$

where $c_{ILn}(pb)$ are concentrations of the different primary ion complexes in the membrane phase boundary (with any stoichiometry n; n = 0 denotes the uncomplexed ion), z is the charge of the primary ion.

To satisfy electroneutrality, for every cation extracted into the membrane from the sample side of the interface there must also be an anion extracted into the membrane from the inner solution side of the interface. Assuming that the anions are not complexed by the ionophore, the charge balance equation can be written as:

$$c_A(pb)^{\cdot} = z\sum_{n=0}^{n_{max}} c_{IL_n}(pb) \tag{3.3}$$

where $c_A(pb)^{\cdot}$ represents the anion concentration at the membrane-inner solution phase boundary. For the remainder of this chapter, the label (pb) will be omitted and it should

be assumed that all concentrations refer to phase boundary concentrations unless stated otherwise.

The amount of complexed primary ion that exists in the membrane is given by the complex formation constant:

$$\beta_n = \frac{c_{IL_n}}{c_I c_L{}^n} \tag{3.4}$$

where c_L is the concentration of uncomplexed ionophore. The mass balance equation for the total ionophore in the membrane, L_T, is written as:

$$L_T = c_L + \sum_{n=0}^{n_{max}} n c_{IL_n} \tag{3.5}$$

It is well established that the phase boundary potential at the sample-membrane interface is a function of any ion existing in two phases in contact with each other and can be described by the following equation in which an applied potential changes the ratio between the two phases:

$$E_{PB} = \frac{RT}{zF} \ln \frac{k_I a_I(aq)}{c_I(org)} \tag{3.6}$$

where R, T and F have their usual meanings, a_I(pb,aq) and c_I(pb,org) are the activity and concentration of the uncomplexed ion, I, in the aqueous and organic phase boundaries,

respectively, and k_I is a direct measure of the standard chemical potential difference of I in both phases. The second phase boundary potential can be expressed as:

$$E_{PB'} = \frac{RT}{F} \ln \frac{k_A a_A(aq)'}{c_A(org)'} = \frac{RT}{F} \ln \frac{k_A a_A(aq)'}{z \sum_{n=0}^{n_{max}} c_{IL_n}(org)} \tag{3.7}$$

where the prime (') refers to the inner side of the membrane. In principle, equations (3.1), (3.2), 3.4), (3.5), (3.8) and (3.9) describe the current–potential relationship for a normal pulse voltammetry experiment in sufficient detail to extract complex formation constants (β_n is assumed to be independent of the applied potential for a given pulse duration). Explicit equations, however, can be obtained after some simplification. If one assumes only one stoichiometry, n, of the ionophore complex, and one considers that at currents below the limiting current, $[I^{z+}]$ must be much smaller than $[IL^{z+}]$, the membrane potential is written by inserting the simplified Equations (3.4), (3.6) and (3.7) into Equation (3.1):

$$E_M(\text{low } i) = \frac{RT}{zF} \ln \frac{k_I a_I(aq) \beta_n c_L{}^n}{c_{IL_n}} + \frac{RT}{F} \ln \frac{k_A a_A(aq)'}{z c_{IL_n}} + iR_{bulk} \tag{3.8}$$

The current–potential relationship at low currents is then obtained by inserting Equation (3.2) into (3.8):

$$E_M(\text{low } i) = \frac{RT}{zF} \ln \frac{-k_I a_I(aq) \beta_n (L_T + ni\delta/AFDz)^n}{i\delta/AFDz} + \frac{RT}{F} \ln \frac{-k_A AFD a_A(aq)'}{i\delta} + iR_{bulk} \tag{3.9}$$

At currents higher than the limiting current, all ionophore is assumed to be in the complexed form, and uncomplexed ions, I, are allowed to be extracted. Consequently, the membrane potential is written as:

$$E_{\mathrm{M}}(\text{high } i) = \frac{\mathrm{RT}}{z\mathrm{F}} \ln \frac{k_{\mathrm{I}} a_{\mathrm{I}}(\mathrm{aq})}{c_{\mathrm{I}}} + \frac{\mathrm{RT}}{\mathrm{F}} \ln \frac{k_{\mathrm{A}} a_{\mathrm{A}}(\mathrm{aq})^{\cdot}}{z(c_{\mathrm{I}} + \mathrm{L_T}/\mathrm{n})} + iR_{bulk} \tag{3.10}$$

For this case, the current–potential relationship is again obtained by inserting the simplified Equation (3.2) into Equation (3.10):

$$E_{\mathrm{M}}(\text{high } i) = \frac{\mathrm{RT}}{z\mathrm{F}} \ln \frac{-k_{\mathrm{I}} a_{\mathrm{I}}(\mathrm{aq})}{\dfrac{i\delta}{\mathrm{AFD}z} + \mathrm{L_T}/\mathrm{n}} + \frac{\mathrm{RT}}{\mathrm{F}} \ln \frac{-k_{\mathrm{A}} \mathrm{AFD} a_{\mathrm{A}}(\mathrm{aq})^{\cdot}}{i\delta} + iR_{bulk} \tag{3.11}$$

The limiting current, i_l, is assumed to describe the situation where the ionophore is fully complexed:

$$i_{\mathrm{l}} = \frac{\mathrm{ADF}z}{\mathrm{n}\delta} \mathrm{L_T} \tag{3.12}$$

Since $\mathrm{L_T}$ is known, the experimentally determined limiting current may be used to estimate the value of AFD/δ in Equations (3.9) and (3.11).

3.3 Experimental

Reagents. Valinomycin was obtained from Aldrich (Milwauke, WI). All other reagents and membrane components were obtained from Fluka Chemical Corp. (Milwaukee, WI). The salts used for aqueous solutions were puriss quality or better and dissolved in Nanopure distilled water. High molecular weight poly(vinyl chloride) (PVC), *o*-nitrophenyl octyl ether (NPOE), tetradodecylammonium tetrakis(4-chlorophenyl) borate (ETH500), selectophore grade tetrahydrofuran (THF), Fluka sodium ionophore ten, Fluka potassium ionophore three (BME-44), Fluka calcium ionophore two (ETH 129), Fluka potassium ionophore two (K-II), Fluka sodium ionophore three (ETH 2120), Fluka lithium ionophore three (ETH 1810) and Fluka calcium ionophore four (ETH 5234) were also used.

Membrane Preparation. Amperometric ion-selective membranes were prepared by dissolving PVC and NPOE (1:2 by weight), 10% by weight ETH500 and 10mmol/Kg of the selected ionophore into 1.5 mL of selectophore grade THF. This cocktail was shaken mechanically for ten minutes and then poured into a glass ring mounted on a microscope slide with an inner diameter of 22 mm. The THF was allowed to evaporate overnight leaving a membrane approximately 200 μm thick.

Experimental Setup. A model AFRDE5 potentiostat (Pine Instruments, Grove City, PA) was used with a three electrode system to measure current versus an applied

potential. The data was recorded using LabView 5.0 program (National Instruments, Austin, TX) on a Macintosh computer equipped with a 16-bit data acquisition board (National Instruments, Austin, TX). A saturated KCl, Ag/AgCl reference electrode containing a 1.0 M lithium acetate bridge electrolyte and a Pt cage counter electrode were immersed in the sample with the working electrode. The working electrodes were prepared by mounting a piece of the ion-selective membrane onto a Philips body electrode (IS-561, Glasbläserei Möller, Zürich, Switzerland) with an i.d. of 4.0 mm and conditioning the electrode overnight in the inner filling solution (0.1 M NaCl except for the sodium ionophore X which was conditioned in 0.1 M KCl). A one-second-uptake pulse at a specified potential was followed by a 30 second stripping pulse at 0.0 V. The current measurements were taken as the average of the last 100 ms of each uptake pulse.

3.4 Results and Discussion

Under an applied potential, charged species can be transferred across an interface between two phases in a selective manner by incorporating a molecule (see ionophores used in this chapter, Figure 3-1) in one phase that effectively lowers the Gibbs standard energy of transfer of the ion.[11,12] Here, the interface is between a solvent polymeric membrane doped with an ionophore and an aqueous solution containing the primary ion that binds selectively to the ionophore. It is the binding characteristics of these ion-ionophore complexes that we wish to study by using normal pulse voltammetry (NPV).

Upon application of a negative potential, cations from the aqueous solution are forced into the membrane where they are complexed by the ionophore. Figure 3-2 shows both the experimental and theoretical current-potential curves using NPV on the interface between 0.1 M KOAc aqueous solution and a NPOE-PVC-ETH 500 membrane doped with 10 mmol/kg of the potassium selective ionophore BME-44. The inner solution in this case was a 0.1 M NaCl aqueous solution. According to theory, there are three regions of this curve that should be distinguished, the potentials below the limiting current (Eq. 3.9), after the limiting current (Eq. 3.11) and at the limiting current (Eq. 3.12). The plateau is the diffusion-limited current arising from the processes of diffusion of the uncomplexed ionophore to the interface and the diffusion of the ion-ionophore complex away from the interface, assuming that the ion transfer from the aqueous to the organic phase is not rate limiting. This was confirmed experimentally by altering the KCl concentration, which only decreased the limiting current at concentrations below 1 mM KCl (data not shown). Moreover, the limiting current decreased with decreasing concentration of ionophore in the membrane, as expected by Equation 3.1 (data not shown).

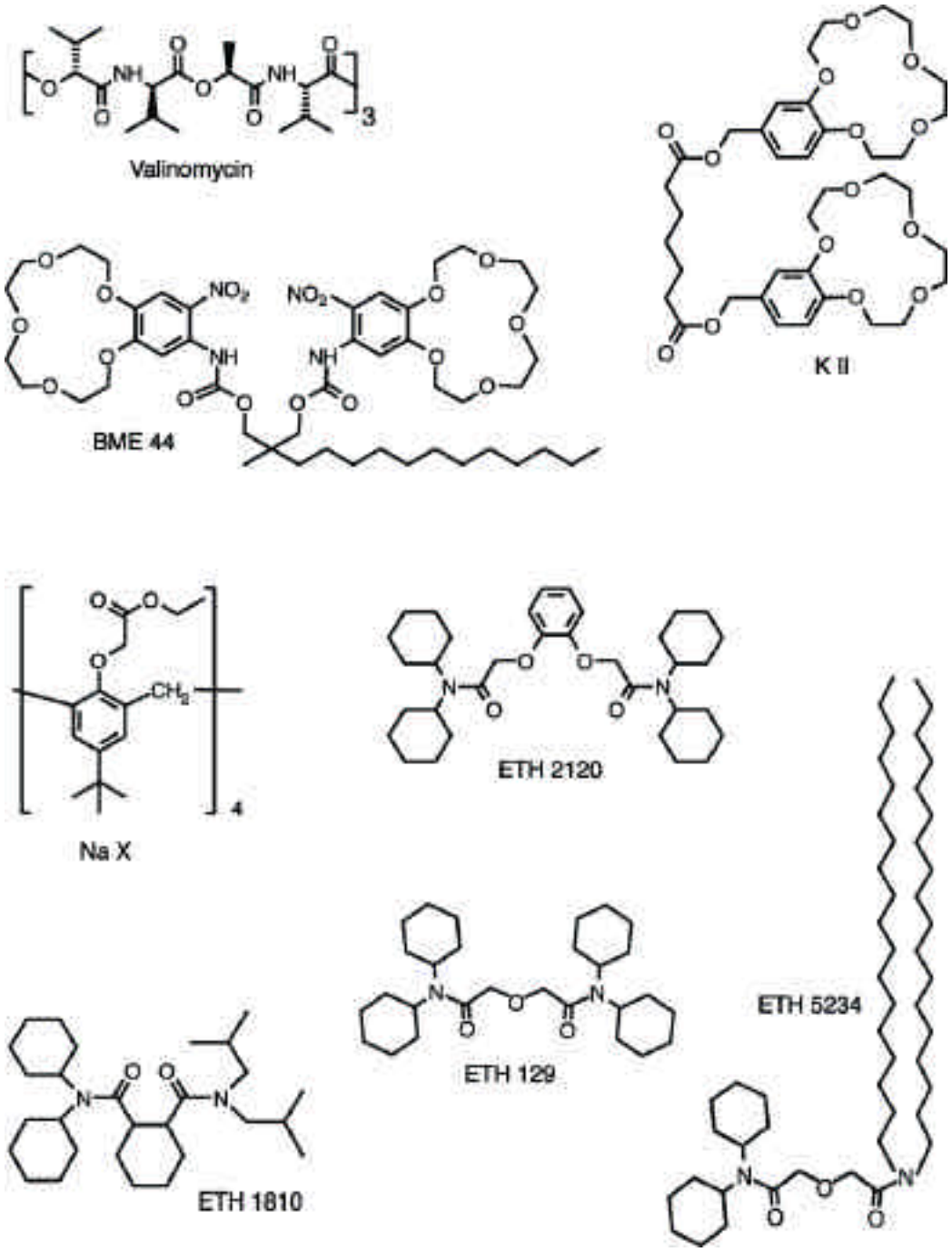

Fig. 3-1 Ionophores considered in this study.

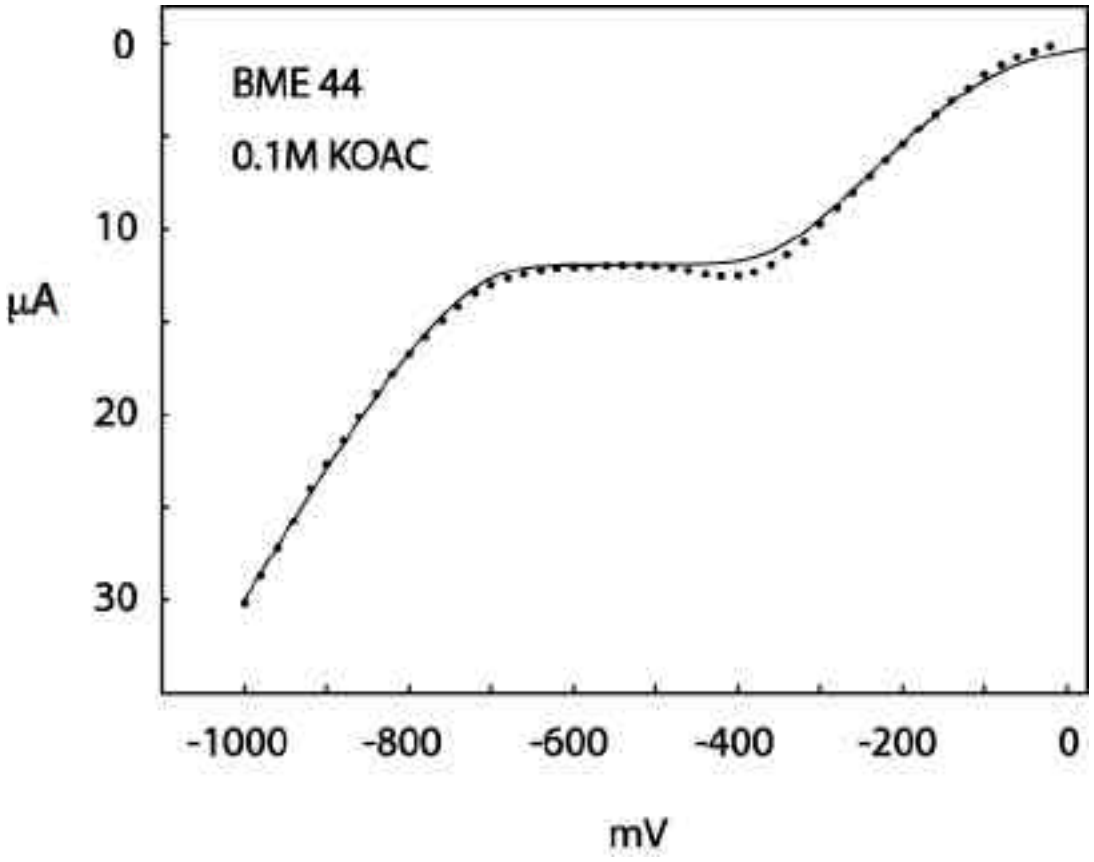

Fig. 3-2 NPV curve shown with theoretical fit for a PVC-NPOE (1:2) membrane containing 9.5 mmol/kg of the potassium iononphore, BME 44, and 10% w/w of the lipophilic salt ETH 500. Each point represents the current from the average of the last 100 milliseconds of each uptake pulse. The NPV scan started at 0 mV and was stepped to -1000 mV in 20 mV increments.

A new voltammetric method is introduced in this chapter to estimate the formation constant between a primary ion and an embedded ionophore within a solvent polymeric membrane. In contrast to previous methods relating differences in potentials[4-6] or absorbance changes[2,3] of separate membranes that depend on reference experiments, carefully buffered solutions and tedious electrode preparation, this method is greatly simplified in its approach. A range of potentials in which the ionophore dominates the extraction and complexation of the primary ion within a single membrane, exhibited by the limiting current plateau, are related through thermodynamic parameters to the complex formation constant. Similar to the other methods, exact concentration of the included neutral ionophore is essential and, in contrast, ion exchange capabilities are not required. Interfering ions are reduced through careful solution preparation and are considered negligible for this NPV experiment. Competing ions and their contribution to the overall potential are a necessity for the other methods, excluding the sandwich membrane technique, along with ion activity ranges that produce valid selectivities. On the other hand, a basic requirement of this method that is not always met is the defining limited current plateau. Without it, values for the complex formation constant can not be estimated using this method.

The observed current–potential curves can be fitted with theory by adjusting several parameters that include the complex formation constant (Eq. 3.4), the coextraction constant $k_I k_A^{z_I}$, the membrane bulk resistance R_{bulk}, and the parameter AFD/δ. This gives a method for estimating the complex formation constant based on data collected

from the NPV scans. As mentioned above, there are three basic regions in these current-potential curves that are separately described by theory (see Figure 3-2), the curve below the limiting current, curve during the limiting current and the curve after the limiting current. As Eq. (3.12) shows, the limiting current may be used to estimate the parameter AFD/δ since the total ionophore concentration is known. It also gives information about the possible complex stoichiometries, n, as a function of the applied potential. Figure 3-2 shows only one limiting current region and therefore just a single complex stoichiometry, n = 1 is assumed for this bis-crown ionophore, as expected. The current-potential curve below the limiting current describes the region where the extracted ions exist in the membrane almost exclusively as complexed ions and the currents increase with increasingly negative applied potentials. After the diffusion limited plateau, the applied potentials are sufficient to force ion transfer of the primary ion without the assistance of the ionophore. The currents again increase, now as a function of the free and complexed primary ions that diffuse into the bulk of the membrane from the interface. Herein lies the principle of this technique. The potential region of the extraction process that is assisted by the ionophore is compared to that of the region where ionophore-mediated extraction is no longer relevant. Figure 3-2 shows the application of the two equations (3.9) and (3.11) used to describe each potential region. After evaluating the term AFD/δ from the limiting current, the potentials at high currents were evaluated first. According to Eq. (3.11), the parameters $k_I k_A^{z_I}$ and R_{bulk}, must be found from the experiment. For the

experiment shown in Figure 3-2, k_A refers to Cl^-, the anion in the inner solution. Recent studies with the so-called segmented sandwich technique have evaluated the coextraction constant of dissociated electrolyte into solvent polymeric membranes. For PVC–NPOE, the value for KCl was found as log $k_K k_{Cl}$ = -12.4, which was obtained indirectly and with membranes without added inert electrolyte.[6] The theoretical curve shown in Figure 3-2 was obtained with log $k_K k_{Cl}$ = -12.6 and with R_{bulk} = 11.2 kΩ. The uncertainty in R_{bulk} directly affects the accuracy of the coextraction constant, which is a limitation of the method that does not exist with the zero-current potentiometry methods. These values were then inserted into Eq. (3.9) to evaluate the potentials at low current. The curve shown in Figure 3-2 was obtained with log β_n = 10.0 which is in agreement with the value found with the sandwich membrane method log β_n = 10.0).[6]

For a potential step experiment, the diffusion-limited current can be described by the Cottrell equation if the interfacial concentrations are unchanged in the course of the experiment, which should be valid in the region of the limiting current:

$$i_l = AFzc_{IL}\sqrt{D/\pi t} \qquad (3.13)$$

In analogy to a planar microelectrode, the interface can be seen as a source of positive charge with the uncomplexed ionophore as the reduced species approaching the interface where it complexes a cation and diffuses away from the interface as an oxidized species. Here, the effects of migration of the ion-ionophore complex are greatly reduced

by the presence of a large excess of the lipophilic salt ETH 500 and we assume that movement of the complex is based on diffusion processes only. This was confirmed earlier with H^+-responsive membranes[13] where imaging experiments confirmed that the ionophore diffusion coefficient was 1.0×10^{-8} cm^2 s^{-1} upon an applied potential of 0.5 V, which was virtually unchanged from its value at zero current. The Cottrell equation provides the current as a function of the sampling time and gives a method for estimating the diffusion coefficients of the charged species in the membrane. In this experiment, a one-second negative uptake potential pulse is applied to the interface in which primary cations are forced into the membrane followed by a 30 s stripping pulse at 0.0 V that should force almost all previously extracted cations back into the contacting aqueous solution.[14,15] This should renew both the Nernst diffusion layer thickness and phase boundary concentration of the primary ion prior to subsequent uptake pulses. The sequence of an uptake pulse followed by a stripping pulse is repeated over the range from 0.0 to -1.0 V with a step of -20 mV. The Cottrell equation predicts that, at the beginning of the one-second uptake pulse, the current should be greatest and should decrease with increasing duration of the pulse. Figure 3-3 shows the Cottrell fit for three uptake pulses at -560, -620 and -700 mV in the region of the limiting current shown in Figure 3-2. In this experiment, we assume that the diffusion coefficients are the same for the complexed and uncomplexed ion in the polymer membrane. The Cottrell equation is valid only in the

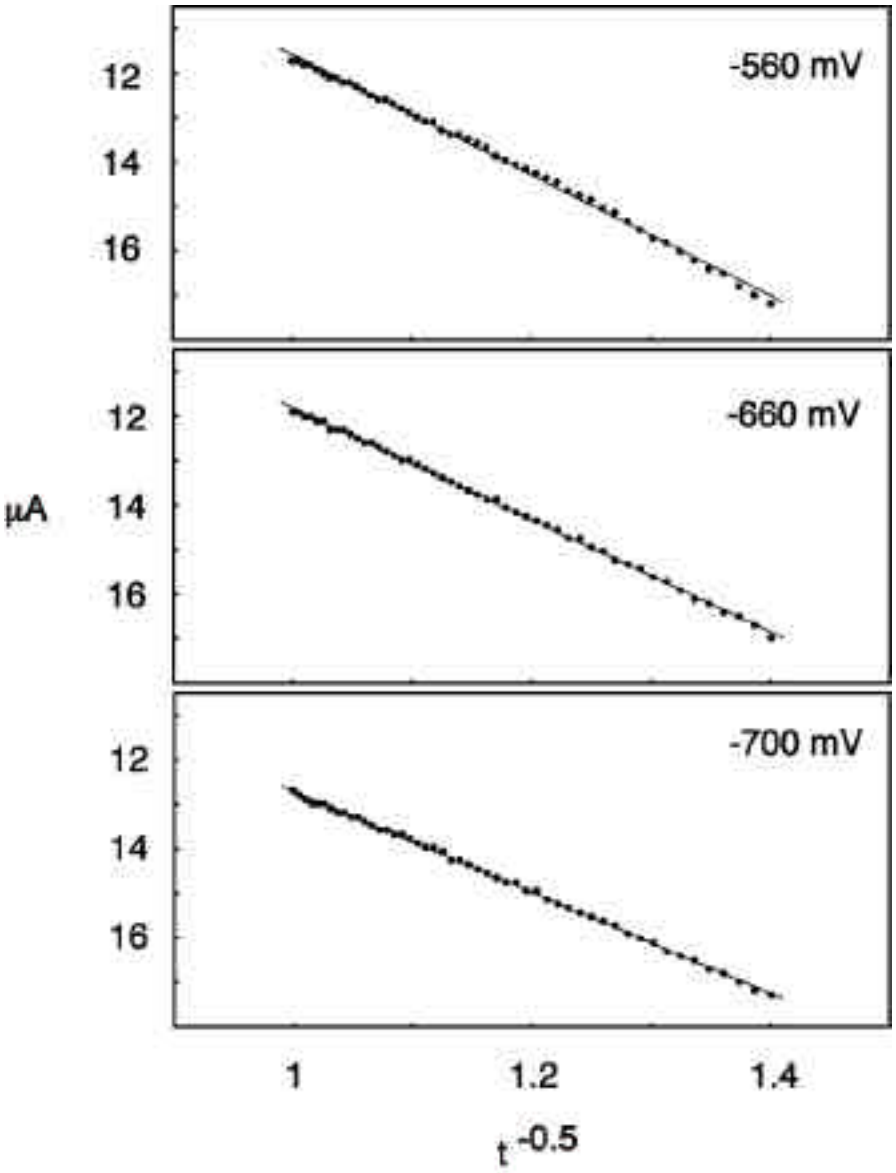

Fig. 3-3 Data points from Fig. 3-2 with Cottrell fits. A value for the diffusion coefficient was estimated for the BME 44/potassium: at -560 mV $D=1.13x10^{-8}cm^2s^{-1}$, at -620 mV $D=9.65x10^{-9}cm^2s^{-1}$ and at -700 mV $D=7.62x10^{-9}cm^2s^{-1}$.

range of potentials in which the current is limited by diffusion, thus, the diffusion coefficients calculated by this method will be heavily weighted towards the complexed ion diffusion coefficient because at these potentials almost all of the primary ion in the membrane exists in the complexed form. The diffusion coefficient for BME-44 was found to be $1.1 \times 10^{-8} cm^2 s^{-1}$.

Figure 3-4 shows normal pulse voltammograms obtained at different pulse durations for a BME-44 based membrane in order to evaluate the robustness of the method. As the length of the current pulse increases, the limiting current decreases in accordance with the Cottrell equation (see above). Each of the voltammograms in Figure 3-4 was evaluated by theory as done above, and the resulting complex formation constants are indicated in the plot. They converge to the same value for pulse times longer than 500 ms, which is the region where the Cottrell equation was found to be valid as well. Along with the diffusion coefficients of the complexed ion in the membrane, the Cottrell equation also allows us to calculate the Nernst diffusion layer thickness as a function of sampling time and gives a calculated theoretical value of about 1.8 µm. In theory, different anions in the inner solution should not influence the complex formation constant. Substituting chloride for acetate did indeed not change the results, although the voltammograms shifted to more negative potentials by 100 mV. This is consistent with Eq. 3.9, since k_A is known to be about 1.5 orders of magnitude less for acetate, with a predicted potential shift of 82 mV.[6]

The voltammetric method was applied to a number of ionophores in PVC–NPOE membranes and the results are summarized in Table 3-1. In most cases, the complex formation constants are in acceptable agreement to the ones found with the sandwich membrane method. However, there are exceptions. Some ionophores did not exhibit a limiting current region (labeled in the Table with "no i_{lim}"), possibly because of electrically charged impurities that lead to a depolarization of the sample–membrane interface. A membrane with substantial ion-exchanger properties is expected to essentially exhibit a feature-less Ohmic response characteristic. In contrast, the zero current potentiometric sandwich method utilizes membranes with added lipophilic ion-exchanger, and electrically charged impurities have little effect on the observed complex formation constant. On the other hand, some ionophores such as valinomycin were difficult to characterize because of their high complex formation constant. This leads to the risk of spontaneous electrolyte coextraction from the sample side, which alters the voltammetric response features. In particular, the limiting current was found to decrease with increasing KCl concentration, and potentials at very low currents could no longer properly be analyzed with Eq. 3.9. Some of these problems were solved by utilizing a hydrophilic counterion such as acetate.

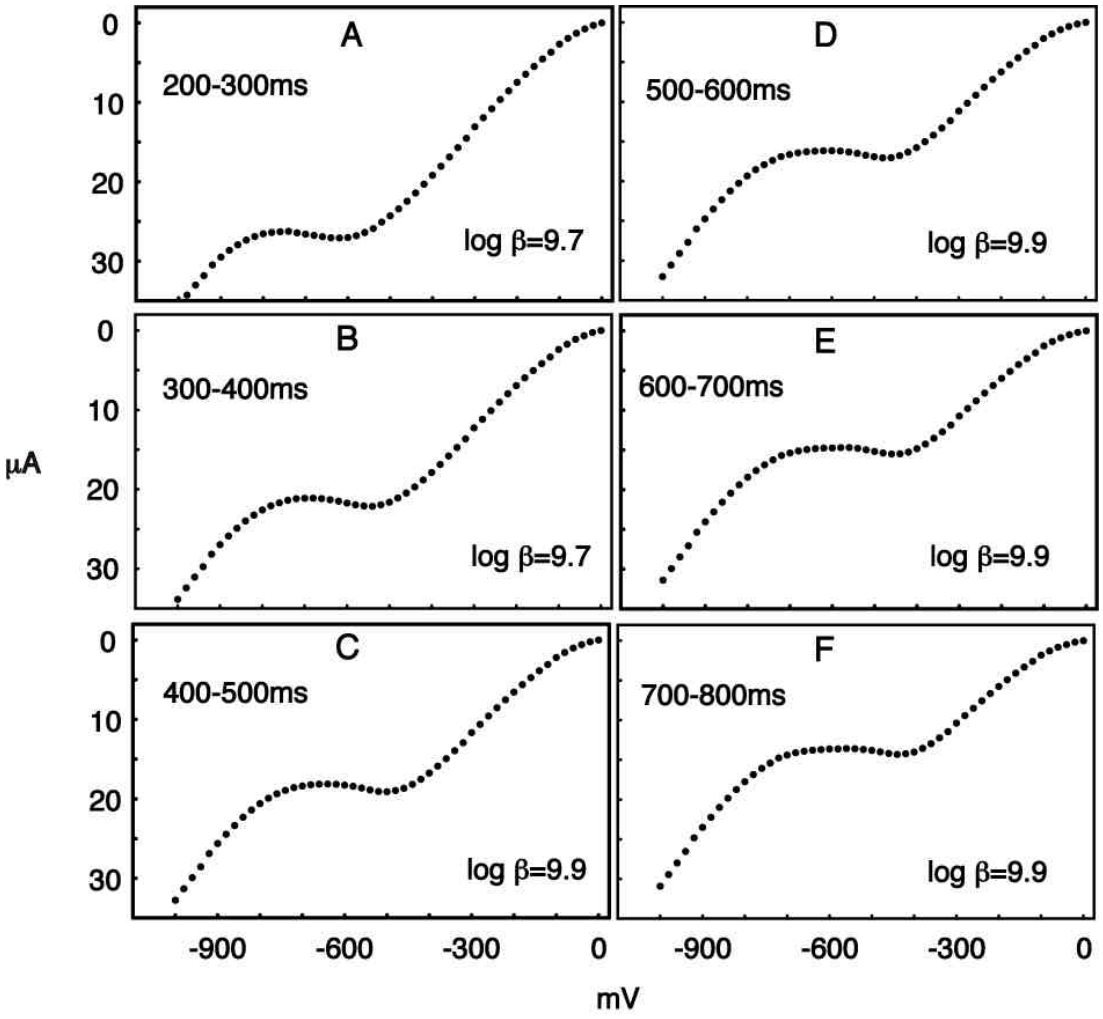

Fig. 3-4 Six NPV curves for BME 44 in 0.1M KOAc at various time segments of the original 1 second uptake pulses at each potential, membrane composition is shown in Fig. 3-1. Curve A: 200-300 ms with log β=9.7, B: 300-400 ms with log β=9.8, C: 400-500 ms with log β=9.9, D: 500-600 ms with log β=9.9, E: 600-700 ms with log β=9.9, F: 700-800 ms with log β=9.9.

Ionophore	Ion I^{z+}	log $k_I^{1/z}k_{Cl}$	log β_n	n	L_T (mmol/kg)	D (cm^2s^{-1})
BME 44	K^+	-12.6	10.0	1	9.5	$1.1x10^{-8}$
ETH 129	Ca^{2+}	-14.7	29.5	3	10.8	$2.1x10^{-8}$
ETH 1810	Li^+	-16.4	11.7	2	9.5	$2.3x10^{-8}$
Na X	Na^+	-14.7	10.8	1	10.4	$3.8x10^{-8}$
Val	K^+	-12.1	10.2	1	9.7	$7.4x10^{-9}$
ETH 5234	Ca^{2+}	-15.0	27.3	3	10.0	$2.0x10^{-8}$
ETH2120	Na^+	no i_{Lim}				
K II	K^+	no i_{Lim}				

Table 3-1 Parameters used to fit the data from the NPV curves for a given ionophore with equations (3.9) and (3.11) along with the average diffusion coefficient (*D*) obtained from the Cottrell equation for at least three uptake potentials within the limiting current range.

Possibly the most striking advantage of a normal pulse voltammetric ionophore screening is the evaluation of ionophore complex stoichiometry. For example, the normal pulse voltammograms for membranes containing the calcium ionophore, ETH 129, is shown in Figure 3-5 (A). The limiting current remains constant for about 600 mV, confirming that this ionophore forms extremely stable complexes with calcium. On the basis of its known crystal structure, the complex stoichiometry for ETH 129 and calcium is n = 3.[1] Astonishingly, this high complex stoichiometry appears to be maintained over the entire limiting current region. At extreme potentials, the membrane appears to prefer the uptake of uncomplexed calcium ions, rather than allowing a lower complex stoichiometry to accomodate more calcium. Another calcium selective ionophore (ETH 5234) also exhibits strong complexes with calcium in the membrane. The potential window of the diffusion-limited current plateau was approximately 500 mV with log β_n of 27.3. A limiting current plateau was also found for Valinomycin (K^+), ETH 1810 (Li^+) and Na-X (Na^+) with the estimated log β_n shown in Table 3-1. The lack of a diffusion-limited plateau was found in the normal pulse voltammograms for ETH 2120 (Na^+) and K-II (K^+).

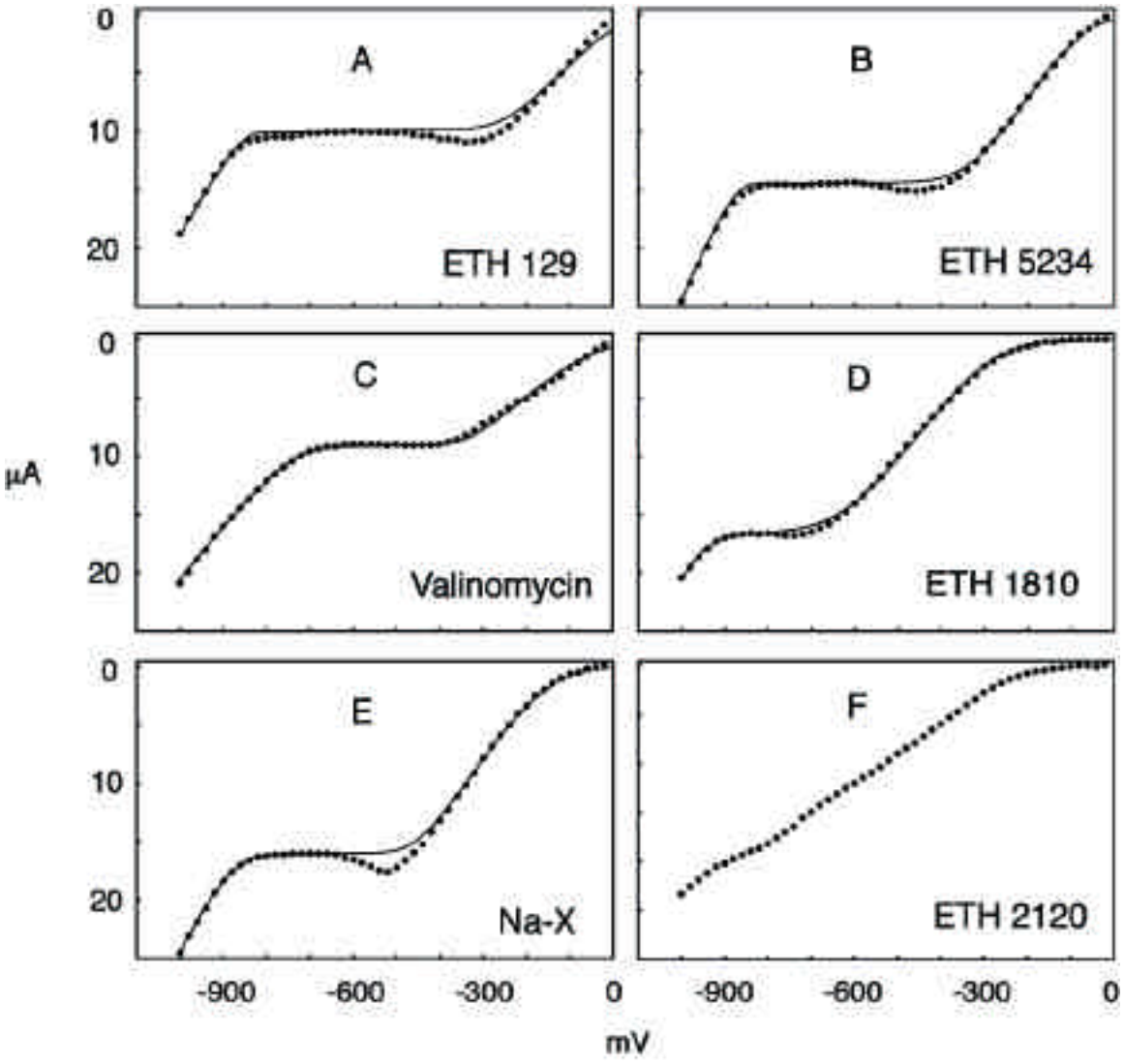

Fig. 3-5 Six NPV curves shown with theoretical fits obtained from Eqs. 3.9 and 3.11. A: calcium selective ETH 129, B: calcium selective ETH 5234, C: potassium selective Valinomycin, D: lithium selective ETH 1810, E: sodium selective Na-X, F: sodium selective ETH 2120 (no limiting current plateau). All NPV scans were performed in 0.1M salt solution of the primary ion.

3.5 Conclusions

The basic response theory for voltammetric ion selective electrodes is extended to accommodate multivalent ions. A term for the complex formation constant is included and a method for establishing its value is determined. Eight different membranes containing neutral ionophores are interrogated using normal pulsed voltammetry. The values for the formation constants are reported. Six of the eight membranes exhibited a diffusion-limited current plateau and the data is used to estimate both the complex formation constant between ion and ionophore and the diffusion coefficient of the complex in the membrane. Ion-ionophore complex stoichiometries for these membranes are also evaluated. The complex formation constants determined voltammetrically are in agreement with previously reported estimates using the zero-current segmented sandwich membrane technique. The values for the diffusion coefficients of the ion-ionophore complex are typical for plasticized PVC membranes with the same composition. Overall, this method is shown to be a useful tool for initial screening of neutral ionophores in PVC-based ion selective sensor membranes.

References

1 Bühlmann, P.; Pretsch, E.; Bakker, E. *Chem. Rev.* **1998**, 98, 1593.

2 Bakker, E.; Willer, M.; Lerchi M.; Seller, K.; Pretsch, E. *Anal. Chem.* **1994**, 66, 516.

3 Bakker, E.; Pretsch, E. *Anal. Chem.* **1998**, 70, 295.

4 Ceresa, A.; Pretsch, E. *Anal. Chim. Acta* **1999**, 395(1-2), 41.

5 Mi, Y.; Bakker, E. *Anal. Chem.* **1999**, 71, 5279.

6 Qin, Y.; Mi, Y.; Bakker, E. *Anal. Chim. Acta* **2000**, 421, 207.

7 Vanysek, P.; Ruth, W.; Koryta, J. *J. Electroanal. Chem*. **1983**, 148, 117.

8 Katano, K.; Senda, M. *J. Chem. Soc. Jpn.* **1997**, 70, 2489.

9 Samec, Z.; Homolka, D.; Marecek. V. *J. Electroanal. Chem*. **1982**, 135, 265.

10 Senda, M.; Katano, K.; Yamada, M. *J. Electroanal. Chem*. **1999**, 475, 90.

11 Reymond, F.; Carrupt, P-A.; Girrault, H.H. *J. Electroanal. Chem*. **1998**, 449, 49.

12 Koryta, J. *Electrochimica. Acta* **1979**, 24, 293.

13 Long, R.; Bakker, E. *Electroanalysis* **2003**, 15(15-16), 1261.

14 Jadhav, S.; Meir, A.J.; Bakker, E. *Electroanalysis* **2000**, 12(16), 1251.

15 Jadhav, S.; Bakker, E. *Anal. Chem.* **1999**, 71, 3657.

Chapter 4

Optical Determination of Ionophore Diffusion Coefficients in Plasticized Poly(vinyl chloride) Sensing Films

4.1 Introduction

Hydrophobic solvent polymeric membranes doped with lipophilic, selective sensing components have been the focus of many studies on ion selective sensors.[1-3] Optimizing membrane components in the polymer matrix is an important aspect in the development of fast, accurate and rugged polymeric ion selective electrodes. In recent years, it was realized that the ion mobility in such sensing membranes may have a pronounced influence on the lower detection limit of ion-selective electrodes.[4,5] Indeed, transmembrane ion fluxes may contaminate the sensing surface with ions from the membrane, and increase the observed detection limit. A minimization of such fluxes may

lead to drastically decreased detection limits down to the low parts per trillion levels, as recently reported for numerous sensing systems.[5-7] Two possibilities to slow the flux of ions in the membrane are covalent immobilization of sensing components[8-10] and increasing the polymer to plasticizer ratio.[10-12] Both will drastically decrease the diffusion coefficient of the ionophore and reduce ion fluxes. Ion mobilities are also very important for the development and characterization of voltammetric and pulsed galvanostatic ion sensors, where the current is often dictated by mass transport in the membrane phase.[13,14] Other examples where ion mobility is crucial for sensing performance include potentiometric polyion sensors, where the measuring range is dependent on the diffusion coefficients in the membrane,[11,12] and optical ionophore-based sensors, where response times are a direct function of the ion mobilities.[15]

In this chapter, an electrically neutral H+-selective chromoionophore, ETH 5294, is characterized in various polymer matrices as a model system. Potentiometric sensors have long employed pH sensitive ionophores for detecting protons.[16] The excellent selectivity and wide range of available pK_a values offered by this class of ionophores makes them good candidates for direct and competitive sensing.[17,18] Such chromoionophores also show a change in optical properties upon protonation. Optical transduction principles, including fluorescence and absorbance, can be utilized in conjunction with clever sensing schemes to gain information on a variety of analytes.[15] Fluorescent PVC-based microspheres have been used to detect sample activity changes

for a variety of cations based on a competitive exchange equilibrium established by the presence of a cation-selective ionophore and a H^+-chromoionophore.[19-21] A spectroscopic technique for the determination of the diffusion coefficients for this class of ionophores has already been reported by the group of Pretsch[9,10]. They used a method of annealing together two halves of a PVC membrane, one with and one without chromoionophore, to image the concentration profiles via absorbance measurements.

This introduces an even more convenient method to determine the diffusion coefficient of the H^+-selective chromoionophore ETH 5294. We take advantage of a potential drawback for many chromoionophores, namely the tendency to photobleach. By using a microscope and light from a mercury lamp, we destroy the absorbance properties of the chromoionophore in a well-defined area of the PVC film containing the chromoionophore. This creates an optical interface, in a single film, between a transparent portion containing photobleached chromoionophore and the section containing undamaged ETH 5294. By imaging the absorbance profiles as a function of time and space, we are able to estimate the diffusion coefficient of the dye in a variety of polymeric membrane environments.

4.2 Experimental

Reagents. High molecular weight poly(vinyl chloride) (PVC), tetradodecylammonium tetrakis(4-chlorophenyl) borate (ETH 500), the plasticizers *o*-

nitrophenyl octyl ether (NPOE) and bis(2-ethylhexyl)sebacate (DOS), and the chromoionophore *N*,*N*-diethyl-5-(octadecanoylimino)-5*H*-benzo[a]phenoxazine-9-amine (ETH 5294), and Selectophore grade tetrahydrofuran (THF) were obtained from Fluka Chemical Corp. (Milwaukee, WI).

Membrane Preparation. All membranes were prepared by solvent casting as reported.[22] Membranes contained 1 wt% ETH 5294 and, optionally, 10 wt% ETH 500. The ratio between PVC and plasticizer was varied as noted. The membranes had a total mass of approximately 65 mg dissolved in 750 µl of THF. This cocktail was poured into a glass ring with an inner diameter of 22 mm mounted on a microscope slide. An ca. 120 µm thick membrane was formed on the slide after overnight evaporation of the solvent, THF.

Instrumentation. The imaging data were collected on a PC using a Nikon Eclipse E400 microscope (Southern Micro Instruments, Marietta, GA) equipped with a Pariss imaging spectrometer (LightForm, Inc., Belle Meade, NJ) and a model 4920 Peltier cooled CCD camera (Cohu, Inc., San Diego, CA). The microscope was equipped with a Nikon Plan Fluor 40x (0.75 NA) objective and a super high-pressure mercury arc lamp (Southern Micro Instruments).[23] A filter cube with a 510-560 nm excitation filter, 565 nm dichroic mirror and 590 nm longpass filter was used in conjunction with the mercury lamp to photobleach the chromoionophore.

Measurements. After solvent evaporation, the polymer membrane was cut along the circumference of the glass ring and remained on the glass microscope slide. The glass ring was removed and the membrane/glass slide was cleaned and placed on the microscope stage. The 40x objective was focused in the center of the membrane using light from a 60-Watt halogen bulb with a controlled voltage source. After focusing, the stage was moved so that the objective was positioned on a portion of the glass microscope slide that was not covered with the polymer membrane. A spectrum was taken with an exposure time of 200 ms and the intensity was adjusted so that the peak intensities in the white light spectrum were between 80% and 90% of the calibration maximum. This spectrum served as the initial intensity for the absorbance measurements. Next, the objective was again centered on the membrane and a spectrum was taken of the purple polymer film. The logarithm of the intensity ratios was calculated to ascertain the wavelength of the absorbance maximum for the chromoionophore ETH 5294. The wavelength range corresponding to the absorbance maximum was dependent on the polymer matrix and was found to be between 535 nm and 550 nm, which is in good agreement with recently reported values.[24] The membrane was then exposed to light passing through the "green" filter from the high-pressure mercury lamp for two minutes. This was sufficient time to photobleach the chromoionophore in a circular area of the membrane with a radius of approximately 1.5 mm. After photobleaching, the objective was quickly positioned so that the vertical view of the microscope crossed perpendicular to the interface between

the purple, chromoionophore-laden polymer and the transparent, photobleached polymer. A snapshot of the interface was comprised of 240 individual spectral lines, with 0.41 μm nominal resolution using the 40X objective, giving a vertical view with a total distance of ca. 100 μm. Spectra were then taken with a set time interval using the PARISS software system in auto scan mode, collecting spectra every minute or every five minutes. These spectra were then analyzed and plotted as a function of the absorbance maximum versus time and space.

Data Analysis. The individual points representing the absorbance profiles of ETH 5294 were recorded as a function of space and time. Each spectrum, taken over fixed time intervals, is a snapshot of the interface and extends into the photobleached portion of the membrane. Overlay of the spectra provides a value for $x = 0$ and A_0, the initial absorbance. The data for each spectrum was fit with Equation 4.1 by inserting A_0, the measured absorbance values $A(x,t)$ and the corresponding position x. A value for Dt, the product of diffusion coefficient and diffusion time, was typically obtained from a running average of approximately the last 50% of the data points extending from the interface to positions were the absorbance/noise ratio becomes small. This value for Dt was inserted into equation 4.3 along with the actual experimental time change Δt, providing a value for D (see Results and Discussion).

4.3 Results and Discussion

Here, the H^+ selective chromoionophore ETH 5294 is used to follow the absorbance changes in a plasticized polymer membrane due to diffusion of the chromoionophore from a region of high concentration to a region of low concentration. Light from a high-pressure mercury arc lamp is used to photo decompose the dye in a well-defined portion of the polymer membrane, leaving a relatively sharp concentration gradient across the interface between the two sections. The photobleached fragments do not possess any absorbance properties, as verified by subsequent spectra in transmission mode, and they are therefore believed to be of no consequence in this experiment. Moreover, since only the chromoionophore may undergo photodegradation during the bleaching step, other membranes properties are not expected to be altered. Consequently, the concentration profile in the membrane changes with time as the chromoionophore enters the membrane section that is devoid of this proton-selective dye. The diffusion of ETH 5294 is monitored as a function of time and space using a microscope, in transmission mode, equipped with a spectrometer and halogen lamp. The light intensity of the halogen lamp in transmission mode was much weaker and photobleaching was estimated to be less than 10% even after 12 h of continuous exposure. Analogous absorbance measurements with essentially the same equipment have been reported recently by Lindner's group and shown to follow Beer's law.[24]

The concentration of the chromoionophore is related to the absorbance, measured with the microscope, through Beer's law. Since a range of wavelengths that incorporate the absorbance maximum were evaluated at discrete time intervals over fixed positions, the following relationship can be used for the diffusion of the chromoionophore into a semi-infinite matrix:[25]

$$A_{(x,t)} = \frac{1}{2} A_0 erfc \frac{x}{2\sqrt{(Dt)}} \tag{4.1}$$

Here, x is the distance from the initial interface in cm, t is the time in s, A_0 is the initial absorbance of the chromoionophore at t = 0, A(x,t) is the absorbance at some position and time, erfc is the error function compliment and D is the diffusion coefficient of the chromoionophore in $cm^2\ s^{-1}$.

Figure 4-1 shows the observed time-dependent absorbance profiles for a representative membrane containing 1% ETH 5294, and 45% PVC, 46% NPOE and 8% ETH 500 by weight. The entire view of the spectral imaging camera using a 40x objective is represented in this figure. The absorbance at 550 nm decreases on the left-hand edge and increases on the right-hand edge symmetrically. In these experiments, the interface between the loaded membrane section and the chromoionophore free section is not perfect as a certain amount of the chromoionophore exists beyond the interface at t = 0. At x = 0, the absorbance should be one half of the original absorbance for all D and t, represented by the point of inflection in Figure 4-1. In subsequent experiments, only the right portion

of this image was recorded and analyzed because of the limited linear range of the CCD detector. Consequently, A_0 was calculated by doubling the absorbance value at x = 0.

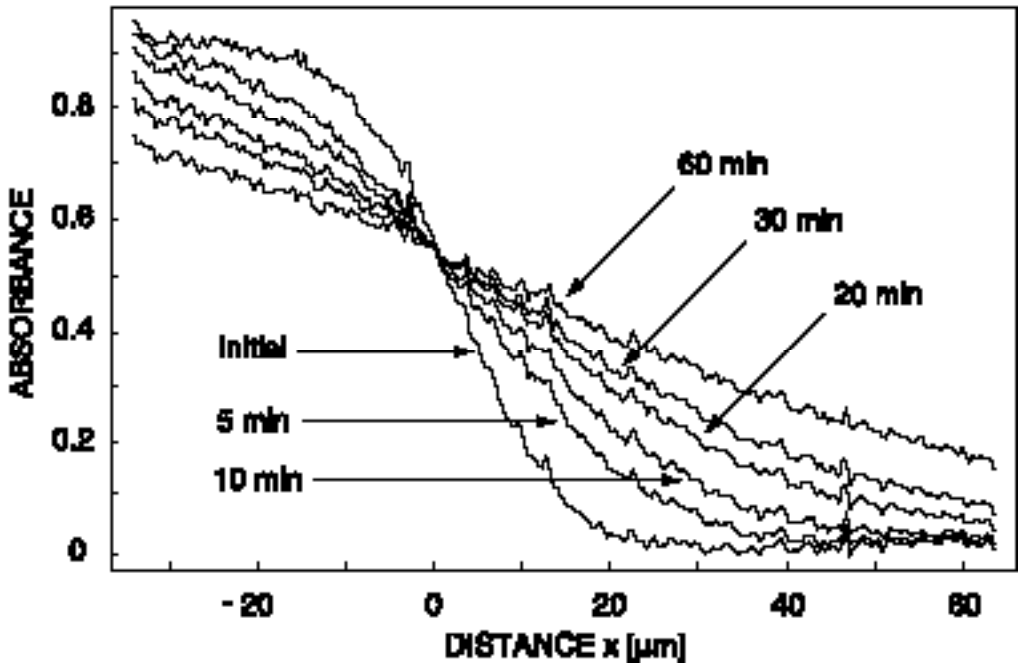

Fig. 4-1 Time-dependent absorbance profiles for the chromoionophore ETH 5294 in a PVC-NPOE (1:1) polymeric sensing film containing the inert lipophilic salt ETH 500. The left side of the plot shows the non-photobleached portion of the membrane exemplified by the increased absorbance while the right side contains, initially, little or no chromoionophore shown here with a vastly decreased absorbance. As the chromoionophore diffuses from left to right, the absorbance decreases and increases, respectively.

To model the diffusion of the chromoionophore into the photobleached section, the experimental data was fitted with equation 4.1, with one modification. In theory, the interface at t = 0 should be a vertical line extending through the inflection point. With the current setup, the initial spectra suggest that the chromoionophore has been diffusing from the interface for some time (t_o) greater than zero. Assuming that the diffusion coefficient of the chromoionophore is constant, we can substitute

$$t = t_0 + \Delta t \tag{4.2}$$

and inserting this relationship into equation 4.1 gives the following:

$$A_{(x,t)} = \frac{1}{2} A_0 erfc \frac{x}{2\sqrt{D(t_0 + \Delta t)}} \tag{4.3}$$

For every recorded absorbance profile, equation 4.1 was used to find the best fit, and a set of Dt values were obtained for all acquisition times (t). From this data set and Eq. 4.3, one can plot Δt versus Dt and obtain a linear relationship whose slope is the diffusion coefficient and whose intercept at t = 0 is Dt_o, as shown in Figure 4-2. This provides a value for the diffusion coefficient and dividing the intercept by the slope provides t_o. Some deviations from linearity were noted at longer times, where the slope of the absorbance profile becomes smaller and more susceptible to influences from noise and the radial diffusion of the chromoionophore. The relative standard deviation in the calculation of the slope (and hence the diffusion coefficient) were quite narrow, in the range of 1 to 7%. For this purpose, non-linear behavior at longer times was excluded from

the analysis. Values of t_0 varied from about 40 s (for 20 wt% PVC) to 250 s (for 60% PVC).

Subsequently, the absorbance data were plotted with the theoretical curve obtained from Eq. 4.3 and a single D and t_0. Figure 4-3 shows the correlation between the experimental data points and the theoretical absorbance profiles predicted by equation 4.3. For this example, D was found as 4.6×10^{-9} cm^2 s^{-1} (SD = 1 %) and t_0 = 120 s. At longer times, the experimental data suggest that a slightly faster diffusion coefficient is required for better correlation or a term for the effects of radial diffusion is needed. However, over short times and small distances the diffusion behaves as if it were indeed in a semi-infinite matrix.

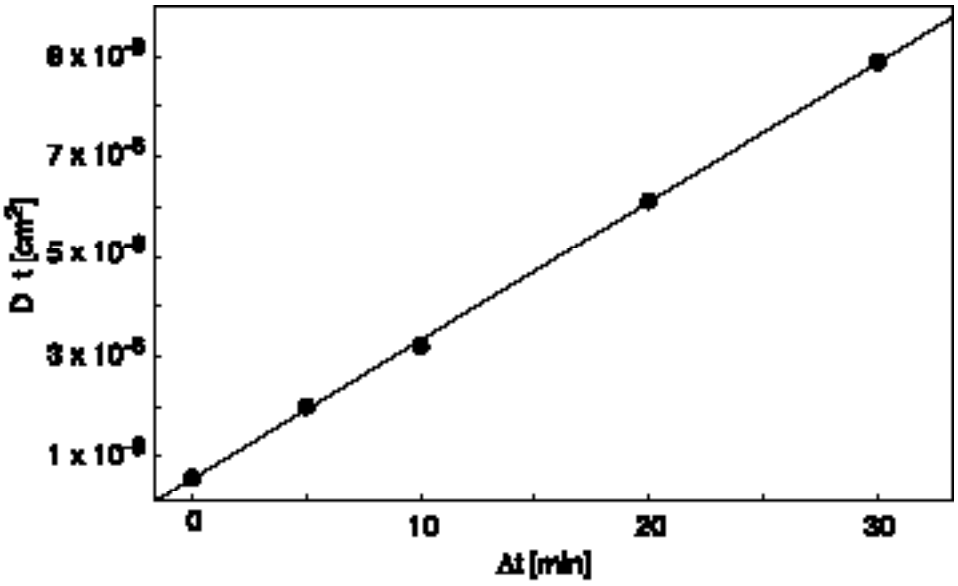

Fig. 4-2 Relationship found between time and the diffusion coefficient for the right side of the data shown in Fig. 4-1 with Eq. 4.3, where $t = t_0 + \Delta t$. From the linear fit the average diffusion coefficient for the entire experiment is determined.

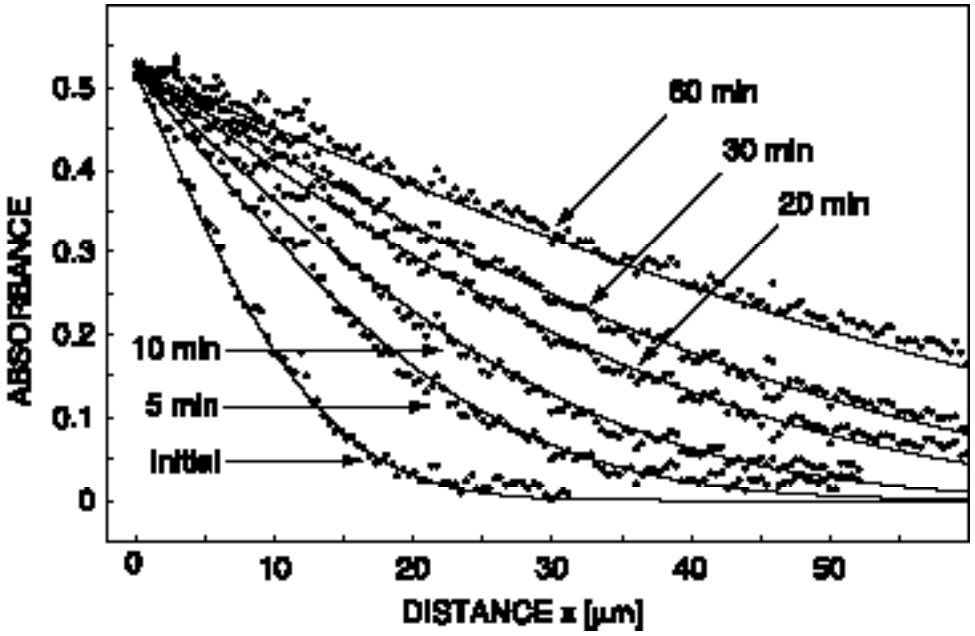

Fig. 4-3 Experimentally obtained time-dependent absorbance profiles shown with curves predicted by theory using equation 4.3. Membrane composition was as shown in Fig. 4-1.

Twenty membranes of various compositions were analyzed to determine the diffusion coefficients of ETH 5294 using the previously mentioned method in each matrix, and the results are summarized in Fig. 4-4. The plot shows an approximately linear relationship between the logarithm of the diffusion coefficient and the polymer content. Obviously, a decrease in the magnitude of the diffusion coefficient is always observed as the polymer content of the membrane is increased, as established earlier.[26] The linear fits shown in Fig. 4-4 are described based on the following equations: For PVC–DOS: log D = -6.17 – 0.0459 wt% PVC. For PVC–DOS–ETH 500: log D = -6.46 – 0.0468 wt% PVC. For PVC–NPOE: log D = -5.89 – 0.0508 wt% PVC. For PVC–NPOE–ETH 500: log D = -6.22 – 0.0473 wt% PVC. Other researchers have previously shown the effects of increased polymer content on the diffusion of a different proton selective dye, ETH 2439, in PVC–DOS.[10] The corresponding linear fit found at the time was comparable: log D = -5.702 – 0.059 wt% PVC (r^2 = 0.964). Specifically, a typical membrane consisting of 33 wt% PVC and 66 wt% DOS containing the chromoionophore ETH 2439, showed a diffusion coefficient of 1.1 x 10^{-8} cm^2 s^{-1} as determined by Schneider and Pretsch.[9] In the paper of Puntener and Pretsch, a PVC–DOS membrane containing 33% PVC showed a predicted diffusion coefficient for ETH 2439 of 2.2 x 10^{-8} cm^2 s^{-1}.[10] Both values are in close agreement with the diffusion coefficient determined in this work, 2.3 x 10^{-8} cm^2 s^{-1}, for ETH 5294 with the same membrane composition. The precision of the data presented here is somewhat improved

over these literature values. Of the four membrane types, the one with the more polar plasticizer NPOE creates a polymer matrix with a greater diffusion coefficient than the less polar DOS. The lipophilic salt ETH 500 is normally added to these membranes to lower the resistance of voltammetric sensing membranes[13] and appears to decrease the diffusion coefficient of the chromoionophore in membranes with either NPOE or DOS as plasticizer. Since the content of ETH 500 is quite high (10 wt%), a membrane with a given weight percent of PVC will contain significantly less plasticizer if ETH 500 is included. Such membranes are indeed expected to show smaller diffusion coefficients so that this result is not too surprising.

The different proportions of PVC and plasticizer studied here will show an overall possible variation of the diffusion coefficient by up to 2 orders of magnitude. The data reported here may give important insights into planning of chemical ion sensors for a number of applications. Obviously, an even more drastic reduction of ion mobilities, for example in view of developing low detection limit ion-selective electrodes, appears to be only achievable by chemical attachment of the ionophore to the polymer matrix.[10,27]

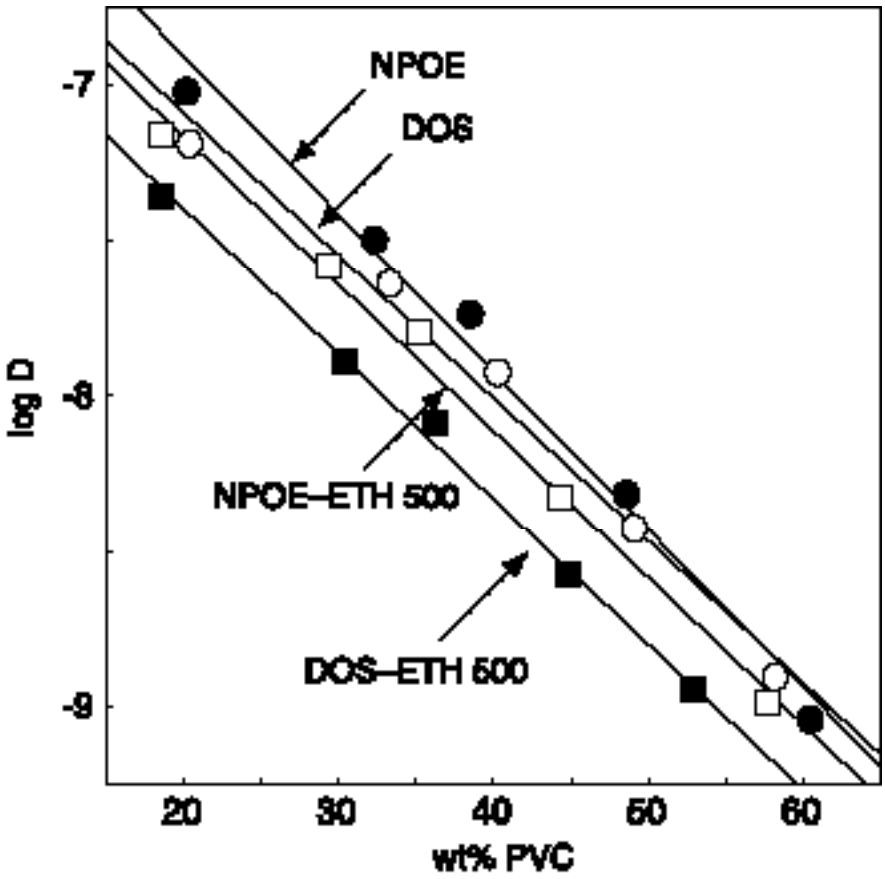

Fig. 4-4 Experimental logarithms of the diffusion coefficient as a function of the polymer content in weight percent for 4 different types of polymeric films. All contain approximately 1 wt% ETH 5294 with the indicated remaining components (plasticizer and, optionally, lipophilic electrolyte ETH 500).

4.4 Conclusions

A spectroscopic method for the determination of the diffusion coefficient of the H^+ selective chromoionophore ETH 5294 in PVC-based liquid polymer membranes is introduced. Four different polymer matrices with two different plasticizers were examined through absorbance and their effects on the diffusion coefficient of the chromoionophore were evaluated. The absorbance profiles of the dye suggest that diffusion can be modeled by assuming a semi-infinite polymer matrix extending from the optical interface. This technique requires relatively short experiments that could provide information on the diffusion coefficients of many compounds. These compounds are limited to those molecules that absorb in the UV/Vis spectrum, are photobleachable and dissolve in the matrix of interest. It is shown that the magnitude of the diffusion coefficient decreases as the content of PVC is increased for all membrane compositions tested and that the more polar plasticizer, NPOE, produces a matrix with a faster rate of diffusion than membranes containing DOS. The addition of the borate salt, ETH 500, appears to slow the diffusion of ETH 5294 in membranes containing either plasticizer if the data are plotted as a function of the weight percent of PVC. This new method offers accurate determination of diffusion coefficients and may aid in maximizing membrane responses by giving insight into the rate of ion transport.

References

1 Umezawa, Y. *Handbook of Ion-Selective Electrodes: Selectivity Coefficients*, CRC Press, Boca Raton, Ann Arbor, Boston, **1990**.

2 Bakker, E.; Bühlmann, P.; Pretsch, E. *Chem. Rev.* **1997**, *97*, 3083.

3 Bühlmann, P.; Pretsch, E.; Bakker,E. *Chem. Rev.***1998**, *98*, 1593.

4 Ceresa, A.; Sokalski,T.; Pretsch, E. *J. Electroanal. Chem*. **2001**, *501*, 70.

5 Bakker, E.; Pretsch, E. *Anal. Chem.* **2002**, *74*, 420A.

6 Ceresa, A.; Radu, A.; Peper, S.; Bakker, E.; Pretsch, E. *Anal. Chem.* **2002**, *74*, 4027.

7 Malon, A.; Radu, A.; Qin, W.; Qin, Y.; Ceresa A.; Maj-Zurawska, M.; Bakker, E.; Pretsch, E. *Anal. Chem.* **2003**, *75*, 3865.

8 Sudholter, E.J.R.; Wal, P.D.V.D.; Skowronska-Ptasinska, M.; Berg, A.V.D.D.; Bergveld, P.; Reinhoudt, D.N. *Anal. Chim. Acta* **1990**, *230*, 59.

9 Schneider, B.; Zwickl, T.; Federer, B.; Pretsch, E.; Lindner, E. *Anal. Chem.* **1996**, *68*, 4342.

10 Puntener, M.; Fibbioli, M.; Bakker, E.; Pretsch, E. *Electroanalysis* **2002**, *14*, 1329.

11 Fu, B.; Bakker, E.; Yun, J.H.; Yang, V.C.; Meyerhoff, M.E. *Anal. Chem.* **1994**, *66*, 2250.

12 Ambrose, T.M.; Meyerhoff, M.E. *Electroanalysis* **1996**, *8*, 1095.

13 Jadhav, S.; Bakker, E. *Anal. Chem.* **2001,** *7*, 380.

14 Rossier, J.S.; Roberts, M.A.; Ferrigno, R.; Girault, H.H. *Anal. Chem.* **1999**, *71*, 4294.

15 Seiler, K.; Simon, W. *Anal. Chim. Acta* **1992**, *266*, 73.

16 Lindner, E.; Cosofret, V.V.; Kusy, R.P.; Buck, R.P.; Rosatzin, T.; Schaller, U.; Simon, W. *Talanta* **1993**, *40*, 957.

17 Bakker, E.; Lerchi, M.; Rosatzin, T.; Rusterholz, B.; Simon, W. *Anal. Chim. Acta* **1993**, *278*, 211.

18 Qin, Y.; Bakker, E. *Talanta* **2002**, *58*, 909.

19 Brasuel, M.; Kopelman, R.; Miller, T.J.; Tjalkens, R.; Philbert, M.A. *Anal. Chem.* **2001**, *73*, 2221.

20 Shortreed, M.; Bakker, E.; Kopelman, R. *Anal. Chem.* **1996**, *68*, 2656.

21 Tsagkatakis, I.; Peper, S.; Retter, R.; Bell, M.; Bakker, E. *Anal. Chem.* **2001**, *73*, 6083.

22 Craggs, A.; Moody, G.J.; Thomas, J.D.R. *J. Chem. Educ.* **1974**, *51*, 541.

23 Tsagkatakis, I.; Peper, S.; Bakker, E. *Anal. Chem.* **2001**, *73*, 315.

24 Gyurcsanyi, R.E.; Lindner, E. *Anal. Chem.* **2002**, *74*, 4060.

25 Crank, J. *The Mathematics of Diffusion*, Oxford University Press, New York, **1993**.

26 Oesch, U.; Simon, W. *Anal. Chem.* **1980**, *52*, 692.

27 Qin, Y.; Peper, S.; Radu, A.; Ceresa, A.; Bakker, E. *Anal. Chem.* **2003**, *75*, 3038.

Chapter 5

Detrmination of Diffusion Coefficients of Chromoionophores in Plasticized Poly(Vinyl Chloride) Films

5.1 Introduction

Polymer membrane electrodes based on ionophore-ion recognition schemes have been at the forefront of the development of ion-selective sensors for the last three decades. A decidedly lopsided tally of cation versus anion sensors has pushed researchers to look at novel compounds for new anion selective ISEs.[1,2] Electrodes based solely on the ion exchange capabilities of the membrane, either from intrinsic impurities[3,4] or added ionic sites,[5] respond to analyte anions according to the Hofmeister selectivity pattern (ClO_4^- > SCN^- > $Salicylate^-$ > I^- > NO_3^- > Br^- > NO_2^- > Cl^- > HCO_3^- > F^-) in which the more lipophilic anion is most preferred.[6]

By the addition of compounds to the membrane that bind reversibly to target anions, the selectivity pattern can be altered from the pure lipophilicity component of ion transfer to assisted ion transfer, yielding an analytically useful sensor. Among the anion ionophores studied recently are the metalloporphyrins. These molecules consist of a metal ion coordinated within the ring-like porphyrin structure of four pyrroles linked by methine bridges. The porphyrins exhibit aromatic characteristics with high stability constants with their coordinated central metal ion.[7] Anion selectivities can be altered from the Hofmeister series by changing the substituents on the porphyrin ring and by changing the central metal ion. Some of the metals incorporated into the porphyrin structures that have recently been examined include In(II),[8-14] Mn(III),[15,16] Al(III),[17] Ga(III),[11,14] Tl(III),[11] Lu(III),[18] Zr(IV)[19,20] and Sn(IV).[21] Useful selectivities generated from the incorporation of these ionophores into the sensing matrix are attributed to the reversible anion to metal binding event at one of the axial positions of the metal within the planar porphyrin ring. In the case of Mn(III) porphyrins, it was shown that an increase in the stability of coordination of less lipophilic anions was achieved by varying the substituents along the periphery of the porphyrin ring. Also, an intramolecularly bound neutral ligand effectively capping one side of the porphyrin was shown to force the membrane to revert back to an ion exchanger with no selective interaction for anions.[15]

Many studies have been conducted in the characterization of In(III) porphyrins in optical and potentiometric sensor applications. One of the recent discoveries was the

ability of the porphyrin to dimerize under certain conditions via a hydroxide bridge. A monomer-dimer equlibrium was demonstrated by UV-Vis spectroscopy and was used to explain the apparent "super-Nernstian" response of the electrodes.[22] In the absence of analyte anions, after bathing in an aqueous solution, it was shown that the metalloporphyrin exists as a positively charged hydroxide bridged dimer within the membrane.[22] The electrodes exhibited a strong pH dependence as a result of the dimer formation. This equilibrium was exploited in the direct monitoring of spectral changes in response to iodide for Mn(III) porphyrins.[23] Also, a series of In(III) porphyrins were recently covalently attached to a methyl methacrylate and decyl methacrylate copolymer essentially preventing the formation of the dimer species yielding a predictable Nernstian response to chloride ions.[10]

In this paper, a previously introduced method,[24] is used to assess the diffusion coefficients of three Indium porphyrins and a Nile Blue derivative (NB-1) in plasticized PVC films without added ionic sites. By estimating the rate of diffusion of these carriers (ionophores), steps toward optimizing the influence of these membrane components to lower detection limits, increase the measuring range, reduce response times and reduce transmembrane ion fluxes can be made.

5.2 Experimental

Reagents. High molecular weight poly(vinyl chloride) (PVC), plasticizers: *o*-nitrophenyl octyl ether (NPOE) and bis(2-ethylhexyl)sebacate (DOS), and Selectophore grade tetrahydrofuran (THF) were all obtained from Fluka Chemical Corp (Milwaukee, WI). 4-hydrobenzoic acid, thionyl chloride, N,N-dimethylformamide, carbon tetrachloride, octaethylporphyrin, indium(III) chloride, orthoformate, methanol, sulfuric acid, 4-hydroxybenzaldehyde, benzaldehyde, pyrrole, propionic acid, acetic acid, acryloyl chloride, triethylamine, 1-octanol and AIBN were purchased from Aldrich (Milwaukee, WI). The monomers methyl methacrylate(99.5%) and *n*-decylmethacrylate(99.9%) were obtained from Polysciences, Inc. (Warington, PA). Hematoporphyrin base was obtained from Frontier Scientific (Logan, UT) and Nile Blue chloride salt was purchased from Strem (Newburyport, MA).

Syntheses. NB-1,chloro(octaethylporphyrinato)indium(III) In(OEP)Cl, chloro(3-[18-(3-acryloyloxypropyl)-7,12-bis(1-methoxyethyl)-3,8,13,17-tetramethylporphyrin-2-yl]-propyl ester)indium (III) In(HEPEAC)Cl and chloro(5-(4-acryloyloxyphenyl)-10,15,20-triphenylporphyrinato)indium(III) In(AOTPP)Cl were all synthesized and polymerized according to literature.[25,10]

Membrane Preparation. Membranes were prepared using the established method for solvent casting.[26] The membranes contained between 0.5-1.5 % (w/w) of the specified free chromogenic ionophore or 5-9 % (w/w) of the MMA-DMA-grafted ionophore, PVC and plasticizer (NPOE or DOS) with a total mass of 100 mg dissolved in 1.2 mL of THF. These membrane cocktails were poured into a glass ring that was mounted on top of a microscope slide. The glass ring had an inner diameter of 22 mm, thus, a ca. 200 μm thick membrane was produced after overnight evaporation of the solvent.

Instrumentation. Absorbance spectra were collected using a Nikon Eclipse E400 microscope (Southern Micro Instruments, Marietta, GA, USA) fitted with a Pariss imaging spectrometer (Lightform Inc., Belle Meade, NJ, USA) and a model 4920 Peltier cooled CCD camera (Cohu, San Diego, CA, USA). The microscope was equipped with a Nikon Plan Fluor 40x (0.75 NA) objective and a super high-pressure mercury arc lamp (Southern Micro Instruments). Imaging data were stored on a PC connected to the CCD camera. The chromogenic ionophores were photobleached by exposure to light from the mercury lamp passing through a filter cube with a 510-560 nm excitation filter, a 565 nm dichroic mirror and a 590 nm longpass filter.

Measurements. After solvent evaporation, the glass ring was removed from the microscope slide. The chromogenic ionophore laden polymer remained on the slide and

was placed on the microscope stage after cleaning the bottom of glass with a piece of cloth and dusting the polymer with a stream of Nitrogen gas. Using the 40x objective, the microscope was focused on the center of the polymer film. The slide was then repositioned to take a spectrum of the glass slide without the polymer film. This initial spectrum was taken and the intensities adjusted to the upper range of the calibration maximum. Next, the slide was again repositioned to take a spectrum of the polymer film. The log of the intensity ratio of the spectra of the blank slide and the polymer film was interrogated to ascertain the absorbance maximum for each ionophore in a particular membrane matrix. The membrane was then exposed to light from the high-pressure mercury arc lamp. The exposure time was dependent on the ionophore interrogated. This exposure photobleached a circular area of the polymer film creating an interface between a section containing the chromogenic ionophore and a section without the chromophore. The microscope stage was then positioned so that the vertical view of the microscope (ca. 100μm) was perpendicular to the photobleached interface and encompassed both the colored and transparent sections. A spectrum was taken immediately and was followed by others every five minutes. The 240 spectral lines with 0.41 nominal resolution provided a snapshot of the interface and followed the progression of the chromogenic ionophore into the photobleached section as a function of time and space.

Data Analysis. The absorbance profiles of the ionophores as a function of time and space provide essential information to fit the experimental data with theory. Overlay

of the spectra provide an intial absorbance value (A_0) at the interface where x=0. The experimental absorbance data $A_{(x,t)}$ with corresponding position (x) for each spectrum were inserted into Eq. 5.1 along with (A_0). A value for Dt, the product of the diffusion coefficient and diffusion time, was obtained from a running average of data points from each spectrum. This value of Dt and the experimental time change (Δt) were inserted into Eq. 5.3, providing a value for the diffusion coefficient (D).

5.3 Results and Discussion

Here, the chromophores NB-1, In(OEP)Cl, In(AOTPP)Cl and In(HEPEAC)Cl (see Figure 5-1) are used to assess their diffusion coefficients in plasticized polymer membranes through absorbance. A spectral microscope follows the absorbance changes as the chromogenic compounds diffuse from a region of the polymer membrane with a high concentration of the ionophore to a region of low concentration. An interface is created by exposing the membrane to light from a high-pressure mercury arc lamp, photo decomposing the ionophore in a discrete area. The properties of the other membrane components are not effected by the photobleaching step and are not of consequence to the experiment. Subsequent absorbance data collected in transmission mode confirm this. The diffusion of these ionophores is followed by recording the absorbance progression as a function of time and space using a microscope equipped with a spectrometer and a halogen lamp, in transmission mode. The weaker intensity of light from the halogen lamp

and the length of exposure during the experiment did not lead to appreciable photobleaching of the ionophores with the absorbance spectra shown in Figure 5-2.

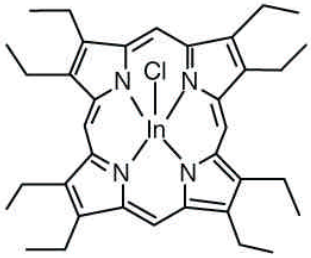

In(OEP)Cl

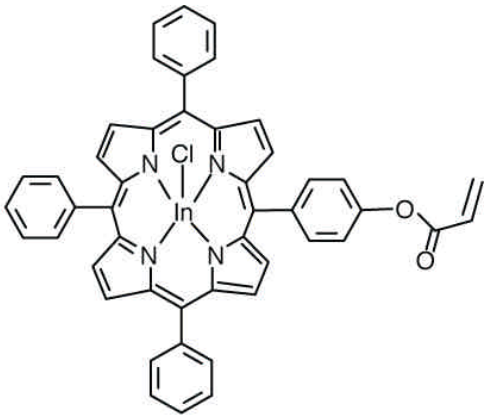

In(AOTPP)Cl

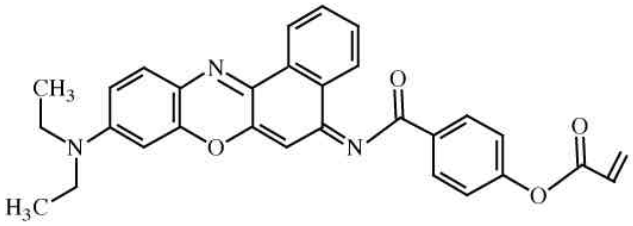

NB-1

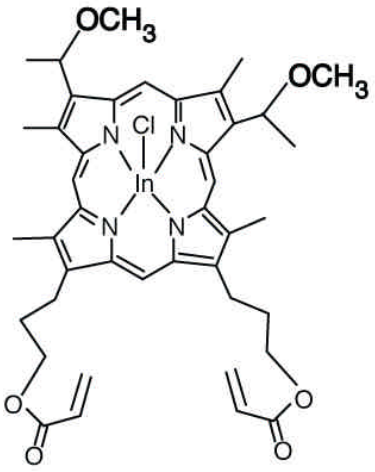

In(HEPEAC)Cl

Fig. 5-1 Structures for NB-1, In(OEP)Cl, In(AOTPP)Cl and In(HEPEAC)Cl.

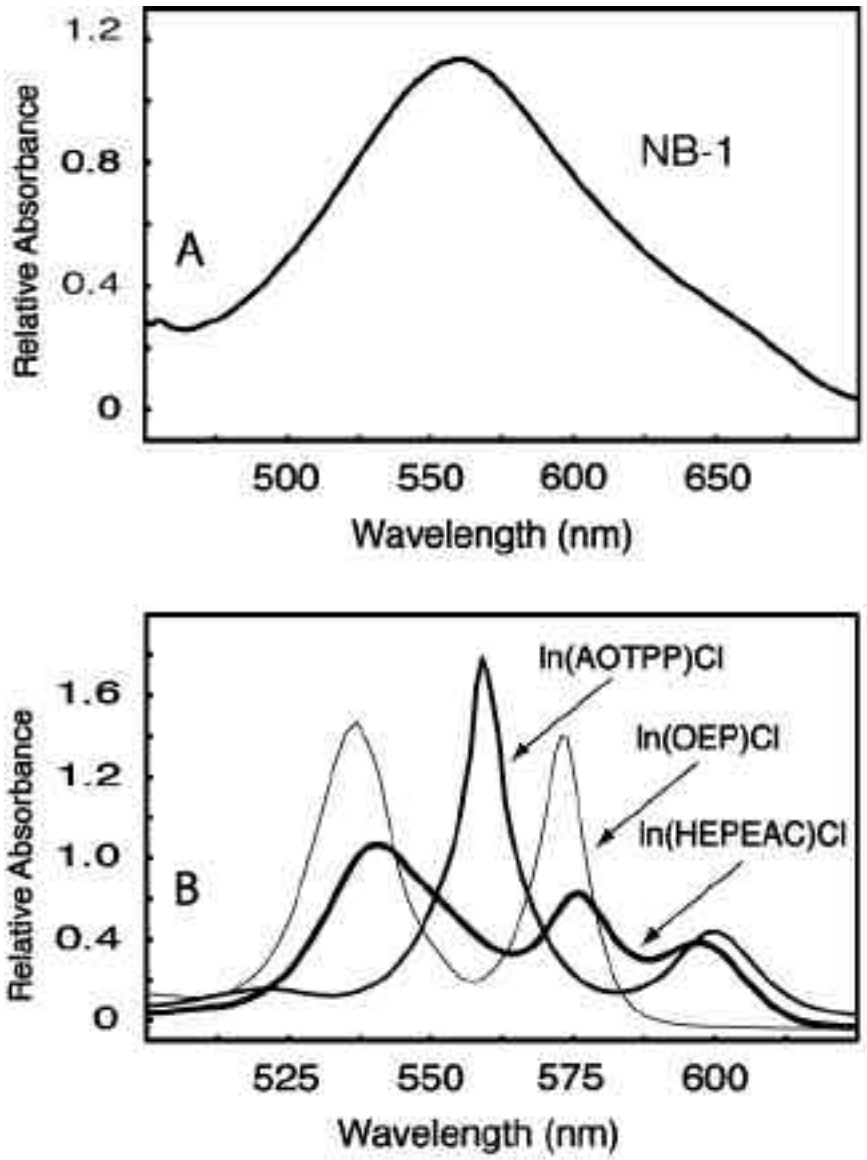

Fig. 5-2 Absorbance Spectra obtained for chromogenic ionophores in a PVC-NPOE (1:2) polymeric film, showing the absorbance maximums used for the diffusion experiments: (A) Nile blue derivative (NB-1): (B) Indium porphyrins- In(OEP)Cl, In(AOTPP)Cl and In(HEPEAC)Cl.

Absorbance profiles of each ionophore were monitored by tracking the wavelengths incorporating the absorbance maximum over discrete time intervals and fixed positions. The data were related to the following model for the diffusion of the species into a semi-infinite matrix:[27]

$$A_{(x,t)} = \frac{1}{2} A_0 erfc \frac{x}{2\sqrt{(Dt)}} \tag{5.1}$$

here, x is distance, t is time, A_0 denotes the initial absorbance of the ionophore at t = 0, $A_{(x,t)}$ denotes the absorbance at some position and time, erfc is the error function compliment and D (cm^2/s) is the diffusion coefficient of the ionophore.

A membrane containing 1.05% In(AOTPP)Cl, 32.8% PVC and 66.15% DOS by weight was interrogated to estimate its rate of diffusion in the polymer matrix according to this method. Figure 5-3 shows the profile of the absorbance change as a function of time and space as the ionophore diffuses from the interface into the photobleached region of the film. The data represents an increase in the absorbance of the polymer film as In(AOTPP)Cl ($\lambda_{max} \approx 560$ nm) diffuses from an area of high concentration to an area of low concentration (left to right). As noted, the initial spectra when t=0 shows an apparent concentration of the ionophore beyond the interface (x=0) into the photobleached region. This deviation from theory suggest that the ionophore has been diffusing from the interface into the membrane film for some time ($t_0>0$). Therefore, assuming a constant diffusion coefficient for the experiment we can substitute:

$$t = t_0 + \Delta t \tag{5.2}$$

After inserting Eq. (5.2) into Eq. (5.1) the following relation is obtained:

$$A_{(x,t)} = \frac{1}{2} A_0 erfc \frac{x}{2\sqrt{D(t_0 + \Delta t)}} \tag{5.3}$$

The absorbance profiles seen in Fig. (5-3) were fit with Eq. (5.1) giving a set of Dt values for all of the acquisition times Δt. This data set was inserted into Eq. (5.3) and a linear relation, shown in Fig. (5-4), between Dt and Δt was obtained providing a value for the diffusion coefficient and t_0. Values for diffusion coefficients were on the order expected for this type of membrane composition.[28,29] Deviation from linearity were observed for longer acquisition times probably due to the non-linear interface between the two polymeric film regions and were excluded from analysis. The relative standard deviations in calculating the diffusion coefficients of the ionophores were between 2-10%. This is similar to results reported previously for a set of plasticized PVC membranes interrogated in the same fashion.[24]

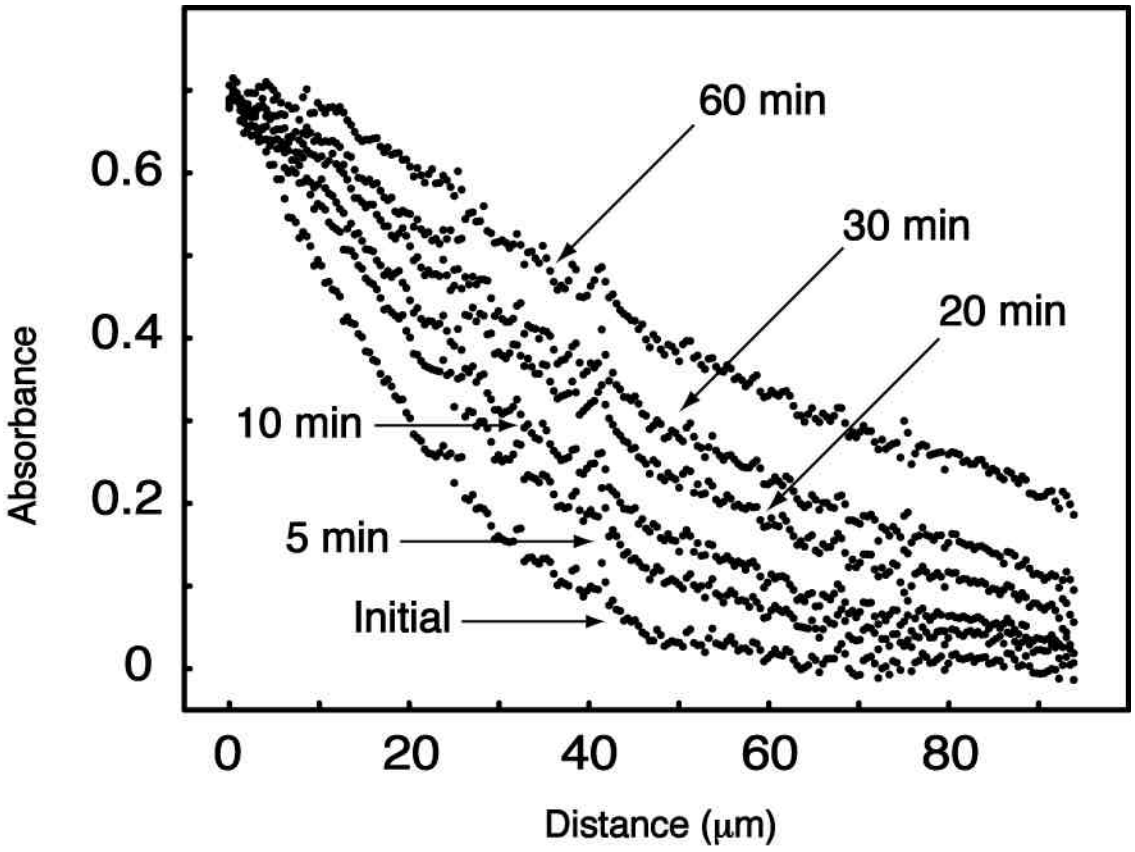

Fig. 5-3 Absorbance profile of a PVC-DOS membrane (1:2) containing 1.05% by weight of the chromogenic ionophore In(AOTPP)Cl. Each point represents the absorbance of an average of wavelengths surrounding the absorbance (λ^{max} ≈560 nm) as a function of time and distance from the iterface where x=0. As the time increases, so does the absorbance further into the photobleached portion of the film.

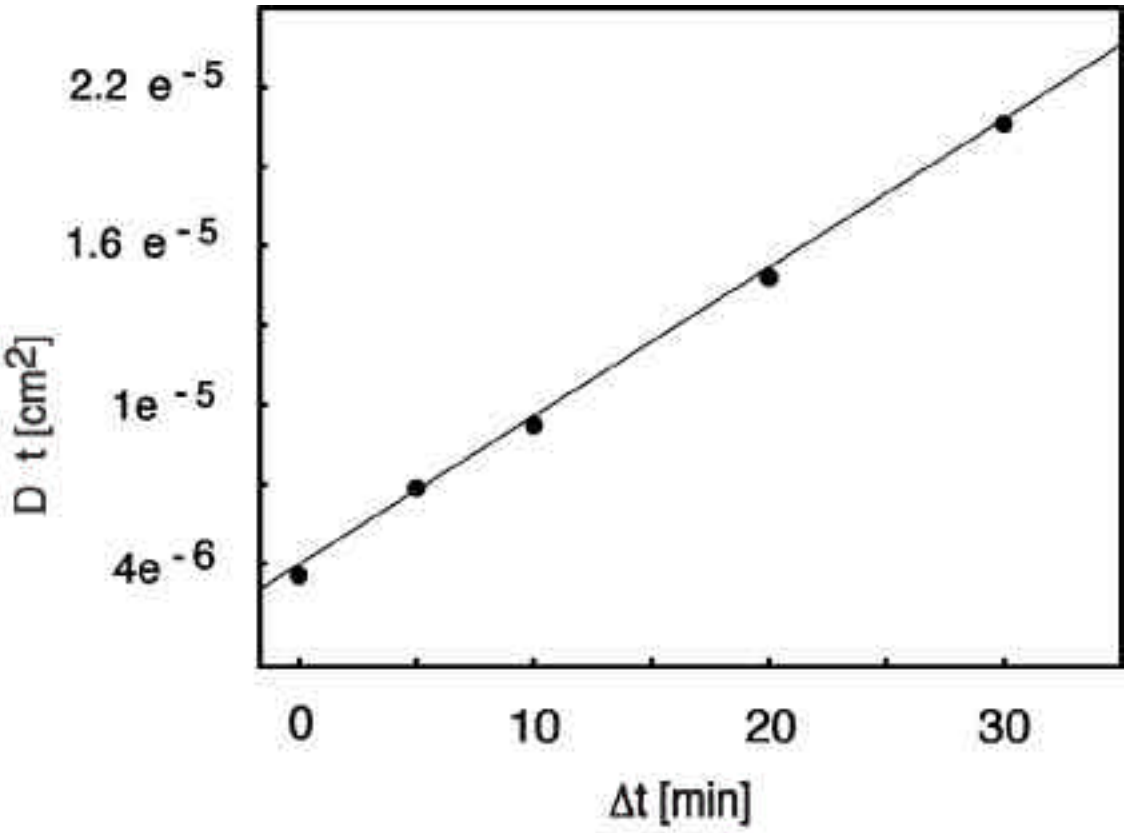

Fig. 5-4 Fit providing an average diffusion coefficient from the data in Fig. 5-3. The line shows the relationship between the diffusion coefficient (D) and time (t) using equation 5.3.

Fig. 5-5 shows the experimental absorbance profiles, shown in Fig. 5-3, fit with curves generated from Eq. (5.3) after inserting a single diffusion coefficient for the entire experiment and t_0, both obtained from the linear relationship between Dt and Δt. In this example, D was found as $9.4 \times 10^{-9} cm^2 s^{-1}$ (S.D. = 1.7%) and a time constant t_0=396s. Good correlation between experimentally obtained data points and theoretical curves demonstrates how useful this simple method can be in determining diffusion coefficients of chromogenic species. In a previous study on ETH 5294, using this method, the time required to photobleach the chromoionophore with light from the high-presure mercury arc lamp was approximately two minutes. In sharp contrast, while the Nile Blue derivative (NB-1) also required 2 minutes to photobleach the porphyrins routinely required 7-9 minutes of continuous exposure to photobleach completely.

The results of the nine membranes analyzed with the above mentioned method are summarized along with the individual membrane compositions in Table 5-1. The data show that in reference to the indium porphyrins examined that the diffusion coefficients for each compound were greater in membranes containing the more polar plasticizer, NPOE, than those with the plasticizer DOS. This is in agreement with a previous study on the diffusion of the chromoionophore ETH 5294 in a similar polymer matrix.[24]

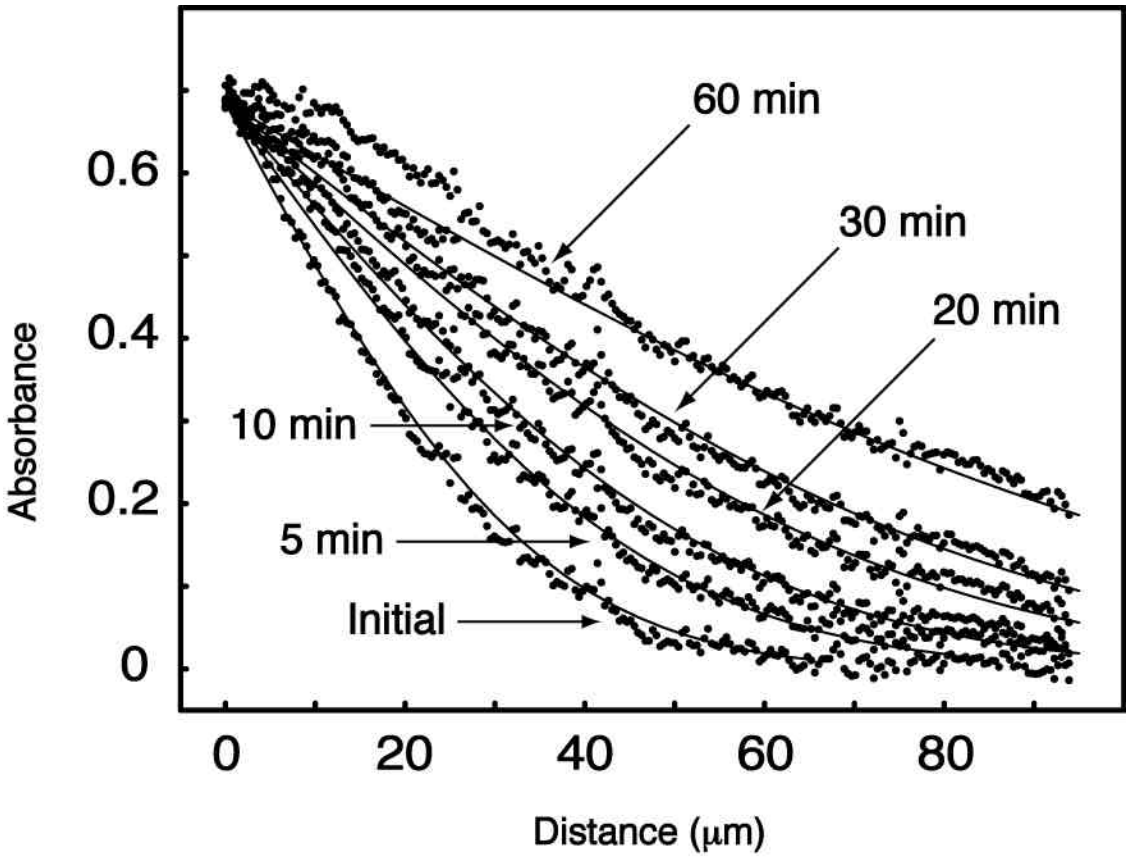

Fig. 5-5 Time dependent absorbance profiles shown in Fig. (5-3) with theoretical fits obtained from Eq. (5.3) using a single diffusion coefficient. The membrane composition was PVC-DOS (1:2) with 1.05% by weight of the chromogenic ionophore In(AOTPP)Cl. The absorbance maximum was approximately 560 nm.

Ionophore (%w/w)		% PVC	Plasticizer	D (cm^2/s)
NB-1	(0.63)	33.7	*o*-NPOE	$2.4x10^{-9}$
In(OEP)Cl	(1.00)	38.7	*o*-NPOE	$8.5\ x10^{-9}$
In(OEP)Cl	(0.83)	50.2	*o*-NPOE	$1.7\ x10^{-9}$
In(OEP)Cl	(0.80)	48.9	DOS	$5.0\ x10^{-10}$
In(AOTPP)Cl	(1.57)	33.0	*o*-NPOE	$1.6\ x10^{-8}$
In(AOTPP)Cl	(1.05)	32.8	DOS	$9.4\ x10^{-9}$
In(HEPEAC)Cl	(1.44)	33.9	*o*-NPOE	$4.9\ x10^{-9}$
In(HEPEAC)Cl	(0.94)	32.9	DOS	$1.3x10^{-9}$

Table 5-1 Calculated Diffusion coefficients from Eq. (5.3) for the reported membrane compositions with calculated weight percents of chromogenic ionophore, PVC and plasticizer.

NB-1 is an acryloyloxybenzoyl derivative of the oxazine-dye, Nile Blue, and has an absorbance maximum of $\lambda^{max} \approx 560$ nm . The derivative of Nile blue was made in order to covalently link the chromoionophore to an MMA-DMA copolymer. Both the free NB-1 and the grafted NB-1-MMA-DMA were interrogated in plasticized PVC membranes. The NB-1-MMA-DMA grafted copolymer did not show appreciable diffusion in the PVC membranes over a two-hour time frame (data not shown) supporting immobilization by covalent attachment. The free NB-1 chromophore did show significant mobility in a PVC:NPOE (1:2) membrane with a calculated diffusion coefficient of $2.4 \times 10^{-9} cm^2 s^{-1}$. This is approximately an order of magnitude slower than its Nile blue analog, ETH 5294, in a similar membrane.[24]

The percent composition of PVC and plasticizer in the membranes containing the chromogenic ionophore In(OEP)Cl were adjusted in an attempt to slow the rate of diffusion and obtain more accurate measurements. In(OEP)Cl has been used in optical[6,7,11] and potentiometric[11,12,14] sensors for the detection of chloride anions. In a PVC:NPOE (1:1) membrane with 0.83 percent by weight of In(OEP)Cl, the measured diffusion coefficient ($1.7 \times 10^{-9} cm^2 s^{-1}$) is on the order of that measured for ETH 5294 with an identical membrane composition.[24]

Both In(HEPEAC)Cl and In(AOTPP)Cl were synthesized so that they could be grafted to the backbone of a MMA-DMA copolymer.[10] The diffusion coefficients for each free ionophore were determined in plasticized PVC membranes with a typical 1:2 weight ratio for both NPOE and DOS. For the In(HEPEAC)Cl ionophore in a

PVC:NPOE membrane, the diffusion coefficient was estimated to be $4.9x10^{-9}cm^2s^{-1}$. While the diffusion coefficient of In(AOTPP)Cl in a similar membrane was estimated as $1.6x10^{-8}cm^2s^{-1}$. In each case, the membranes containing the more polar plasticizer, NPOE, exhibited a greater rate of diffusion. Also, both grafted ionophores demonstrated a greatly decreased linear mobility into the photobleached portion of the membrane with an example shown in Fig. (5-6).

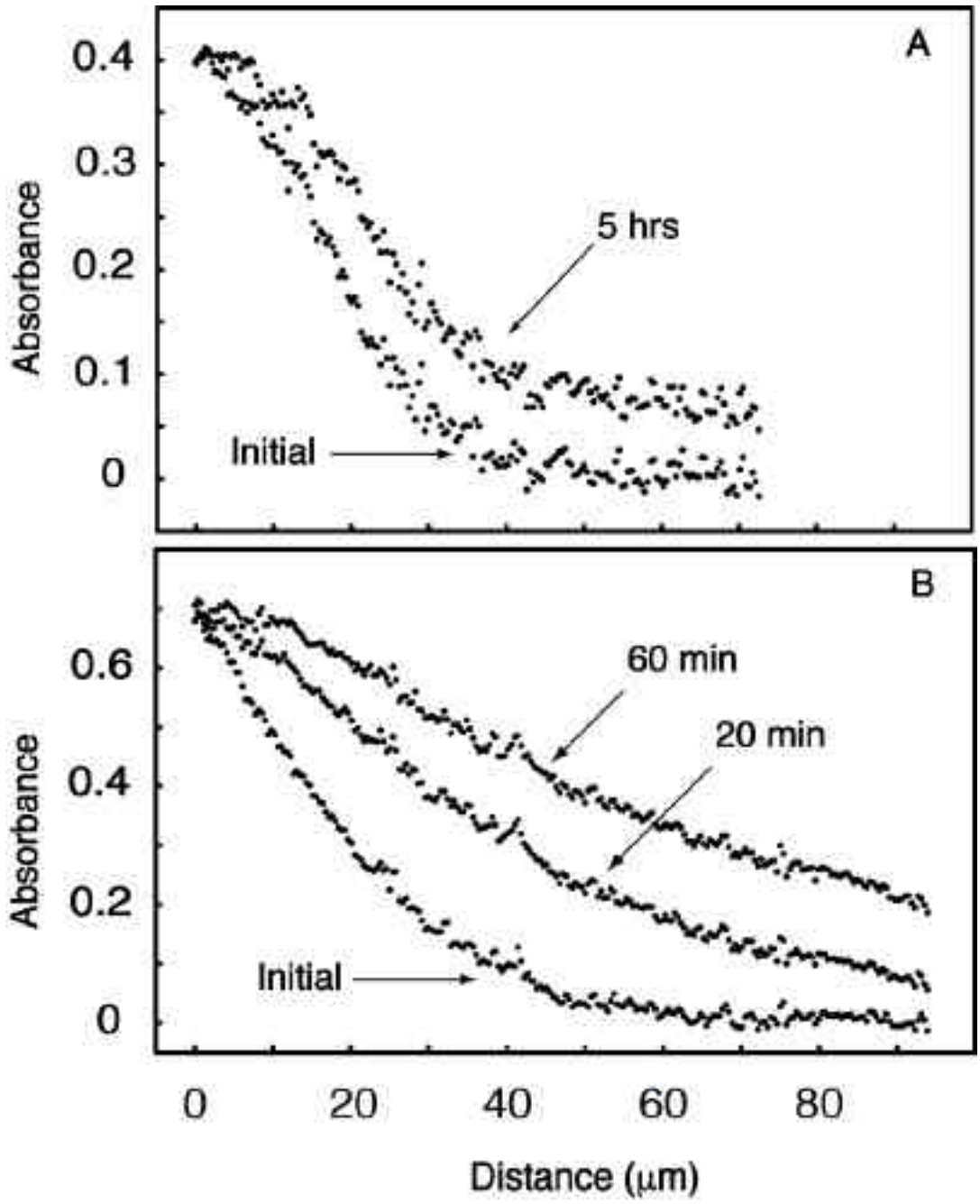

Fig. 5-6 Diffusion profiles in PVC-DOS (1:2) membranes of A: Grafted In(AOTPP)-MMA-DMA copolymer and B: Free In(AOTPP)Cl.

5.4 Conclusions

A previously introduced spectroscopic method for determining the diffusion coefficients of chromogenic ionophores in PVC based liquid polymer membranes is used to interrogate three novel ionphores [NB-1, In(HEPEAC)Cl and In(AOTPP)Cl] and one established ionophore [In(OEP)Cl]. Through absorbance measurements, an accurate value for the diffusion coefficients of each compound is estimated in PVC by modeling the membrane matrix as semi-infinite plane. The plasticizer was varied between NPOE and DOS showing an increased rate of diffusion in membranes with the more polar plasticizer (NPOE). The three novel ionophores investigated were indeed synthesized to be grafted onto a MMA-DMA copolymer. The grafted form of each exhibited a vast decrease in diffusion rate through the plasticized PVC membranes.

References

1 Bakker, E.; Bühlmann, P.; Pretsch, E. *Chem. Rev*. **1997**, 97, 3083.

2 Bühlmann, P.; Pretsch, E.; Bakker, E. *Chem. Rev*. **1998**, 98, 1593.

3 van den Berg, A.; van der Wal, P.D.; Skowronska-Ptasinska, M.; Sudholter, E.J.R.; Reinhoudt, D.N.; Bergveld, P. *Anal. Chem.* **1987**, 58, 2827.

4 Morf, W.E.; Simon, W. *Helv. Chim. Acta* **1986**, 69, 1120.

5 Morf, W.E.; de Rooij, N.F.; Pretsch, E. *J. Electroanal. Chem.* **2005**, 581 265.

6 Hofmeister, F. *Arch. Exp. Pharmakol.* **1888**, 24, 247.

7 Biesaga, M.; Pyrzynska, K.; Trojanowicz, M. *Talanta* **2000**, 51, 209.

8 Zhang, W.; Rozniecka, E.; Malinowska, E.; Parzuchowski, P.; Meyerhoff, M.E. *Anal. Chem.* **2002**, 74, 4548.

9 Qin, W.; Parzuchowski, P.; Zhang, W.; Meyerhoff, M.E. *Anal. Chem.* **2003**, 75, 332.

10 Qin, Y.; Bakker, E. *Anal. Chem.* **2004**, 76, 4379.

11 Steinle, E.D.; Schaller, U.; Meyerhoff, M.E. *Anal. Sci*. **1998**, 14, 79.

12 Pimenta, A.M.; Araujo, A.N.; Conceicao, M.; Montenegro, B.S.M.; Pasquini, C.; Rohwedder, J.J.R.; Raimundo Jr., I.M. *J. Pharm. Biomed. Anal*. **2004**, 36, 49.

13 Wang, E.; Romero, C.; Santiago, D.; Syntilas V. *Anal. Chim. Acta* **2001**, 433, 89.

14 Malinowska, E.; Niedzolka, J.; Meyerhoff, M.E. *Anal. Chim. Acta* **2001**, 432, 67.

15 Chaniotakis, N.A.; Chasser, A.M.; Meyerhoff, M.E. *Anal. Chem.* **1988**, 60, 188.

16 Ammann, D.; Huser, M.; Krautler, B.; Rusterholz, B.; Schulthess, P.; Lindemann, B.; Halder, E.; Simon, W. *Helv. Chim. Acta* **1986**, 69, 849.

17 Badr, I.H.A.; Meyerhoff, M.E. *Anal. Chem.* **2005**, 77, 6719.

18 Messik, M.S.; Krishnan, S.K.; Hulvey, M.K.; Steinle, E.D. *Anal. Chim. Acta* **2005**, 539, 223.

19 Gorski, L.; Meyerhof, M.E.; Malinowska, E. *Talanta* **2004**, 63, 101.

20 Malinowska, E.; Gorski, L.; Meyerhoff, M.E. *Anal. Chim. Acta* **2002**, 468, 133.

21 Chaniotakis, N.A.; Park, S.B.; Meyerhoff, M.E. *Anal. Chem.* **1989**, 61, 566.

22 Steinle, E.D.; Amemiya, S.; Bühlmann, P.; Meyerhoff, M.E. *Anal. Chem*. **2000**, 72, 5766.

23 Wang, E.; Meyerhoff, M.E. *Anal. Chim. Acta* **1993**, 283, 673.

24 Long, R.; Bakker E. *Anal. Chim. Acta* **2004**, 511, 91.

25 Qin, Y.; Bakker, E. *Submitted.*

26 Craggs, A.; Moody, G.J.; Thomas, J.D.R. *J. Chem. Edu.* **1974**, 51, 541.

27 Crank, J. *The Mathematics of Diffusion*, Oxford University Press, New York, **1993**.

28 Schneider, B.; Zwickl, T.; Federer, B.; Pretsch, E.; Lindner, E. *Anal. Chem*. **1996**, 68, 4342.

29 Puntener, M.; Fibbioli, M.; Bakker, E.; Pretsch, E. *Electroanalysis* **2002**, 8, 1329.

Chapter 6

Conclusions

An amperometric pH sensor was demonstrated based on the same membrane components as the traditional solvent polymeric ion-selective electrodes. By measuring the potential from a series of normal pulse voltammograms (NPV) that resulted in identical currents for the amperometric sensor containing the chromoionophore ETH 5294, a pseudo-Nernstian response curve was generated relating the current from sample solutions at different pH. The membrane was devoid of ion-exchanger sites and was made with a high weight percent of the inert lipophilic electrolyte ETH 500, which lowered the membrane resistance and decreased ion migration. The response range for this sensor compared well with the potentiometric counterpart. The NPV curves provided information on the diffusion coefficient of the H^+/chromoionophore complex from Cottrell fits of the current response within the limiting current region. Imaging experiments were also done following the absorbance of the chromoionophore under an

applied potential to assess its diffusion coefficient based on the theory of diffusion into a semi-infinite matrx. The values obtained corresponded to the Cottrell fits and to reported values for this membrane composition.

The amperometric theory of the response for these sensors was expanded to accommodate multi-valent ions including terms and conditions relating the NPV to the complex formation constants of the ion-ionophore complex. The results from nine ionophores were reported along with experimental protocols. Again, using the Cottrell equation, diffusion coefficients were reported for the neutral ionophores that exhibited a diffusion-limited current region. The values for both the complex formation constants and the diffusion coefficients were in agreement with those reported from other methods.

A new method was introduced to assess the diffusion coefficients of chromogenic species within a single solvent polymeric membrane. The method involved photobleaching a circular area of the membrane and following the absorbance of the chromogenic species as it diffused into the newly created transparent region. Twenty membranes containing various polymer:plasticizer ratios were examined to obtain the diffusion coefficients of the chromoionophore ETH 5294. It was shown that the rate of diffusion of ETH 5294 decreased linearly in response to increased weight percent of the polymer (PVC), and that membranes with added lipophilic salt ETH 500 also showed a decrease in the rate of diffusion.

This method was also used to determine the diffusion coefficients of four other chromogenic species in solvent polymeric membranes. Three chromogenic ionophores

that were derivatized for covalent attachment to an MMA-DMA copolymer and one underivatized ionophore were examined. The values obtained for the diffusion coefficients of these species were in agreement with those expected for this membrane composition. The derivatized ionophores were attached to the MMA-DMA copolymer and included in the PVC membranes showing a vast decrease in their rates of diffusion.